

# **MODELING EVAPOTRANSPIRATION USING REMOTELY SENSED SPATIAL CONTEXTUAL INFORMATION**

**Thesis**

**Submitted in partial fulfilment of the requirements for the degree of  
DOCTOR OF PHILOSOPHY**

**By**

**SANJAY SHEKAR N C**



**DEPARTMENT OF APPLIED MECHANICS AND HYDRAULICS  
NATIONAL INSTITUTE OF TECHNOLOGY KARNATAKA,  
SURATHKAL, MANGALORE – 575025  
NOVEMBER, 2019**

# **MODELING EVAPOTRANSPIRATION USING REMOTELY SENSED SPATIAL CONTEXTUAL INFORMATION**

**Thesis**

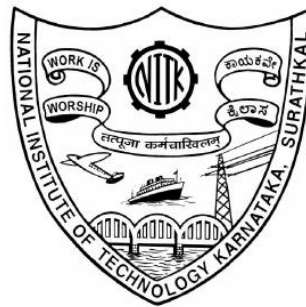
**Submitted in partial fulfilment of the requirements for the degree of  
DOCTOR OF PHILOSOPHY**

**By**

**SANJAY SHEKAR N C**

**Under the Guidance of**

**Prof. LAKSHMAN NANDAGIRI**



**DEPARTMENT OF APPLIED MECHANICS AND HYDRAULICS  
NATIONAL INSTITUTE OF TECHNOLOGY KARNATAKA,  
SURATHKAL, MANGALORE – 575025**

**NOVEMBER, 2019**

## **D E C L A R A T I O N**

*By the Ph.D. Research Scholar*

I hereby *declare* that the Research Thesis entitled “**Modeling Evapotranspiration using Remotely Sensed Spatial Contextual Information**” which is being submitted to the **National Institute of Technology Karnataka, Surathkal** in partial fulfilment of the requirements for the award of the Degree of **Doctor of Philosophy** in **Applied Mechanics and Hydraulics Department** is a *bonafide report of the research work* carried out by me. The material contained in this Research Thesis has not been submitted to any University or Institution for the award of any degree.

135070AM13P02, SANJAY SHEKAR N C

(Register Number, Name & Signature of the Research Scholar)

Department of Applied Mechanics and Hydraulics

Place: NITK-Surathkal

Date:

## C E R T I F I C A T E

This is to *certify* that the Research Thesis entitled “**Modeling Evapotranspiration using Remotely Sensed Spatial Contextual Information**” submitted by SANJAY SHEKAR N C (Register Number: AM13P02) as the record of the research work carried out by him, is *accepted as the Research Thesis submission* in partial fulfilment of the requirements for the award of degree of **Doctor of Philosophy**.

Dr. Lakshman Nandagiri

Professor

Research Guide

(Name and Signature with Date and Seal)

Chairman - DRPC

(Signature with Date and Seal)

## ACKNOWLEDGEMENTS

---

I want to express the sincere gratitude to supervisor Prof. Lakshman Nandagiri, who has been continually and convincingly conveyed in guiding me to render a shape for my research work. Without his guidance and tenacious help, this dissertation would not have been possible.

I want to thank Research Progress Committee members, Prof. Paresh Chandra Deka, Prof. Arkal Vittal Hegde, Department of Applied Mechanics and Hydraulics and Prof. Sunil B M, Department of Civil Engineering, for their continuous support, fruitful encouragement and pragmatic critique during research progress presentations.

I am greatly indebted to Prof. Subba Rao, Prof. Dwarakish G S and Prof. Mahesha A the former Head of the Department of Applied Mechanics and Hydraulics, NITK, Surathkal and Prof. Amba Shetty, the present Head of the Department, for granting me the permission for data collection and to use the departmental computing facilities available for necessary research work to the maximum extent, which was very vital for the completion of the computational aspects relevant to this research.

I thank the Director of the NITK, Surathkal, for granting permission to use the institutional infrastructure facilities, without which this research work would have been impossible.

I sincerely acknowledge the help and support rendered by all the Faculties, staffs and Research scholars of the Department of Applied Mechanics & Hydraulics.

I can never forget to mention friends and peers for the support, help, appreciation and immensely valuable suggestions during research work. Especially, I would like to thank Dr. Keerthi Laxmi for teaching me MATLAB and her countless support throughout the research period. Also, I would like to thank Dr. Kumar Raju B C, Dr. Sanjeev Gadad and Dr. Bhojraja B E for their encouragement and selfless assertiveness. I want to acknowledge the help and support by all the fellow friends

and all other well-wishers for their direct or indirect assistance at various stages of this research work.

I want to thank the supporting staff of the department Mr. Jagadish, Mr. Balakrishna, Mrs. Prathima, Mr. Harish, Mr. Gopal, Mr. Anand and Mr. Niranjana for all their logistics and other indirect help during PhD work. Timely support rendered by the administrative staff of NITK is gratefully acknowledged. My thanks are also to each and everyone who has directly or indirectly helped.

I express heartfelt gratitude to authors of all those research publications which have been referred to in this thesis and also like to thank all the Government Departments and Organizations for providing required data.

Finally, I wish to express gratitude, love, and affection to beloved family members for their encouragement and moral support on the road to the completion of the research.

## ABSTRACT

---

Characterization of the spatial and temporal variabilities of Actual Evapotranspiration (AET) or Latent Heat Flux ( $\lambda$ ET) from heterogeneous landscapes is essential in studies related to hydrology, climate, agriculture, irrigation, water resources engineering and management and environmental impact assessments. AET/ $\lambda$ ET is influenced by a large number of factors related to climate, vegetation and soil moisture and therefore its direct measurement is rendered difficult especially over large spatial domains. The only feasible and convenient way to map AET over regional or catchment-scales is through the use of remote sensing technology and accordingly, numerous world-wide studies have focussed on this approach. Among these, the Penman-Monteith (PM) and Priestley-Taylor (PT) methods have proved to be most popular on account being simple but yet providing reasonably accurate estimates of regional AET. However, most previous studies have implemented satellite-based PM and PT AET estimation approaches to crop lands located in arid to semi-arid regions.

Therefore, the main focus of the present study is to develop satellite-based AET estimation methods which can be applied to wet tropical regions possessing natural vegetation. The current research work is aimed at the development, application and evaluation of methodologies for estimation of AET/ $\lambda$ ET by the PM approach using Moderate Resolution Imaging Spectrometer (MODIS) satellite imagery. The feasibility of extracting the bulk surface conductance ( $G_s$ ); an important parameter in the PM model, from the spatial contextual information present in a scatter plot of Land Surface Temperature (LST) versus Fraction of Vegetation (Fr) is explored in this study. Also, few studies seemed to have compared the performances of the PM and the PT model and other similar models using the same dataset and therefore this exercise was taken up.

Using a general expression for  $G_s$  derived by assuming a two-source total  $\lambda$ ET (canopy transpiration plus soil evaporation) approach proposed by previous researchers, minimum and maximum values of  $G_s$  for a given region can be inferred from a trapezoidal

scatter plot of pixel-wise values of LST and corresponding Fr. Using these as limiting values, Gs values for each pixel can be derived through interpolation and subsequently used with the PM model to estimate  $\lambda ET$  for each pixel. The proposed methodology was implemented in 5 km x 5 km areas surrounding each of four AsiaFlux tower sites located in different countries of tropical south-east Asia which were selected based on certain specific criteria. MODIS data products of MOD11A1 product of Land Surface Temperature (LST) at 1000 m resolution, MOD09GA product of Land Surface Reflectance (LSR) at 1000 m resolution, MOD15A2 product of Leaf Area Index (LAI) as eight days average composited at 1000 m resolution and Digital Elevation Model (DEM) at 30 m resolution were used. Preliminary processing of images was performed using MODIS reprojection tool (MRT) and was converted to a standard format that can be read by MATLAB software. Geo-referencing, subsetting and pixel-wise analysis corresponding to the study area were performed using ArcGIS and ERDAS IMAGINE. Model evaluation was carried out using the following performance measures- coefficient of determination ( $R^2$ ), root mean squared error (RMSE), percent bias (PBIAS) and the intercept (a) and slope (b) terms of a linear regression fit ( $y = a + bx$ ). Excellent comparisons were obtained between tower measured  $\lambda ET$  and those estimated by the proposed approach for all four flux tower locations ( $R^2 = 0.85 - 0.96$ ; RMSE = 18.27 – 33.79 W/m<sup>2</sup>). The proposed methodology was compared with two alternative methods proposed by previous researchers. Performances of all three approaches were comparable indicating the robustness of the methodology proposed in the present study.

The PM method proposed in the present study was implemented in the Hemavathi sub-basin which is located in the Cauvery River Basin, Karnataka, India to map spatial patterns of daily AET. MOD16A2 product of actual evapotranspiration (AET) as eight day average composited at 500 m resolution was used for validation purposes. Climate records for the Belur station were used. The analysis was carried out for two dates in summer and two dates in winter separately for the years 2007 (wet year) and 2012 (dry year). For each date, trapezoidal scatter plots of MODIS-derived LST values versus Fr were plotted by considering 1 km<sup>2</sup> pixels in the study area of 304 km<sup>2</sup>. For each day, estimated AET values



by the PT approach ( $AET_{PT}$ ), PM model of the present study with Ga computed using Leuning equation ( $AET_{PM}$ ) and with Ga computed using Choudhary equation ( $AET_{PMCH}$ ) for each of the 304 pixels were extracted and compared with the corresponding pixel-wise MOD16A2 ET estimates.

Results of the performance evaluation of AET estimation methods relative to MOD16A2 showed that the PM model proposed in the present study with Ga computed using the Leuning equation ( $AET_{PM}$ ) performed reasonably well for both the wet and dry years. High values of  $R^2$  (0.77 – 0.90) and reasonably low values of RMSE (0.28 – 0.38 mm/day) were obtained but the PBIAS values were somewhat high (-7.04 – -12.41). Also, the PM model yielded relatively poorer estimates for the winter days of the drier year 2012. The performance of the PT model was quite similar to the PM model with similar performance statistics being recorded. However, slightly lower RMSE values were obtained for this model on some days. The PM model proposed in the present study with Ga computed using the Choudhary equation turned out to be the best model as indicated by the lowest values of RMSE (0.19 – 0.25 mm/day), although  $R^2$  values were similar. Also, use of the Choudhary equation reduced PBIAS values significantly for all days considered. Using the pixel-wise values of  $AET_{PMCH}$ , maps showing the spatial variability were prepared for the Hemavathi sub-basin for all the dates considered in 2007 and 2012. The variations of AET over the basin appear to be influenced by topography, type of LU/LC, LST and moisture availability conditions.

The satellite-based spatial contextual information approach adopted in the present study for the first time with the PM model has proved to be a simple, calibration-free and accurate method. As demonstrated by previous studies and also the present study, use of the LST- $F_r$  plot does not require additional hydrological data for optimization of the AET model parameters. The framework for implementing the spatial contextual information approach to derive operational estimates of daily AET over large spatial domains has been developed and validated in this study.

## TABLE OF CONTENTS

Title Page.....	<i>i</i>
Declaration.....	<i>ii</i>
Certificate.....	<i>iii</i>
Acknowledgements.....	<i>iv-v</i>
Abstract.....	<i>vi-viii</i>
Table of Contents.....	<i>ix-xii</i>
List of Figures.....	<i>xiii-xiv</i>
List of Tables.....	<i>xv</i>
List of Abbreviations.....	<i>xvi-xvii</i>
List of Notations.....	<i>xviii-xxi</i>
<b>CHAPTER 1</b>	<b>Pg.no</b>
<b>INTRODUCTION.....</b>	<b>1-10</b>
1.1 GENERAL.....	1
1.2 IMPORTANCE OF AET.....	2
1.3 MEASUREMENT OF AET.....	2
1.4 ESTIMATION OF AET.....	3
1.5 SATELLITE-BASED AET ESTIMATION APPROACHES.....	5
1.6 STUDY OBJECTIVES.....	7
1.7 SCOPE OF THE PRESENT STUDY.....	8
1.8 OVERALL METHODOLOGY.....	9
1.9 OUTLINE OF THE THESIS.....	9
<b>CHAPTER 2</b>	
<b>REVIEW OF LITERATURE.....</b>	<b>11-32</b>
2.1 GENERAL.....	12
2.2 PENMAN-MONTEITH EQUATION.....	12
2.3 PRIESTLEY-TAYLOR EQUATION.....	19

2.4	RELATIONSHIP BETWEEN PT PARAMETER ( $\varphi$ ) AND BULK SURFACE RESISTANCE ( $R_s$ ).....	25
2.5	COMPARISON OF SPATIAL AET ESTIMATES WITH MOD16A2.....	29
2.6	SUMMARY.....	31
<b>CHAPTER 3</b>		
	<b>STUDY AREAS AND DATA USED.....</b>	<b>33-39</b>
3.1	STUDY AREAS.....	33
3.2	FLUX TOWER SITES .....	33
3.3	HEMAVATHI CATCHMENT.....	35
3.4	DATA PREPARATION.....	36
3.4.1	Satellite data acquisition .....	36
3.4.2	MODIS satellite data products .....	37
3.4.3	Meteorological data.....	37
3.4.4	Land Use/Land Cover (LU/LC) Map.....	38
3.4.5	Preprocessing and software used.....	39
<b>CHAPTER 4</b>		
	<b>METHODOLOGY FOR ESTIMATION OF AET.....</b>	<b>40-63</b>
4.1	GENERAL.....	40
4.2	METHODOLOGY OF PENMAN-MONTEITH APPROACH.....	41
4.3	METHODOLOGY OF PRIESTLEY-TAYLOR APPROACH.....	43
4.4	COMPUTATION OF VARIABLES IN PM AND PT EQUATION.....	44
4.4.1	Estimation of net radiation ( $R_n$ ).....	45
4.4.1.1	Incoming solar radiation ( $R_s$ ).....	46
4.4.1.1.1	Inverse relative earth-sun distance ( $d_r$ ).....	46
4.4.1.1.2	Two-way atmospheric transmissivity ( $\tau_{sw}$ ).....	47
4.4.1.1.3	Solar zenith angle ( $\theta$ ).....	47
4.4.1.2	Long wave downward radiation ( $R_{i\downarrow}$ ).....	47
4.4.1.2.1	Atmospheric emissivity ( $\varepsilon_a$ ).....	48

4.4.1.3	Long wave upward radiation ( $R_i\uparrow$ ).....	48
4.4.2	Computation of albedo ( $\alpha$ ).....	48
4.4.3	Estimation of soil heat flux ( $G$ ).....	49
4.4.4	Slope of saturation vapour pressure curve ( $\Delta$ ).....	49
4.4.5	Psychrometric constant ( $\gamma$ ).....	49
4.4.6	Estimation of Normalized Differential Vegetation Index (NDVI).....	50
4.4.7	Estimation of Fraction of Vegetation (Fr).....	50
4.4.8	Saturated vapour pressure ( $e_s$ ).....	51
4.4.9	Actual vapour pressure ( $e_s$ ) .....	51
4.4.10	Air density at constant pressure ( $\rho_a$ ).....	51
4.4.11	Altitudinal correction of LST.....	52
4.4.12	Computation of daily net radiation ( $R_{n \text{ daily}}$ ).....	53
4.4.12.1	Extraterrestrial solar radiation ( $R_a$ ).....	53
4.4.13	Estimation of aerodynamic conductance ( $G_a$ ).....	54
4.4.14	$G_s$ estimation from the trapezoidal scatter plot (LST versus Fr).....	54
4.4.15	Deriving pixel-wise $G_s$ and $\phi$ values from the LST-Fr scatter plot.....	58
4.4.16	Cleugh et al., (2007) bulk surface conductance model.....	60
4.4.17	Leuning et al., (2008) bulk surface conductance model.....	61
4.4.18	Estimation of evaporative fraction (EF).....	62
4.4.19	Calculation of daily AET.....	62
<b>CHAPTER 5</b>		
<b>VALIDATION OF ALGORITHMS.....</b>		<b>64-83</b>
5.1	GENERAL.....	64
5.2	APPLICATION OF ALGORITHMS TO FLUX SITES.....	64
5.3	RESULTS.....	65
5.3.1	Variation of $G_{s_{\max}}$ with climatic variables.....	65
5.3.2	LST-Fr scatter plots.....	66
5.3.3	Computed $G_{s_{\max}}$ values .....	72
5.3.4	Pixel-wise variability of computed $G_s$ and $\lambda ET_{PM}$ values.....	72

5.3.5	Comparison of computed and measured values of latent heat flux by PM approach.....	74
5.3.6	Comparison with Laxmi and Nandagiri (2014).....	79
5.3.7	Comparison with Cleugh et al., (2007).....	79
5.3.8	Comparison with Leuning et al., (2008) .....	80
5.3.9	Discussion.....	81
<b>CHAPTER 6</b>		
<b>APPLICATION TO THE HEMAVATHI SUB-BASIN.....</b>		<b>84-101</b>
6.1	GENERAL.....	84
6.2	APPLICATION OF THE VALIDATED PM AND PT ALGORITHMS .....	84
6.3	RESULTS AND DISCUSSION.....	85
6.3.1	LST-Fr scatter plots.....	85
6.3.2	Pixel-wise variability of computed Gs and $\phi$ with AET values.....	88
6.3.3	Pixelwise comparison of estimated AET by PM and PT approaches using MOD16A2.....	90
6.3.4	Aerodynamic conductance estimation by Choudhary et al. (1986).....	93
6.3.5	Spatial AET estimated by PM, PT and PMCH approaches.....	98
<b>CHAPTER 7</b>		
<b>SUMMARY AND CONCLUSIONS.....</b>		<b>102-105</b>
7.1	GENERAL.....	102
7.2	CONCLUSIONS.....	102
7.3	LIMITATIONS OF THE STUDY.....	104
7.4	SCOPE FOR FUTURE STUDIES.....	105
Appendix A	REFERENCES.....	<b>106-118</b>
Appendix B	PAPERS PUBLISHED FROM THIS RESEARCH.....	119
Appendix C	RESUME.....	120

## LIST OF FIGURES

Sl. No	Fig. No.	Caption	Page No.
1	2.1	Simplified representation of the (bulk) surface and aerodynamic resistances for water vapour flow	12
2	3.1	Location map and DEM of Hemavathi catchment sub-basin	36
3	3.2	LU/LC map of the Hemavathi sub-basin	38
4	4.1	Flowchart depicting the steps involved in the estimation of AET by the Penman-Monteith method	42
5	4.2	Flowchart depicting the steps involved in the estimation of AET by the Priestley-Taylor method	43
6	4.3	Surface Atmosphere Energy Exchange	45
7	4.4	Solar zenith angle	47
8	4.5	Triangular and trapezoidal scatter plot of LST versus Fr	55
9	5.1	Response of $G_{S_{max}}$ (Equation 4.35) to $D_a$ for different values of $(R_n - G)$ at constant air temperature (T) of $30^0$ C	65
10	5.2	Trapezoidal scatter plots of LST versus Fr for MKL flux tower	67
11	5.3	Trapezoidal scatter plots of LST versus Fr for PDF flux tower	68
12	5.4	Trapezoidal scatter plots of LST versus Fr for IRI flux tower	69
13	5.5	Trapezoidal scatter plots of LST versus Fr for SKR flux tower	70
14	5.6	Variability of computed pixel-wise $\lambda ET_{PM}$ values for selected dates in each flux site area	74
15	5.7	Comparison of instantaneous latent heat flux values computed by the Penman-Monteith method proposed in the present study ( $\lambda ET_{PM}$ ) with those measured ( $\lambda ET_{Meas}$ ) on selected dates/times at the flux towers located at (a) MKL (b) PDF (c) IRI and (d) SKR	77
16	6.1	Trapezoidal scatter plots of LST versus Fr	86
17	6.2	Variability of computed pixel-wise min, max and mean $G_s$ values and values of $G_{S_{max}}$ computed using Eq. 4.35	88
18	6.3	Variability of computed pixel-wise min, max and mean $AET_{PMCH}$ values	89
19	6.4	Variability of computed pixel-wise min, max and mean $\phi$ values	90

20	6.5	Variability of computed pixel-wise min, max and mean AET <sub>PT</sub> values	90
21	6.6	Comparison of average AET estimated by PM and MOD16A2 for sample days (a) Day 57, 2007 (b) Day 57, 2012 (c) Day 345, 2007 (d) Day 353, 2012	91
22	6.7	Comparison of average AET estimated by PT and MOD16A2 for sample days (a) Day 57, 2007 (b) Day 57, 2012 (c) Day 345, 2007 (d) Day 353, 2012	92
23	6.8	Comparison of average AET estimated by PMCH and MOD16A2 for sample days (a) Day 57, 2007 (b) Day 57, 2012 (c) Day 345, 2007 (d) Day 345, 2012	94
24	6.9	Spatial variation of AET by PM approach in Hemavathi sub-basin for a) Day 57, 2007 (b) Day 65, 2007 (c) Day 345, 2007 (d) Day 353, 2007 (e) Day 57, 2012 (f) Day 65, 2012 (g) Day 345, 2012 (h) Day 353, 2012	98
25	6.10	Spatial variation of AET by PT approach in Hemavathi sub-basin for a) Day 57, 2007 (b) Day 65, 2007 (c) Day 345, 2007 (d) Day 353, 2007 (e) Day 57, 2012 (f) Day 65, 2012 (g) Day 345, 2012 (h) Day 353, 2012	99
26	6.11	Spatial variation of AET by PMCH approach in Hemavathi sub-basin for a) Day 57, 2007 (b) Day 65, 2007 (c) Day 345, 2007 (d) Day 353, 2007 (e) Day 57, 2012 (f) Day 65, 2012 (g) Day 345, 2012 (h) Day 353, 2012	100

## LIST OF TABLES

Sl. No	Table. No.	Caption	Page No.
1	2.1	Review of the Penman-Monteith equation	13
2	2.2	Review of the Priestley-Taylor equation	20
3	2.3	Review of the relationship between $\phi$ and $r_s$	26
4	2.4	Review of the comparison of spatial AET estimates with MOD16A2	30
5	3.1	Details of selected flux tower sites in south-east Asia	35
6	3.2	Annual rainfall totals (mm) for Belur rain gauge	38
7	3.3	LU/LC class composition in the Hemavathi sub-basin	39
8	5.1	LST values extracted from trapezoidal scatter plots on selected dates and times for each flux tower site	71
9	5.2	Variability of computed pixel-wise $G_s$ values for selected dates in each flux site area and values of $G_{s_{max}}$ computed using Equation 4.35	74
10	5.3	Performance measures computed using latent heat flux values measured on six dates at each of the four flux towers ( $\lambda ET_{Meas}$ ) and flux values obtained by the approach proposed in the present study ( $\lambda ET_{PM}$ )	77
11	5.4	Performance measures computed using latent heat flux values measured on six dates at each of the four flux towers ( $\lambda ET_{Meas}$ ) and flux values obtained by the PT ( $\lambda ET_{PT}$ ), PMC ( $\lambda ET_{PMC}$ ) and PML ( $\lambda ET_{PML}$ ) approaches	78
12	6.1	LST values extracted from trapezoidal scatter plots on selected dates	87
13	6.2	Performance measures computed comparing pixel-wise MOD16A2 values in the Hemavathi sub-basin on eight dates with AET estimates obtained by the PM ( $AET_{PM}$ ), PT ( $AET_{PT}$ ) and PMCH ( $AET_{PMCH}$ ) approaches	96



## LIST OF ABBREVIATIONS

<b>Abbreviation</b>	<b>Description</b>
AET	Actual Evapotranspiration
ASTER	Advanced Spaceborne Thermal Emission and Reflection Radiometer
AVHRR	Advanced Very High Resolution Radiometer
DEM	Digital Elevation Model
EF	Evaporative Fraction
ET	Evapotranspiration
ETM	Enhanced Thematic Mapper
EVI	Enhanced Vegetation Index
FAO	Food and Agriculture Organization
GIS	Geographic Information System
HDF-EOS	Hierarchical Data Format – Earth Observing System
IMD	Indian Meteorological Department
LAI	Leaf Area Index Obtained from MODIS Remote Sensing
LISS	Linear Imaging Self-scanning Sensor
LPDAAC	Land Processes Distributed Active Archive Centre
LSR	Land Surface Reflectance
LST	Corrected Land Surface Temperature
LU/LC	Land Use Land Cover
MATLAB	MATric LABoratory
MODIS	Moderate Resolution Imaging Spectroradiometer
MRT	MODIS Reprojection Tool

NASA	National Aeronautics and Space Administration
NDVI	Normalized Difference Vegetation Index
PML	Leuning et al. (2008) Bulk Surface Conductance Model
PMC	Cleugh et al. (2007) Bulk Surface Conductance Model
PET	Potential evapotranspiration
PM	Penman-Monteith
PT	Priestley-Taylor
SEBAL	Surface Energy Balance Algorithm for Land
SP	Soil Physics
SS	Sunshine Hours
TM	Thematic Mapper
TT	Turbulent Transfer

## LIST OF NOTATIONS

Abbreviation	Description
$c_p$	Specific Heat of the Air
$c_L$	Mean Surface Conductance Per Unit Leaf Area Index
$d$	Zero Plane Displacement Height
$D_a$	Vapor Pressure Deficit
$D_{50}$	Vapour Pressure Deficit at Which Stomatal Conductance Is Half
$d_r$	Inverse Relative Earth-Sun Distance
$e_a$	Actual Vapor Pressure
$e_s$	Saturation Vapour Pressure
$E_s$	Evaporation Rate from Soil
$ET_0$	Potential or Reference crop Evapotranspiration
$e^0(LST)$	Saturation Vapour Pressure at air temperature
$e^0(LST_{min})$	Saturation Vapour Pressure at minimum air temperature
$e^0(LST_{max})$	Saturation Vapour Pressure at maximum air temperature
$f$	Ratio of Evaporation Rate from Soil to the Equilibrium Evaporation Rate
$F_r$	Fraction of Vegetation
$G$	Soil Heat Flux
$g_{min}$	Surface Conductance Controlling Soil Evaporation
$g_{sx}$	Maximum Stomatal Conductance
$G_a$	Aerodynamic Conductance
$G_c$	Conductance Data Dominated by the Canopy

$G_s$	Surface Conductance
$G_i$	Climatological Conductance
$G_{sc}$	Solar Constant at the Atmosphere Top
$H$	Sensible Heat Flux
$J$	Julian day
$k$	Von Karman's Constant
$k_A$	Extinction Coefficient for Available Energy
$k_Q$	Extinction Coefficient for Shortwave Radiation
$K_0$	Solar Constant
$K_c$	Crop Coefficient
$LST_i$	Image Pixel Temperature
$P_0$	Standard air Pressure
$P$	Atmospheric Pressure
$PM-G_s$	Penman-Monteith Surface Conductance Approach
$PT$	Priestley-Taylor
$Q_h$	Flux Density of Visible Radiation at the Top of Canopy
$Q_{50}$	Visible Radiation Flux when Stomatal Conductance is Half
$r_a$	Aerodynamic Resistance
$r_s$	Surface Resistance
$R$	Gas Constant
$RH$	Relative Humidity
$RH_{min}$	Minimum Relative Humidity
$RH_{max}$	Maximum Relative Humidity

$R_i \downarrow$	Longwave Downward Radiation
$R_i \uparrow$	Longwave Upward Radiation
$R_n$	Net Radiation
$R_n$ daily	Daily Average Net Radiation
$R_n$ 24	Net Radiation per Day
$R_s$ daily	Daily Average Incoming Shortwave Radiation
$R_s$	Incoming Solar Radiation
$S$	Solar Declination
$T_a$	Air Temperature
$T_s$	Surface Air Temperature
$T_r$	Radiometric Temperature
$T_v$	Virtual Temperature
$u_z$	Wind Speed at Height $z_m$
$VI$	Vegetation Index
$VI-T_s$	Vegetation Index – Surface Temperature
$Z$	Elevation
$z_m$	Height of Wind Speed and Humidity Measurements
$z_{om}$	Roughness Lengths Governing the Transfer of Momentum
$z_{ov}$	Roughness Lengths Governing the Transfer of Water Vapour
$\alpha$	Surface Albedo
$\delta$	Solar Declination
$\epsilon_a$	Atmospheric Emissivity
$\epsilon_s$	Surface Emissivity
$\gamma$	Psychometric Constant

$\phi$	Priestley-Taylor Parameter
$\lambda E$ or $\lambda ET$	Latent Heat Flux
$\theta$	Solar Zenith Angle
$\theta_s$	Surface Potential Temperature
$\rho_a$	Mean Air Density
$\rho_w$	Density of Water
$\sigma$	Stefan-Boltzmann Constant
$\tau_{sw}$	Two-way Atmospheric Transmissivity
$\omega_s$	Sunset Hour Angle
$\psi$	Latitude of Each Pixel
$\Delta$	Slope of Saturation Vapour Pressure Curve
$\tau$	Fraction of Total Available Energy Absorbed by Soil Surface
$\beta$	Thermal Expansion Coefficient
$g$	Gravitational Acceleration
$Ri_B$	Richardson Number

## CHAPTER 1

### INTRODUCTION

---

#### 1.1 GENERAL

Evapotranspiration (ET) is the combination of two separate processes whereby water is transferred from land to atmosphere through evaporation from wet surfaces and by transpiration from vegetation. ET constitutes a major portion of the water balance and since it results in large amounts of water being removed from land it a major determinant of prevailing hydrological and climatic conditions of a given region/catchment. It is estimated that between 40-60% of annual precipitation is returned back to the atmosphere by ET. The ET process is extremely complex and is influenced by a large number of factors related to climate, surface/vegetation and soil moisture. In an effort to reduce the complexity, hydrologists and agronomists use the concept of Potential or Reference Crop Evapotranspiration ( $ET_0$ ).  $ET_0$  is the rate at which moisture removed is from a hypothetical green grass or alfalfa crop under existing climate when soil moisture supply is unlimited. Since  $ET_0$  is a function of climate, it may be computed using recorded climate variables. Standardized procedures (e.g., Allen et al., 1998) involving the use of crop/vegetation characteristics and soil moisture levels are available for converting  $ET_0$  values to the desired Actual Evapotranspiration (AET) rates.

AET is the rate at which water is actually removed from a given vegetated surface under existing climate when soil moisture supply is either unlimited or limited. Accordingly, it is evident that while  $ET_0$  is useful as an index of the atmospheric demand for moisture, in hydrological studies and water resources assessments, it is AET that must be characterized. While the total amount of water transferred to the atmosphere from a given land unit during a given period of time is denoted by AET and expressed in volume ( $m^3/\text{time}$ ) or depth ( $\text{mm}/\text{time}$ ) units, the instantaneous rate of water transfer is denoted as the latent heat flux ( $\lambda ET$ ) and expressed in units of  $W/m^2$ .

## 1.2 IMPORTANCE OF AET

Characterization of the spatial and temporal variabilities of AET from heterogeneous landscapes is essential in studies related to hydrology, climate, water resources engineering and management, and environmental impact assessments. AET rates from a given location in natural landscapes show reasonably conservative temporal variations dictated by variations in climatic variables and soil moisture levels. However, the spatial variations in AET from a heterogeneous catchment can be significant on account of differences in climate, vegetation and soil moisture. Because of this spatiotemporal variability, characterization of AET is crucial in a variety of hydrological studies.

In the limited water systems, spatial and temporal patterns of AET have significant impacts on streamflow variability and storm responses. Urbanization can affect the local water balance and AET patterns in numerous ways due to changes in land use/land cover (LULC). Replacing vegetation with impervious surfaces may decrease AET, as well as increasing storm runoff and annual stream flow. Prediction of AET rates will aid in better water allocation, estimation of water demand for agriculture, environmental impact assessments and watershed modeling.

## 1.3 MEASUREMENT OF AET

Hydrological, micrometeorological and plant physiological approaches are most commonly used AET measurement methods.

Hydrological approaches:

(1) Catchment/soil Water balance (2) Weighing or Drainage Lysimeters

Micrometeorological approaches:

(1) Energy balance and Bowen ratio (2) Aerodynamic method (3) Eddy covariance

Plant physiology approaches:

(1) Sap flow method (2) Chambers system

Each method has its limitations and drawbacks which result in no single method being acceptable under all conditions. Also, methods vary in terms of spatial coverage ranging from point-scale (lysimeters, plant physiological methods), landscape-scale



(eddy covariance flux towers) to catchment/regional-scale (water balance, energy balance). Routine and continuous use of direct measurement methods is expensive, cumbersome and requires regular monitoring. However, some of these methods are accurate and invariably used for calibration/validation of AET estimation methods. In the present study, eddy covariance flux tower measurements were used to validate the AET/ $\lambda$ ET estimation techniques developed.

## 1.4 ESTIMATION OF AET

Given the difficulties associated with direct measurement of AET, methods have been proposed for its estimation which may be classified as follows:

### 1.4.1 Indirect method

This approach seeks to estimate AET using a three step procedure – 1) computation of reference crop evapotranspiration ( $ET_0$ ) using available ground-based climate data 2) conversion of  $ET_0$  to crop evapotranspiration ( $ET_{crop}$ ) using a crop coefficient ( $K_c$ ) specific to the crop of interest and 3) reducing  $ET_{crop}$  to actual evapotranspiration ( $ET_a$ ) by accounting for the existing level of soil moisture availability. This popular indirect approach to estimation of AET has been standardized by the United Nations Food and Agriculture Organization (FAO) through a series of reports (Doorenbos and Pruitt, 1977; Doorenbos and Kassam, 1979; Allen et al., 1998). Although the focus of this method is on computing crop and irrigation water requirements for a wide variety of crops grown in different agroclimatic zones of the world, the same procedure is adopted in hydrological models too.

However, this method is highly data intensive and also upscaling AET estimates to regional/catchment scales in the presence of spatial heterogeneity in climate, crops and soils give rise to large uncertainties.

### 1.4.2 Direct methods

Attempts to estimate AET/ $\lambda$ ET directly with empirical to semi-empirical equations using regularly recorded ground-based climate data have been made. An example of this approach is application of the empirical radiation-based Priestley-Taylor (PT) equation (Priestley and Taylor, 1972). Although this equation has been widely used to

estimate PET by assuming a value of 1.26 for the coefficient in the equation ( $\phi$ ), attempts have been made to estimate AET instead by assuming that the coefficient varies with soil moisture levels (e.g., Mukammal and Neumann, 1977; De Bruin, 1983).

The Penman-Monteith (PM) equation (Monteith, 1965) has also been applied to estimate  $\lambda$ ET by computing the bulk surface/canopy and aerodynamic conductances from secondary data (e.g., Beven, 1979; McNaughton and Jarvis, 1983) and using routinely recorded climate records.

The Complementary Relationship approach is yet another direct method which provides estimates of regional AET using only routinely recorded climate data (e.g., Brutsaert and Stricker, 1979; Morton, 1983). The advantage of this approach is that it circumvents the need for data on vegetation and soils and yet provides reasonably accurate estimates of AET. However, this method cannot be applied in regions close to environmental discontinuities.

As with the indirect method, the PM and PT approaches when implemented using ground-based data suffer from the uncertainties inherent in upscaling point estimates to regional scales.

Energy Balance algorithms are based on the rationale that ET is a change of the state of water using available energy in the environment for vaporization. Remote sensing based energy balance algorithms converts satellite sensed radiances into land surface characteristics such as albedo, leaf area index, vegetation indices, surface roughness, surface emissivity, and surface temperature to estimate ET as a “residual” of the land surface energy balance equation. SEBAL approach is more complex which requires more data inputs compared to simple PM and PT approaches.

## 1.5 SATELLITE-BASED AET ESTIMATION APPROACHES

Efforts to upscale AET estimation approaches to spatially heterogeneous catchments have been made with varying degrees of success for the past few decades. Such efforts have benefited significantly with the advent of satellite remote sensing and Geographic Information System (GIS) techniques (Kustas and Norman, 1996; Patel et al., 2006; Gamage et al., 2011). In recent decades, several studies have demonstrated that the only feasible way to map ET over large spatial domains is through the use of satellite remote sensing imagery. Remote sensing provides temporal and spatial measurements of various surface biophysical variables which may be used to estimate ET (or latent heat flux  $\lambda ET$ ) using diverse methods (e.g. Anderson et al. 2008, Fisher et al. 2008, Glenn et al. 2007, Senay et al. 2007, Zhang et al. 2016). Satellite-based approaches to estimation of regional ET patterns have been aided by the free availability of data from sensors such as the Moderate Resolution Imaging Spectrometer (MODIS) and Landsat Thematic Mapper at reasonably fine spatial and temporal resolutions. Sensor measurements from various bands of the electromagnetic spectrum provide information on different surface characteristics of the landscape such as Normalized Difference Vegetation Index (NDVI), Leaf Area Index (LAI) and surface albedo from visible and near-infrared bands, and surface emissivity and Land Surface Temperature (LST) from mid and thermal infrared bands. The temporal and spatial variabilities of these characteristics are then used to compute variables and parameters involved in estimation of regional ET.

Remote sensing has been employed to develop practical evapotranspiration estimation methods. Remote sensing allows us to obtain regional land surface information easily and decreases the required manpower in field observations.

While residual methods can be applied over large spatial domains, they provide spatially averaged estimates of AET. On the other hand, the semi-empirical and empirical equations when applied with ground-based climate records provide only point estimates. Therefore, a major challenge in hydrology has been to develop methods that can map the spatial patterns of AET at regional/catchment scales. It is now recognized that the only feasible way to map AET over large spatial domains is

through use of satellite remote sensing technology and accordingly, numerous world-wide studies have focussed on the use of this technology. A detailed review of literature of such studies is included in the thesis. Remote sensing provides temporal and spatial measurements of various surface biophysical variables which may be used to estimate AET/ $\lambda$ ET. A large number of such previous efforts have attempted spatially distributed applications of the surface energy balance (SEB) using remote sensing inputs to derive regional AET patterns. However, it has been noted that this approach is complex and highly data-intensive.

Remote sensing methods are recognized as the only feasible means to map regional and mesoscale patterns of AET on the Earth's surface in a globally consistent and economically viable manner. Remote sensing technology offers several distinct advantages over ground-based direct point measurement:

1. It can deliver significant and constant spatial coverage.
2. It costs less than conventional ground-based approaches.
3. It is best suited for ungauged areas where ground-based measurements are not available.

Modeling AET is complex and direct measurement to the large basin scale is challenging. The only feasible way to map AET over the large spatial domain is remote sensing technology. Therefore, numerous studies have been carried out to estimate AET throughout the world using remote sensing imagery which is suitable and modest. Many efforts used attractive PM and PT empirical satellite-based approaches to estimate AET at regional scale patterns. Remote sensing provides various temporal and spatial measurements for global monitoring of surface biophysical variables affecting AET.

Remote sensing provides various temporal and spatial measurements for global monitoring of surface biophysical variables affecting AET (e.g. Anderson et al., 2008, Fisher et al., 2008, Glenn et al., 2007, Senay et al., 2007, Zhang et al., 2016). Satellite-derived inputs are used to derive the parameters related to the surface energy balance such as albedo ( $\alpha$ ), Normalized Difference Vegetation Index (NDVI),

Fraction of Vegetation (Fr) and Land Surface Temperature (LST) may be computed to characterize different characteristics of different LU/LC classes in a landscape. Numerous literature review studies shown that MODIS data products provide LU/LC characteristics information for estimating AET conveniently and cost-effectively (e.g., Cleugh et al., 2007; Leuning et al., 2008; Mu et al., 2007; Zhang et al., 2009). Therefore, abundant studies have been carried out to estimate AET throughout the world using remote sensing imagery which is suitable and modest (e.g., Allen et al., 2007; Ayenew, 2003; Garcia et al., 2013; Loukas et al., 2005; Scanlon et al., 2015; Yang et al., 2017; Zhang et al., 2009). Among them, PM and PT are attractive empirical approaches to estimate AET using ground-based point measurements (e.g., Sumner and Jacobs, 2005; Utset et al., 2004; Yao et al., 2013). Penman-Monteith (PM) and Priestley-Taylor (PT) are attractive empirical methods implementing to estimate evapotranspiration of a regional scale using satellite data products. Therefore, significant research has been invested in satellite-based applications of the simpler and less data-intensive PM and PT methods. This approach was adopted in the present study.

A review of previous work reported in the literature about the estimation of regional AET by empirical PM and PT models using satellite imagery data inputs along with few climatic data is presented in the next chapter.

## 1.6 STUDY OBJECTIVES

1. To evaluate the applicability of a MODIS-based Penman-Monteith (PM) model to estimate latent heat flux ( $\lambda$ ET) in humid tropical regions of south-east Asia
2. To explore the feasibility of using the trapezoidal scatter-plot of MODIS-derived land surface temperature (LST) versus fraction of vegetation (Fr) to estimate the bulk surface conductance parameter ( $G_s$ ) in the Penman-Monteith (PM) model

3. To evaluate the relative performances of the PM model with the MODIS-based Priestley-Taylor (PT) model and other similar models proposed by previous researchers using latent heat flux ( $\lambda$ ET) measurements made at flux towers located in different types of landscapes in south-east Asia
4. To develop a methodology for application of the validated PM and PT models to map spatial variability of daily AET in a tropical catchment and to evaluate model accuracies

### 1.7 SCOPE OF THE PRESENT STUDY

The current research work is aimed at the development, application and evaluation of methodologies for estimation of regional AET/ $\lambda$ ET by the PM and PT approaches using Moderate Resolution Imaging Spectrometer (MODIS) satellite imagery. While most previous studies have implemented these approaches to crop lands located in arid to semi-arid regions, the focus of the present study is to apply them to wet tropical regions possessing natural vegetation and evaluate their performances. The primary principle in satellite-based applications of the PT is based on pixel-based characterization of the PT parameter ( $\phi$ ) from a scatter plot of Land Surface Temperature (LST) versus Fraction of Vegetation (Fr). In the present study, the feasibility of extracting the bulk surface conductance ( $G_s$ ); an important parameter in the PM model, from a scatter plot of LST-Fr is explored. Also, few studies seemed to have compared the performances of the PM and the PT model and other similar models using the same dataset and therefore this exercise was taken up in the present study. Lastly, in previous studies validation of AET/ $\lambda$ ET estimates obtained from satellite-based PM/PT models have been achieved through comparisons with water balance or SEB estimates in some cases and with flux tower measurements in other cases. In the present study, after model validations with flux tower measurements, spatial AET estimates have been validated with the MODIS ET product – MOD16.

## 1.8 OVERALL METHODOLOGY

Based on a review of the literature, the PM and PT models were chosen due to its ease, data input requirements and reasonably good accuracy. The primary effort of the current research is to evaluate the applicability of a MODIS-based Penman-Monteith (PM) model to estimate latent heat flux ( $\lambda ET$ ) in humid tropical regions of south-east Asia and to explore the feasibility of using the trapezoidal scatter-plot of MODIS-derived land surface temperature (LST) versus fraction of vegetation (Fr) to estimate the bulk surface conductance parameter ( $G_s$ ) in the Penman-Monteith (PM) model. Relative performances of the PM model with the MODIS-based Priestley-Taylor (PT) model and other similar models proposed by previous researchers is to be evaluated using latent heat flux ( $\lambda ET$ ) measurements made at flux towers located in different types of landscapes in south-east Asia. Methodology for application of the validated PM and PT models to map spatial variability of daily AET in a tropical catchment and to evaluate model accuracies is to be developed. Since the river basin did not have sufficient ground-based climatic measurements, the AET models must be framed to use only satellite data. Also, no data on measured AET was available in the basin for the validation of developed PM and PT models. Therefore, the accuracy of the developed AET algorithms were tested using Asian flux towers data available in different types of landscapes. The validated algorithms are then applied to estimate pixel-wise AET values and to compare the results with MOD16A2 in the Hemavathi river sub-basin on selected days of summer and winter to understand seasonal variations in the years 2007 and 2012.

## 1.9 OUTLINE OF THE THESIS

This thesis includes seven chapters, list of references and additional annexures.

**Chapter 1:** The first chapter briefly introduces to the AET importance, components, measurement and estimation. Also, it describes the advanced knowledge which identifies the semi-empirical to empirical PM and PT methods of estimation of AET, advantages of spatial approaches using remote sensing imagery for AET estimation, study objectives and scope of the research methodology implemented.

**Chapter 2:** This chapter deals with the literature review for the estimation of AET using empirical attractive PM and PT methods using satellite imagery. This chapter also presents the relationship between the PT parameter and bulk surface resistance for modeling bulk surface conductance parameter and comparison of estimated AET by PM and PT approaches with MOD16A2.

**Chapter 3:** The chapter presents the study areas descriptions selected for the study. Detailed features of the flux tower sites and Hemavathi river sub-basin are provided, along with a description of ground based measurements data, flux towers data, satellite imagery and the softwares used for pre and post processing the data.

**Chapter 4:** This chapter describes the attractive PM and PT algorithms developed for the estimation of AET. Novel features incorporated in the algorithm like the estimation of surface conductance, alternative datasets for ground based measurements are highlighted.

**Chapter 5:** This chapter explains the application of the developed PM and PT algorithms to four flux tower sites for evaluating its accuracy by comparing the estimated latent heat flux values with measured by flux towers.

**Chapter 6:** In this chapter, the validated PM and PT models are later applied to the Hemavathi sub-basin to estimate AET and to compare the results with MOD16A2.

Finally, **Chapter 7:** Lists out conclusions, limitations and scope for future research work on this study topic.



## CHAPTER 2

### REVIEW OF LITERATURE

---

#### 2.1 GENERAL

In the previous section, as discussed there are several methods for estimating AET, but they are more data-intensive and difficult to estimate to a large basin scale. So, those methods are used for the validation purpose for other methods.

In recent times, numerous attempts have been made to estimate AET over various catchments through the application of the PM and PT approaches. Since these methods originated from direct point estimates of AET for homogeneous areas, but the implementation of same techniques to large scale heterogeneous catchment areas requires accurate spatial characterization of relevant input data. Many studies have shown that satellite data products provide land use and land cover characteristics information conveniently and cost-effectively. These remote sensing imagery based approaches integrated with ground-based measurement data can estimate more precise AET estimation.

Remote sensing methods provide various temporal and spatial measurements for global monitoring of surface biophysical variables affecting the AET. Hence the only feasible way to map AET over the large spatial domain is remote sensing technology since it is best suited even for ungauged areas where ground-based measurements were difficult. Abundant researches have shown to predict AET throughout the world using satellite data products that are appropriate and modest. Among them, the Penman-Monteith (PM) equation and the Priestley-Taylor (PT) equation are the most attractive methods for direct point estimates, but estimating in the large basin scale is challenging. According to the literature review done, satellite imagery with ground based measurements integrated with PM and PT approaches are the most commonly used methods for spatial mapping of AET.

An overview of the commonly applied PM and PT approaches for estimating AET using remotely sensed data and ground based measurements data is given in further

sections of this chapter to provide insight into the various methods for development and application of AET to a regional scale.

## 2.2 PENMAN-MONTEITH EQUATION

The Penman equation refers to evaporation ( $E$ ) from an open water surface which is developed by Howard Penman in 1948 by combining the energy balance with the mass transfer method. It requires daily mean temperature, wind speed, relative humidity, and solar radiation to predict  $E$ . Monteith (1965) replaced the wind function with the crop canopy and aerodynamic resistance to decrease the regional variation forming the Penman-Monteith (PM) method.

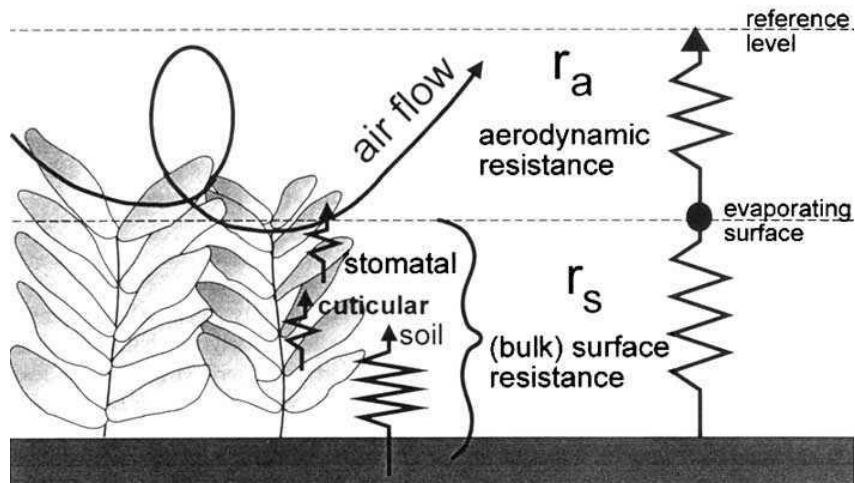


**Figure 2.1: Simplified representation of the (bulk) surface and aerodynamic resistances for water vapour flow (Source: Allen et al., 1998)**

Many researchers further developed the so-called Penman (1948) combination approach and extended to cropped surfaces by introducing aerodynamic resistance and surface resistance factors. Penman-Monteith equation is sensitive to vegetation parameters like stomatal resistance or conductance. The resistance of the vapor flow through stomatal openings and from total leaf area is known as the surface resistance ( $1/G_s$ ) (Fig. 2.1). The resistance of the vapor from the vegetation to flow upward and involves friction from air flowing over vegetative surfaces is known as the aerodynamic resistance ( $1/G_a$ ). The United Nations Food & Agriculture Organization (FAO) used

PM as a standard method for modeling evapotranspiration (Allen et al., 1998). The PM approach is a biophysically sound and strong framework for predicting AET at regional scales using satellite imagery.

The Penman-Monteith equation for latent heat flux estimation is given by;

$$\lambda ET_{PM} = \frac{\Delta(R_n - G) + \rho_a c_p \frac{(e_s - e_a)}{r_a}}{\Delta + \gamma \left[ 1 + \frac{r_s}{r_a} \right]} \quad (2.1)$$

Where,  $\lambda ET_{PM}$  = latent heat flux estimation by PM approach ( $W/m^2$ ),

$r_a$  = aerodynamic resistance (s/m),

$r_s$  = bulk surface resistance (s/m),

$R_n$  = net radiation of surface ( $W/m^2$ ),

$G$  = Soil heat flux ( $W/m^2$ ),

$\Delta$  = slope of saturated vapor pressure curve ( $kPa/^\circ C$ ),

$\gamma$  = psychrometric constant ( $kPa/^\circ C$ ),

$c_p$  = specific heat of moist air at constant pressure ( $MJ/kg/^\circ C$ ),

$\rho_a$  = mean density of air at constant pressure ( $kg/m^3$ ),

$D_a$  = vapor pressure deficit ( $e_s - e_a$ ) in which

$e_s$  = saturation vapor pressure (kPa) at air temperature and

$e_a$  = actual vapor pressure (kPa) at air temperature .

**Table 2.1: Review of the Penman-Monteith equation**

Author	Objective	Remarks
Cleugh et al., 2007	To develop a global model for monitoring AET	PM model satisfactorily estimated AET, but surface conductance model needs to be improved
Mu et al., 2007	To develop a global AET algorithm	Surface conductance model is improved by incorporating changes in the Cleugh et al., (2007) approach

		PM model yielded more accurate estimates of AET than Cleugh et al., (2007) approach
Leuning et al., 2008	To develop a simple surface conductance model to estimate AET	PM equation provided reliable estimates of evaporation rates Parameters $g_{sx}$ and $f$ are to be optimized
Zhang et al., 2009	To Improve rainfall-runoff modeling by remotely sensed AET	Calibrated the surface conductance model with mean annual ET inferred from runoff measurements and then using the calibrated model with the PM approach to map AET
Yuan et al., 2010	To estimate AET and gross primary production based on MODIS and global meteorology data	Yuan et al., (2010) modified Mu et al., (2007) model by calculating the $F_r$ using LAI instead of EVI and by adding air temperature constraint to stomatal conductance  Comparisons with observed GPP at flux towers showed a significant underestimation of ET and GPP due to lower net radiation of MERRA satellite dataset
Zhang et al., 2010	To parameterize surface conductances and calculate AET	Calibrated a Budyko curve-based hydrometeorological model by using gridded climate data to estimate grid-wise mean annual AET

		PM approach showed satisfactory agreement with high correlation values for estimating AET
Mu et al., 2011	To improve Mu et al., (2007) AET algorithm	Improved AET algorithm is the official global terrestrial MOD16 ET product PM model yielded more accurate estimates of AET than Mu et al., (2007) AET algorithm
Yebra et al., 2013	To estimate AET and canopy conductance by evaluating of optical remote sensing	Compared estimates of AET with six vegetation measures derived from the MODIS  Generated gridded and tabulated conductance data dominated by the canopy to facilitate the application of their results to a large scale AET estimation
Li et al., 2014	To examine the performance of the Mu et al., (2011) remote sensing PM model over various ecosystem types	Results indicated that the mean annual AET was ranging spatially between 484 and 521 mm/yr which is higher than the world average, with a mean value of 500 mm/yr
Autovino et al., 2016	To model bulk surface resistance by MODIS data and	Calibrated an empirical relationship between bulk surface resistance and MODIS-derived LST for an olive crop

	assessment of MOD16A2	Obtained reasonably accurate estimates of daily ET with the PM model
--	-----------------------	--

PM model despite being data and parameter intensive provides reasonably accurate estimates of AET and circumvents deficiencies inherent in the application of more elaborate surface energy balance schemes (e.g., Leuning et al., 2008; Mu et al., 2011). Numerous studies have successfully implemented the PM model using ground-based datasets and satellite imagery (e.g., Cleugh et al., 2007; Mu et al., 2007; Leuning et al., 2008; Zhang et al., 2009; Yuan et al., 2010; Zhang et al., 2010; Mu et al., 2011, Yebra et al., 2013; Li et al., 2014; Autovino et al., 2016). Significant research efforts have focused on scaling up stomatal/leaf-scale resistances to model bulk surface resistances which are required for regional AET estimation by the PM model (e.g., McNaughton and Jarvis 1983; Kelliher et al., 1995). Recent studies estimated AET by empirical approaches at regional to global scales have modeled the bulk surface conductance using satellite imagery data such as Leaf Area Index (LAI), Normalized Difference Vegetation Index (NDVI), fraction of vegetation cover, etc.

Cleugh et al., (2007) developed surface conductance model using a linear relationship with MODIS LAI data. Despite its simplicity, their model was able to estimate satisfactorily estimate the magnitude and seasonal variations of ET measured at two flux tower sites in Australia. Mu et al., (2007) developed an improved surface conductance model by incorporating a few changes in the approach proposed by Cleugh et al., (2007) significant among them being the inclusion of vapor pressure deficit and minimum air temperature constraints and the addition of a soil evaporation component. Validation at 19 flux tower sites in the USA indicated that their algorithm yielded more accurate estimates of PM ET. Leuning et al., (2008) introduced a simple biophysical model for surface conductance for use with MODIS derived Leaf Area Index (LAI) data and the PM ET model. The six parameters in the surface conductance model were optimized using measured daily mean ET at 15 flux tower sites located in different parts of the globe and they found that only two parameters representing maximum

stomatal conductance and ratio of soil evaporation to equilibrium evaporation were sensitive. Other parameters could be held constant without loss of much accuracy. Overall results showed that the Leuning et al., (2008) approach provided reasonably accurate estimates of daily mean ET at kilometre spatial scales. However, despite being biophysically-based, use of the Leuning et al., (2008) bulk conductance model with the PM equation requires optimization of model parameters using observed ET values. Their approach is data intensive and involves the use of six unknown parameters; associated uncertainties may constrain the accuracy of estimated ET values. Mu et al., (2011) introduced many modifications to Cleugh et al., (2007) Gs model and developed a MODIS-based global ET estimation algorithm that yielded extremely accurate ET estimates at 46 American flux tower sites. This algorithm was adopted to develop the MODIS evapotranspiration product (MOD16A2).

Previous researchers have demonstrated the applicability of the developed satellite-based PM models to derive ET estimates at the catchment or regional scales. Zhang et al., (2009) demonstrated how the Leuning et al., (2008) ) attempted refinements to the Leuning et al., (2008) Gs model approach which is applied at catchment-scale by first calibrating the surface conductance model with mean annual ET inferred from runoff measurements and then using the calibrated model with the PM approach to map ET in the Murray Darling Basin, Australia. Yuan et al., (2010) modified Mu et al., (2007) global evapotranspiration model by calculating the Fr using LAI instead of EVI and by adding of the constraint of air temperature to stomatal conductance. Comparison between estimated gross primary production (GPP) and simulated GPP from flux measurements showed that model performance differed significantly between ecosystem kinds. In general, most models performed better in estimating the temporal variations and magnitude of GPP analysis in deciduous broadleaf and mixed forests than in evergreen broadleaf forests and shrublands. Zhang et al., (2010) developed an operational procedure by combining a simple biophysical surface conductance model (Leuning et al., 2008) by using remotely sensed LAI data along with the PM equation approach to estimate surface conductance and ET for the entire Australian continent. Budyko-curve hydro meteorological model is the novelty of this paper to estimate mean

annual evaporation rates. PM approach showed satisfactory agreement with high correlation values between 8-day average evaporation rates. Mu et al., (2011) improved the 2007 PM approach by 1) calculating soil heat flux; 2) improving the methods to estimate stomatal conductance, aerodynamic resistance, and boundary layer resistance; 3) simplifying the calculation of vegetation cover fraction; 4) calculating ET as the sum of daytime and night-time components; 5) separating transpiration from the dry surface and evaporation from the wet canopy surface; and 6) separating actual evaporation from the moisture surface and potential evaporation from the saturated wet surface. This improved ET algorithm is the official MOD16 ET algorithm used to produce the official global terrestrial MOD16 ET product. Yebra et al., (2013) compared estimates of AET with six vegetation measures derived from the MODIS and three different approaches using measurements from flux towers at 16 FLUXNET sites located worldwide in various land cover types. Meteorological and flux data derived from flux towers as well as reflectances derived from MODIS were used to test three different approaches to estimate AET; (i) linear regression, (ii) PET scaling and (iii) PM conductance method. None of the three most successful methods were uniformly superior across all land cover types. Based on the mean of the three best methods, they generated gridded and tabulated conductance data dominated by the canopy to facilitate the application of their results to large scale AET estimation. They obtained average  $RMSE = 38 \text{ W m}^{-2}$  and  $R^2 = 0.72$  at 16 FLUXNET sites located worldwide in various land cover types. Li et al., (2014) examined the performance of the Mu et al., (2011) remote sensing PM model over various ecosystem types using ET measurement of 34 eddy covariance sites within China. Regional patterns of AET at a spatial resolution of  $10 \times 10 \text{ km}$  were measured using a Modern Era Retrospective-analysis for Research and Applications reanalysis products, meteorology dataset from 753 meteorological stations and satellite data such as the AVHRR LAI. Results indicated that the mean annual AET was ranging spatially between 484 and 521 mm/yr which is higher than the world average, with a mean value of 500 mm/yr, which accounted for approximately 5.6-8.3% of the world's total land-surface ET. Autovino et al., (2016) used flux tower measurements of ET in an irrigation district of Sicily and calibrated an



empirical relationship between bulk surface resistance ( $R_s$ ) and MODIS-derived LST for an olive crop.

### 2.3 PRIESTLEY-TAYLOR EQUATION

In the Penman-Monteith equation, the main uncertainty is the parameterization of the resistances. To avoid this problem, a simpler version to estimate AET is developed by Priestley and Taylor (1972). In the PT approach, they replaced the aerodynamic term formulation for radiation-based equilibrium conditions and atmospheric demand with a more straightforward empirical multiplier termed as PT coefficient ( $\phi$ ). This Empirical coefficient ( $\phi$ ) accounts for the water vapor entrainment as air moves over an extensive well-watered in the evaporating region. This equation is most suitable for estimating AET, which uses fewer ground-based data sets and providing reasonably accurate results.

The PT equation for latent heat flux estimation is given by:

$$\lambda ET_{PT} = \phi \left[ (R_n - G) \frac{\Delta}{\Delta + \gamma} \right] \quad (2.2)$$

Where,  $\lambda ET_{PT}$  = Latent heat flux estimation by PT approach ( $W/m^2$ ),

$\phi$  = Priestley-Taylor parameter,

$R_n$  = net radiation of surface ( $W/m^2$ ),

$G$  = Soil heat flux ( $W/m^2$ ),

$\Delta$  = slope of saturated vapor pressure curve ( $kPa/^\circ C$ ) and

$\gamma$  = psychrometric constant ( $kPa/^\circ C$ ).

**Table 2.2: Review of the Priestley-Taylor equation**

<b>Author</b>	<b>Objective</b>	<b>Remarks</b>
Goward et al., 1985	To develop a contextual information-based approach to estimate the $\phi$ using a pixel-wise scatter plot	Popularly known triangle or trapezoid method is first developed which showed realistic variations to moisture and temperature conditions
Jiang and Islam, 1999	To subsequently refine contextual information-based triangle method of the Goward et al., (1985)	Results showed consistent and realistic considering the complexity associated with the residual method for the estimation of spatially distributed latent heat flux
Jiang and Islam, 2001	To develop a simple triangular method (Jiang and Islam, 1999) to estimate surface evaporation over large heterogeneous areas using remote sensing data	Results are more reliable and easily applicable for operational estimation of evaporation over large areas where ground-based data are not readily available
Nishida et al., 2003	To develop an operational remote sensing algorithm of land surface evaporation by using trapezoid approach	Evaporative fraction product can capture variations of surface energy partitioning and water exchange which will help in several climatological and hydrological applications of remote sensing
Batra et al., 2006	To develop the LST–VI triangle method by using AVHRR data.	The proposed ET estimation algorithm, primarily driven by satellite data, appears to be robust

		and can produce spatially distributed ET map over large heterogeneous areas.
Wang et al., 2007	To estimated EF from a combination of day and night LST and NDVI	Results predicted AET under a wide range of soil moisture contents and different land use and land cover types
Hassan et al., 2007	To develop a wetness index by using MODIS LST and NDVI in the humid region	Results demonstrated a practical way to estimate the spatiotemporal variability in surface wetness conditions in a forest-dominated, topographically-diverse region
Ambast et al., 2008	To estimate AET by computing sensible heat and later to estimate AET	Results show that the change in mean sensible heat flux estimation is less than 5% and indicated the acceptability of the model against the uncertainties
Tang et al., 2010	To simplify PT formulation for estimating AET using only remotely sensed data	Proposed a novel method for accurate determination of dry and wet edges and results indicated that their approach was accurate for the estimation of regional AET
Tang et al., 2011	To refine further Tang et al., (2010) approach by applying in a semi-arid region	The triangular approach is best suited for arid or semi-arid regions since in humid region Fr values for some of the pixels are well above 0.8 would plot outside the right side of the triangular space

Yao et al., 2011	To develop a triangular VI method using albedo and fraction of vegetation cover from MODIS data	Results of estimated and observed ground-based measured ET data collected from the Yingke site showed good agreement between them
Laxmi and Nandagiri, 2014	To estimate PT parameter in a humid tropical region by using trapezoidal relationship	The novel methodology developed provided reasonably accurate estimates of latent heat flux at a humid tropical location
Wang et al., 2015	To estimate the PT parameter by combining LST and vegetation index (VI)	AET estimated to match the flux observations well, which indicates the effectiveness of the proposed method
Sun, 2016	To estimate evaporative fraction (EF) over a crop area by using the trapezoidal approach	Comparisons at six eddy covariance systems indicated that trapezoid approach is more effective at estimating EF and demonstrates the evolution of the LST/Fr space from the triangular to the trapezoidal form.

Numerous earlier PT model studies have shown that the use of satellite imagery is a simpler alternative to other more complex and data-intensive methods and yet provides reasonably accurate estimates of ET at kilometre spatial scales and daily time steps. However, as with the PM model, the challenge of implementing the PT model is to estimate the unknown model parameter ( $\phi$ ). Goward et al., (1985) were the first to propose a contextual information-based approach to estimate the PT parameter ( $\phi$ ) using a pixel-wise scatter plot of land surface temperature (LST) versus an appropriate

index of vegetation such as NDVI, Vegetation Index (VI) or fraction of vegetation (Fr). This approach, more popularly known as the triangle or trapezoid method, was subsequently refined and implemented by Jiang and Islam (1999, 2001) by plotting MODIS LST versus VI. Jiang and Islam (2001) proposed a simple method to estimate surface evaporation over large heterogeneous areas using remote sensing data. They modified the Priestley-Taylor parameter and enhanced the applicability over large heterogeneous areas. The Modified Priestley-Taylor parameter ( $\phi$ ) ranges from 0 to 1.26. They proposed a two-step interpolation scheme to estimate  $\phi$  from the dry and wet edges of the triangular space. They were shaped in a plot of pixel-wise values of LST versus corresponding values of vegetation index (VI) such as NDVI (Jiang and Islam, 1999) in the selected region. Nishida et al., (2003) developed an algorithm for estimating EF globally. EF is expressed as a ratio of AET to the available energy (sum of ET and sensible heat flux) using AVHRR data. They used vegetation index-surface temperature diagram for estimating EF from bare soil and vegetation. Remote sensing data is used for determining EF but flexible enough to ingest ancillary data when available. For the formulation of EF, they used the complementary relationship of the actual and the potential ET. Validation of the algorithm is done by using EF at AmeriFlux stations (standard error = 0.17 and  $R^2 = 0.71$ ). Batra et al., (2006) also demonstrated that the LST–VI triangle method could also be successfully applied using AVHRR data. The contextual approach has also been used to investigate vegetation features and for estimation of soil moisture. Wang et al., (2007) estimated EF from a combination of day and night land surface temperatures ( $T_s$ ) and normalized difference vegetation index (NDVI): a new method to determine the Priestley-Taylor parameter. Ground-based measurements were collected by Energy Balance Bowen Ratio systems located at the Southern Great Plains of the United States were analyzed to identify parameterization of EF. The modification of the Priestley-Taylor parameter by the Jiang and Islam (2001) enhanced the applicability of the Priestley-Taylor equation over large heterogeneous areas. Ambast et al., (2008) proposed and tested a remote sensing-based approach to estimate the sensible heat flux by combining with the local meteorological conditions, and in turn determined the regional evapotranspiration of Western Yamuna Canal system, India. They estimated the average ET for a well-watered wheat crop by

the proposed model as well as the Penman-Monteith equation, which indicated a difference of less than 10%. Results revealed that the percentage change in mean sensible heat flux for the image was less than 5%. Tang et al., (2010) applied the parameterization of Jiang and Islam (1999) in which a simplified PT formulation in which AET was estimated using only remotely sensed data. The PT parameter was estimated from the scatter plot of Ts (Land Surface Temperature) and VI (Vegetation Index) under conditions of full ranges of soil moisture availability and vegetation cover in arid and semi-arid regions. Parameter  $\phi$  was derived using a two-step interpolation scheme from the dry and wet edges in the Ts-VI triangular space. They proposed a novel method for accurate determination of dry and wet edges. Results indicated that their approach was accurate enough at least in most cases for the estimation of regional AET by showing RMSE of this comparison as 25.07 W/m<sup>2</sup>. Tang et al., (2011) further refined this approach and demonstrated its applicability in a semi-arid region of the USA. The triangular approach is best suited for arid or semi-arid regions since in humid region Fr values for some of the pixels are well above 0.8 would plot outside the right side of the triangular space (e.g., Hassan et al., 2007) and also in tropical regions, abundant vegetation may experience water stress. Yao et al., (2011) developed a triangular VI method using albedo of the reflectance bands and fraction of vegetation cover from MODIS data to estimate the PT parameter for AET estimation in arid and semi-arid regions. Evaporative fraction (EF) was first estimated using remote sensing imagery. The results of estimated and observed ground-based measured ET data collected from the Yingke site showed good agreement between them. The bias of estimated daily ET deviating from the corresponding ground-measured ET is -8.66 W/m<sup>2</sup> and the RMSE is 21.55 W/m<sup>2</sup>. Laxmi and Nandagiri (2014) estimated actual evapotranspiration (AET) by an approach based on the PT method using only MODIS satellite data products. A trapezoidal relationship was adopted to estimate PT parameter in forested regions in the humid tropical Mae Klong region, Thailand.  $\lambda$ ET estimates were estimated and validated with observed  $\lambda$ ET at a flux tower located in the area. Corresponding to the study area MODIS remote sensing satellite data products were used to inputs required by the PT approach. Comparison of estimated and measured fluxes in 2003 yielded root mean square error (RMSE) of 64.73 W/m<sup>2</sup> which reduced

to  $18.65 \text{ W/m}^2$  when one day was treated as an outlier because of instrument error. Wang et al., (2015) combined land surface temperature (LST) and vegetation index (VI) by using the trapezoidal relationship to estimate PT parameter in the PT equation. This approach mainly consists of: (1) construction of trapezoidal space between the LST versus VI for calculating the LST; (2) estimating the PT parameter for individual pixel using trapezoidal space with respect to the position of the observed at a point; (3) To estimate AET of each pixel using the PT equation. Estimated ET matches the observations of the Landsat-8 images and ground-based data for a semi-humid area in China well. Sun (2016) estimated evaporative fraction (EF) over a crop area in Yingke along the middle reaches of Heihe River Basin in China using a new interpretation of land surface temperature and fractional vegetation coverage (LST/Fr) space. In the triangular space, the fully vegetated surface temperature is assumed to be invariant, and bare soil surface temperature ( $T_s$ ) is variable. In the trapezoidal area, both  $T_v$  and  $T_s$  are assumed to vary simultaneously in the conventional trapezoid. To validate the rationality of the trapezoid model, the new SimSphere model is used to simulate the LST/Fr space. Simulations indicate that the trapezoid is more consistent with the simulated LST/Fr space. Comparisons at six eddy covariance systems showed that the trapezoid is more efficient at estimating EF than the conventional approach.

#### **2.4 RELATIONSHIP BETWEEN PT PARAMETER ( $\phi$ ) AND BULK SURFACE RESISTANCE ( $R_s$ )**

Several studies were conducted to estimate  $\phi$  using triangular and trapezoidal scattered plot approach (e.g., Jiang and Islam 1999, 2001; Nishida et al., 2003; Batra et al., 2006; Wang et al., 2007; Hassan et al., 2007; Tang et al., 2010; Yao et al., 2011; Laxmi and Nandagiri 2014; Sun, 2016). Modeling surface resistance ( $R_s$ ) parameter is difficult which uses complex ground-based measurements data. In developing countries like India, the computation of  $R_s$  using flux measurements is not available. Hence the main objective of the present study is to find the modest approach for modeling  $R_s$  parameter in a simple method which is similar to  $\phi$  estimation. So, literature review relating to the relationship between  $\phi$  and  $R_s$  is given below.

**Table 2.3: Review of the relationship between  $\phi$  and  $R_s$** 

<b>Author</b>	<b>Objective</b>	<b>Remarks</b>
De, 1983	To investigate the PT parameter model coupled to the PM equation as an extension	Found that under the conditions for a typical sunny summer day, surface resistance values showed good agreement with PT parameter for a bright summer day
Nemani and Running, 1989	To estimate surface resistance from NDVI and AVHRR Data	The slope of LST and NDVI provided a useful parameterization of surface resistance in regional AET research
McNaughton and Spriggs, 1989	To find relationship between the PT coefficient and $R_s$ by averaging the AET estimated rates	Calculations of PT values tend to be similar over a range of weather conditions and to vary only a small amount of surface resistance values from 0 to about 60 s/m only for water bodies and dense vegetation
Huntingford and Monteith, 1998	To derive the PT coefficient and $R_s$ from a convective boundary layer (CBL) approach developed by McNaughton and Spriggs (1989).	Results by running the CBL model multiple times demonstrated that the reciprocal of PT parameter increases almost linearly with surface resistance values
Pereira, 2004	To present evidence that the PT parameter can be set equal to the inverse of the McNaughton-Jarvis decoupling factor	The results showed that the PT parameter and decoupling factor ( $\omega$ ) relation exists almost linear.



Autovino et al., 2016	To find an empirical relationship between $R_s$ and MODIS-derived LST for an olive crop	Calibrated an empirical relationship between bulk surface resistance and MODIS-derived LST for an olive crop  Obtained reasonably accurate estimates of daily ET with the PM model
Amazirh et al., 2017	To model ET of irrigated wheat crops in Morocco by computing SI using LST	Subsequent implementation of the PM model with the calibrated $R_s$ -SI relationship provided spatial ET estimates with good accuracy
Er-Raki et al., 2018	To establish a relationship between $R_s$ and a Stress Index	The proposed approach has a great potential for detecting crop water stress and estimating crop water requirements by estimating $R_s$ over large areas along the agricultural season

In the present study, we pose the question as to whether the contextual information-based approach involving the use of a scatter plot between LST versus  $R_s$  can be used to estimate pixel-wise values of PM model bulk surface conductance ( $G_s$ ) like the estimation of the PT parameter ( $\phi$ ). Significant findings worthy of consideration in support of an answer to the above question are first, proof of a significant relationship between the slope of LST-NDVI plot and canopy resistance provided by Nemani and Running (1989). Secondly, studies have shown the existence of a relationship between the Priestley-Taylor (PT) parameter ( $\phi$ ) and surface resistance ( $R_s$ ). De (1983) investigated the PT parameter model using a simplified atmospheric boundary layer model coupled with the Penman-Monteith equation as an extension. In this approach, they combined an atmospheric boundary layer model with a more physically realistic

boundary layer sub-model concerning the dynamics. It was found that under the conditions for a typical sunny summer day, surface resistance values showed good agreement with PT parameter for a bright summer day in the Netherlands. Nemani and Running (1989) estimated surface resistance from NDVI and AVHRR Data. The slope of LST and NDVI provided a useful parameterization of surface resistance in regional AET research. McNaughton and Spriggs (1989) demonstrated the relationship between the calculated PT coefficient and surface resistance by averaging the evaporation rates over the simulated period of surface resistance ranging from 0 to 10000 s/m by using observed ground-based data inputs. Hence, they calculated the PT coefficient for a range of surface resistance values by using McNaughton-Jarvis decoupling factor. Calculations of PT values tend to be similar over a range of weather conditions and to vary only a small amount of surface resistance values from 0 to about 60 s/m only for water bodies and dense vegetation. Huntingford and Monteith (1998) derived the PT coefficient from a convective boundary layer (CBL) developed by McNaughton and Spriggs (1989). They used a control set of driving environment conditions to run the full CBL model. The numerical code of CBL model was run for twenty surface resistance values ranging from 10 to 200 s/m corresponding to well waters to moderately stressed vegetation. Results by running the CBL model multiple times demonstrated that the reciprocal of the PT parameter increases almost linearly with surface resistance values. Pereira (2004) presented evidence that the PT parameter can be set equal to the inverse of the McNaughton-Jarvis decoupling factor by using two extensive data sets of daily lysimetric measurements of reference ET under climatic conditions ranging from humid tropical to semi-arid. This approach does not require any calibrations for the PT parameter since several statistical measures to indicate a good alternative to the PM with the parameterization scheme. The results showed that the PT parameter and decoupling factor ( $\omega$ ) relation exists almost linear. More recent studies have tried to establish empirical relationships between the PM model bulk surface resistance ( $R_s$ ) and LST. Autovino et al., (2016) used flux tower measurements of ET in an irrigation district of Sicily and calibrated an empirical relationship between bulk surface resistance ( $R_s$ ) and MODIS-derived LST for an olive crop. They obtained reasonably accurate estimates of daily ET with the PM model.

Using eddy covariance and ground-based measurements in an orange orchard in Morocco, Er-Raki et al., (2018) established a two-part relationship between  $R_s$  and a Stress Index (SI) which was derived from LST measured using infrared thermometers. Interestingly, the computation of SI involved the use of minimum (wet) and maximum (dry) LST values (end members) and provided PM ET estimates with less than 20% error. Amazirh et al., (2017) used a similar approach to model ET of irrigated wheat crops in Morocco but computed SI using Landsat-derived LST values. The end members were simulated using a surface energy balance model and subsequent implementation of the PM model with the calibrated  $R_s$ -SI relationship provided spatial ET estimates with good accuracy. These studies provide sufficient justification and the basis for pursuing the idea of estimating  $G_s$  from a scatter plot of LST-VI further.

## **2.5 COMPARISON OF SPATIAL AET ESTIMATES WITH MOD16A2**

As already discussed in the previous chapters that in developing countries like India, computation of AET using ground-based climate measurements is hampered by non-availability of flux towers and accurate ground-based measurements. Integration of both the ground-based climatic data and the satellite-based inputs would provide spatially distributed estimates of evapotranspiration. Due to non-availability of ground-based measurements, the estimated spatial pixel-wise AET values by PM and PT approaches are compared with MOD16A2 to check performance measures. Mu et al., (2011) introduced many modifications for Mu et al., (2007) approach and developed a MODIS-based global ET estimation algorithm that yielded extremely accurate ET estimates at 46 American flux tower sites. This algorithm was adopted to develop the MODIS evapotranspiration product (MOD16A2). So, literature review relating to spatial pixel-wise AET estimates comparison with MOD16A2 are presented.

**Table 2.4: Review of the comparison of spatial AET estimates with MOD16A2**

Author	Objective	Remarks
Ruhoff et al., 2013	To estimate AET over vegetated surfaces by using ground-based measurements of fluxes obtained from eddy covariance sites	Comparison between 8-day average MOD16A2 estimates and flux tower measurements yielded $R^2$ of 0.78 to 0.81, mean RMSE of 0.78 and 0.46 mm/day
Cherif et al., 2015	To improve the accuracy of estimating AET by using raster meteorological data	Results were compared with MOD16A2, attaining $R^2$ of 0.61 and an RMSE of 0.92 mm/day.
Autovino et al., 2016	To estimate AET by using PM approach by modeling $R_s$	Comparison between MOD16A2 and the proposed PM approach showed that MOD16A2 overestimated AET by reporting mean RMSE of 0.83 mm/day
Ke et al., 2017	To proposed spatial-temporal fusion (STF)-integrated approach in order to generate AET based spatial estimates	Results showed that fusion of Landsat VIs produced the best accuracy of predicted AET ( $R^2 = 0.52-0.97$ , RMSE = 0.47–3.0 mm/8 days when compared with MOD16A2

Ruhoff et al., (2013) estimated AET over vegetated land surfaces by using ground-based measurements of energy fluxes obtained from eddy covariance sites installed in tropical biomes and from a hydrological model (MGB-IPH) were used to validate MOD16 products at local and regional scales. Later examined the accuracy of the MOD16A2 algorithm at the sugar-cane plantation and natural savannah vegetation. Comparison between 8-day average MOD16A2 estimates and flux tower

measurements yielded  $R^2$  of 0.78 to 0.81, mean RMSE of 0.78 and 0.46 mm/day, at PDG and USE, respectively. Cherif et al., (2015) improved the accuracy of estimating AET by using raster meteorological data integrated with remotely sensed energy balance model to achieve time series of Terra Moderate Resolution Imaging Spectroradiometer (MODIS) satellite images and results were compared with MOD16A2, attaining  $R^2$  of 0.61 and an RMSE of 0.92 mm/day. Autovino et al., (2016) estimated daily AET by using PM approach, where the surface resistance term was computed by using MODIS Land Surface Temperature (LST). The model was then later validated by an independent database collected over four different years. The estimated AET by PM model was later compared with measured AET fluxes showed a mean RMSE of 0.52 mm/day. Also, the comparison between MOD16A2 and the proposed PM approach showed that MOD16A2 overestimated AET by reporting mean RMSE of 0.83 mm/day. Ke et al., (2017) proposed machine learning and spatial-temporal fusion (STF)-integrated approach in order to generate AET based spatial estimates with three schemes. Results showed that fusion of Landsat VIs produced the best accuracy of predicted AET ( $R^2 = 0.52-0.97$ , RMSE = 0.47–3.0 mm/8 days when compared with MOD16A2. The downscaled 30 m AET had good agreement with MOD16A2 (RMSE = 0.42–3.4 mm/8 days).

## 2.6 SUMMARY

Review of the literature is evident that several studies have been undertaken for modeling regional evapotranspiration. Most commonly used algorithms are Penman-Monteith and Priestley-Taylor equations. These research studies have adopted different methods, satellites, algorithm structures, methodology and spatial scales. However, no standardized procedure seems to be available with researchers to estimate AET using equations. The present research is to use Penman-Monteith and Priestley-Taylor equations for estimating actual evapotranspiration. The most critical issues concerning

implementing a trapezoidal based method to estimate bulk surface conductance in the PM model for regional AET estimation may be summarized as follows:

1. Numerous studies shown the existence of a relationship between the Priestley-Taylor (PT) parameter ( $\phi$ ) and bulk surface resistance ( $R_s$ ) (e.g., De, 1983; Nemani and Running, 1989; McNaughton and Spriggs 1989; Huntingford and Monteith 1998; Pereira 2004; Autovino et al., 2016; Amazirh et al., 2017; Er-Raki et al., 2018).
2. Even though numerous studies were conducted to improve and simplify the estimation of  $\phi$  using triangular and trapezoidal scattered plot approach (e.g., Jiang and Islam 1999, 2001; Nishida et al., 2003; Batra et al., 2006; Wang et al., 2007; Hassan et al., 2007; Tang et al., 2010; Yao et al., 2011; Laxmi and Nandagiri 2014; Sun, 2016).
3. Scatter plots in a trapezoidal than the triangular shape of LST versus  $F_r$  are best suited for heterogeneous landscapes which are more representative of the relative proportions of soil and vegetation (Laxmi and Nandagiri 2014).
4. However, an important issue that remains completely unresolved is the way such spatial AET estimates should be validated in the data scarcity region. So, AET estimates derived from PM and PT methods are compared with MOD16A2 to evaluate the relative performances after validating the PM and PT algorithms by using flux tower observations in different types of landscapes of Asia Flux Network.

## CHAPTER 3

### STUDY AREAS AND DATA USED

---

---

#### 3.1 STUDY AREAS

In order to achieve the objectives of this study, two study areas were considered. For the purpose of validating  $\lambda$ ET values obtained by the PM model and also for relative comparisons with other models, four AsiaFlux tower sites located in different countries of tropical south-east Asia were selected based on certain specific criteria. For the validation purpose, since the basin did not possess ground-based measurements of AET required for validation purposes, the PM and PT approaches were validated using Asia Flux network ([asiaflux.net](http://asiaflux.net)) of Asia. The data from flux sites Mae Klong (MKL), Palangkaraya drained forest (PDF), IRRI Flux Research Site (IRI) and Sakaerat (SKR) were used which are located in different types of landscapes. Measured latent heat flux data from the flux towers were used to validate the developed PM and PT AET algorithms and subsequently applied to the Hemavathi sub-basin. In order to demonstrate the applicability of the methodology for spatial mapping of daily AET using the PM and PT models, a sub-basin in the Hemavathi catchment located in the Cauvery River Basin in Karnataka State, India was selected. Complete descriptions of the physical, climatic and topographic characteristics of the study areas, data related to meteorology and satellite imagery are presented in this chapter.

#### 3.2 FLUX TOWER SITES

AsiaFlux (<http://asiaflux.net>) comprises a network of 36 flux towers located in different countries of South Asia which have been installed to measure exchanges of carbon dioxide, water vapor, and energy. In this study, four flux tower sites which are part of this network were selected for validation of PM and PT approaches. The data for validation from four flux sites Mae Klong (MKL), Palangkaraya drained forest (PDF), IRRI Flux Research Site (IRI) and Sakaerat (SKR).  $\lambda$ ET is measured using the eddy covariance technique. The radiometer is used to measure net radiation ( $R_n$ ), and platinum resistance thermometer is used to measure air temperature. An area of 25

km<sup>2</sup> surrounding the flux tower was considered for the analysis. Considering a 5 km × 5 km area centred on each flux tower site (Table 3.1), corresponding satellite imagery were downloaded for the selected dates.

The requirement constrained the selection of sites that flux measurements should be available on clear-sky days when cloud-free MODIS imagery for the regions was also available. Additionally, an effort was also made to select sites which provided measured data on days representing different seasons (summer, monsoon, and winter). Table 3.1 provides details of climate, mean annual temperature, mean annual rainfall, vegetation type, position, terrain type, measurement height and location of the selected flux tower sites. Except for one flux tower which is located in paddy fields (IRI) the others are located in forested areas. At all sites, water vapor flux is measured using the eddy covariance technique at a sampling frequency of 4 Hz or 10 Hz and averaging time of 30 mins or 60 mins. Complete details of the instrumentation at each site are provided at <http://asiaflux.net>.

Recorded measurements pertaining to climatic variables and latent heat flux were downloaded for each selected date for the four flux sites from the Asia Flux database ([https://db.cger.nies.go.jp/asiafluxdb/?page\\_id=16](https://db.cger.nies.go.jp/asiafluxdb/?page_id=16)). For each date, climate variables and flux values were extracted for the averaging period corresponding to satellite overpass at the site (Table 3.1) to enable comparisons of measured and estimated values of instantaneous latent heat flux. In a few instances, the next nearest averaging period had to be considered due to missing data or erroneous measurements. Measured values of  $R_n$ ,  $G$ , air temperature ( $T$ ), and relative humidity (RH) are used for implementation of Equation (4.1 and 4.2). Since measured values of  $G$  were available only at the MKL and PDF sites,  $G$  was estimated using a function proposed by Bastiaanssen (2000) at the other two sites.



**Table 3.1: Details of selected flux tower sites in south-east Asia**

Attribute code	MKL	PDF	IRI	SKR
Climate	Monsoon	Tropics	Tropical	Tropical-desert
Mean annual air temperature (°C)	25	26.3	27.5	24
Mean annual precipitation (mm)	1500	2231	2075	1300
Vegetation type	Tropical seasonal deciduous forest	Tropical evergreen forest	Rice	Tropical seasonal evergreen forest
Position	14° 34' 34.6" N, 98° 50' 38.0" E	02° 20' 42" S, 114° 02' 11" E	14° 08' 42.11" N, 121° 15' 39.38" E	14° 29' 32.5" N, 101° 54' 58.7" E
Elevation (m)	231	30	21	543
Terrain type	On the ridge	Flat	Flat agricultural land	Approximately flat
Measurement height ( $z_m$ ) (m)	42	41	2.25	45
Canopy height (h) (m)	30	26	1	35
Location	Watershed Research Station, Thailand.	Central Kalimantan, Indonesia.	Los Banos, Laguna, Philippines.	Nakonrachasima, Thailand.
Satellite overpass time (hour)	11.15	11.00	11.30	11.15

### 3.3 HEMAVATHI CATCHMENT

The Hemavathi catchment (Figure 3.1) is part of the Upper Cauvery River Basin, Karnataka, India. A sub-basin in the catchment which lies between 13°03'30" to 13°18'30" North latitudes and 75°43'30" to 75°59'45" East longitudes with a catchment area 304 km<sup>2</sup> was considered. The annual rainfall in the Hemavathi catchment varies from a maximum of 1725 mm to a minimum of 692 mm with an average annual rainfall of 1222 mm. The catchment area is a typical example of a tropical monsoon type of climate with June-October being the rainy season. The area under study is a hilly catchment with steep to moderate slope. The slope is very high in the upper reaches and reduces gradually in the lower reaches. The general elevation of the basin ranges from 748 m to 1853 m above mean sea level. The entire basin may be

classified as hilly lands, moderately sloping and low lands (valley lands). The LU/LC in the basin is mainly comprised of agricultural land and plantations/orchards.

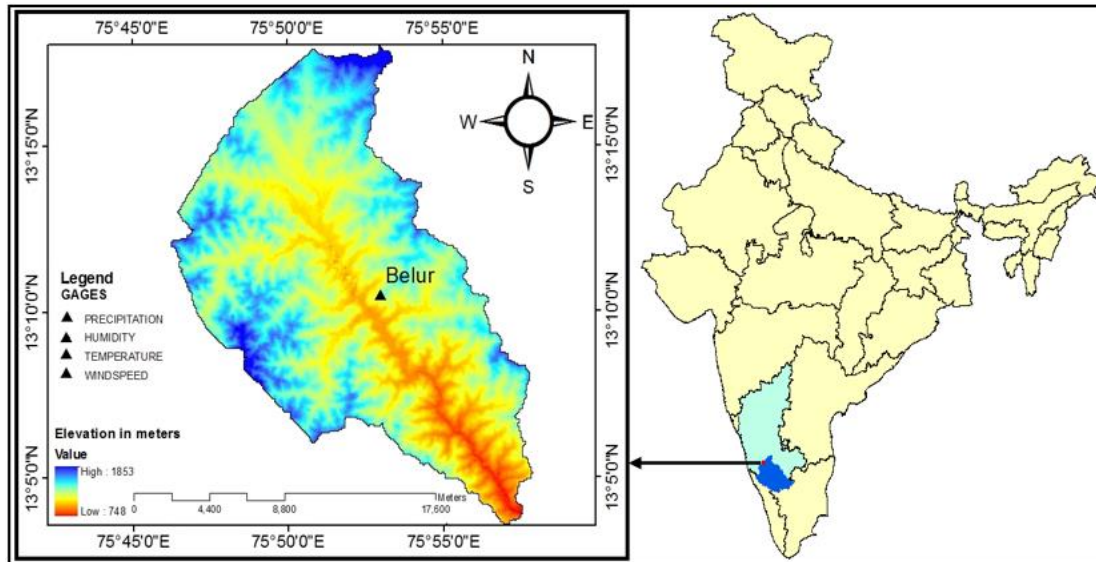


**Figure 3.1: Location map and DEM of Hemavathi catchment sub-basin**

### 3.4 DATA PREPARATION

Satellite data and meteorological data are used for AET estimation which are obtained from relevant agencies and websites.

#### 3.4.1 Satellite data acquisition

In this study, data from the MODIS sensor are used. MODIS is an earth-viewing sensor that is mounted on the Earth Observing Systems, namely Terra and Aqua satellites, which were launched in December 1999 and May 2002 respectively. MODIS has a swath of 2330 km (cross-track) by 10 km (a long-track at nadir). It scans the earth from a polar-orbiting sun-synchronous platform at an altitude of 705 km. All images captured by MODIS are in the sinusoidal projection. The MODIS data are provided in the HDF - EOS format (Hierarchical Data Format-Earth Observing System format) developed by the National Centre for Supercomputing Applications (NSCA). According to NASA (National Aeronautics and Space Administration) policies, the processed MODIS data are freely available. Details of MODIS band specifications are available at [https://lpdaac.usgs.gov/products/modis\\_products\\_table](https://lpdaac.usgs.gov/products/modis_products_table).

### 3.4.2 MODIS satellite data products

MODIS data products of MOD11A1 product of Land Surface Temperature (LST) at 1000 m resolution, MOD09GA product of Land Surface Reflectance (LSR) at 1000 m resolution, MOD15A2 product of Leaf Area Index (LAI) as eight days average composited at 1000 m resolution, MOD16A2 product of actual evapotranspiration (AET) as eight day average composited at 500 m resolution, MCD12Q1 product of Land Cover Type and Digital Elevation Model (DEM) at 30 m resolution were used in the present study. Preliminary processing of images was performed using MODIS reprojection tool (MRT) and was converted to a standard format that can be read by MATLAB software. Geo-referencing, subsetting and pixel-wise analysis corresponding to the study area were performed using ArcGIS and ERDAS IMAGINE. Considering a 5 km × 5 km area centered on each flux tower site (Table 3.1), corresponding MOD11A1, MOD15A2 and MOD09GA products were downloaded for the selected dates. The MCD12Q1 product was resampled to 1000 m resolution and ground elevations for each MODIS pixel were derived for each flux tower study area. Similarly, all the MODIS products were prepared for 1000 m resolution for the selected dates of modeling for the Hemavathi sub-basin (Figure 3.1).

### 3.4.3 Meteorological data

Daily ground-based measurements of rainfall, temperature, relative humidity, wind speed and sunshine hours for the Belur climate station located in the Hemavathi sub-basin were used for AET estimation. Data was obtained from India Meteorological Department (IMD) and Agricultural Department, Mangalore.

Upon examination of rainfall records of the recent past (2006 - 2013), it was found that year 2012 experienced rainfall significantly less than the normal and 2007 was an above than the normal. Rainfall records of the rain gauges for the years from 2006 to 2013 are shown in Table 3.2 from which it is clear that 2012 is a relatively dry year and 2007 is a relatively wet year. Therefore, these two years were selected to evaluate inter-annual differences in LU/LC characteristics as influenced by rainfall regime.

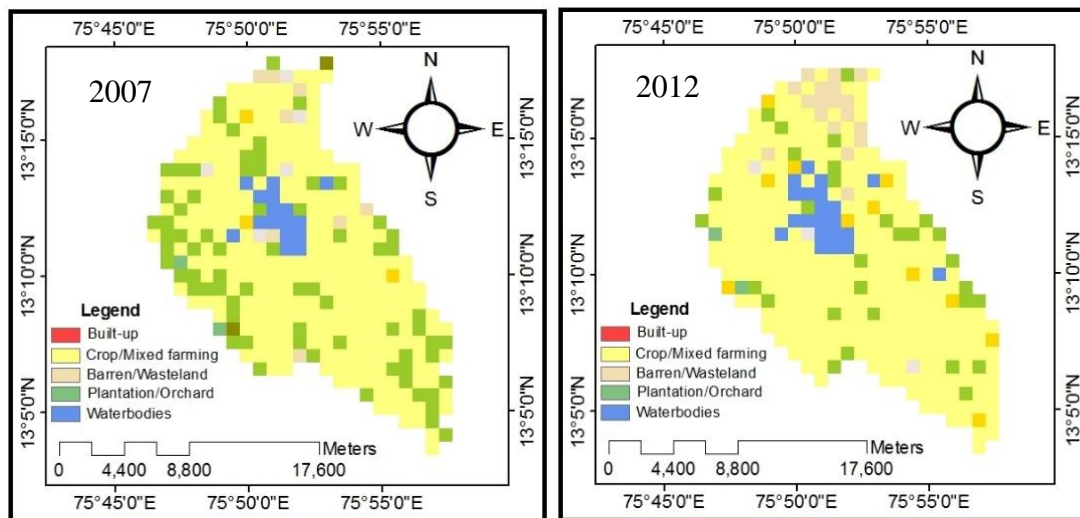
**Table 3.2: Annual rainfall totals (mm) for Belur rain gauge**

Year	2006	2007	2008	2009	2010	2011	2012	2013	Average=
Rainfall (mm)	1423	1725	1251	1350	1235	1088	692	1012	1222

For the analysis two dates of 2007 and 2012, two corresponding to the summer season (pre-monsoon) and two corresponding to the winter season (post-monsoon) were selected to evaluate intra-annual differences in vegetation characteristics as influenced by season.

### 3.4.4 Land Use/Land Cover (LU/LC) Map

LU/LC maps for the Hemavathi sub-basin for the years 2007 and 2012 were downloaded from Bhuvan - Thematic services website. The data used in the present study is of scale 1:250000 derived from Resourcesat-1 satellite's Linear Imaging Self-scanning Sensor LISS - III data. This data consists of 19 classes (2<sup>nd</sup> level), but only five classes were found in the Hemavathi river sub-basin. The derived LU/LC maps for the Hemavathi sub-basin are shown in Figure (3.2). It was found that crops and Plantation/Orchard are the predominant class in the Hemavathi river basin.

**Figure 3.2: LU/LC map of the Hemavathi sub-basin**

**Table 3.3: LU/LC class composition in the Hemavathi sub-basin**

LU/LC Class	Year 2007		Year 2012	
	% of total pixels	Area (km <sup>2</sup> )/ No. of pixels	% of total pixels	Area (km <sup>2</sup> )/ No. of pixels
<b>Crop/Mixed farming</b>	83	252	82	249
<b>Plantation/Orchard</b>	7	21	7	20
<b>Barren/Wasteland</b>	4	11	5	16
<b>Built-up</b>	1	3	2	5
<b>Waterbodies</b>	6	17	5	14
<b>Total</b>	100	<b>304</b>	100	<b>304</b>

### 3.4.5 Preprocessing and Software used

Preliminary processing of images was performed using MODIS reprojection tool (MRT) and was converted to a standard format that can be read by MATLAB software. Geo-referencing, subsetting and pixel-wise analysis corresponding to the study area were performed using ArcGIS and ERDAS IMAGINE. The MODIS images were resampled to 1000 m resolution and ground elevations for each MODIS pixel were derived for the study area. Pixel-wise calculations using all the above necessary equations for each date of acquired MODIS images were carried out using MATLAB software.

## CHAPTER 4

## METHODOLOGY FOR ESTIMATION OF AET

## 4.1 GENERAL

From the previous research studies, it is obvious that numerous studies have been undertaken for modeling regional AET by different methods. PM and PT models are evidenced to be more attractive because of modest which requires available satellite data inputs along with few ground based inputs by providing reasonably accurate estimates of AET. Hence the present research work aims to concentrate on the modest PM and PT approaches to estimate AET by using data inferred from MODIS satellite imagery. PM and PT approaches are validated using flux towers data of Asia network, then applied to map AET in a Sub-humid tropical Hemavathi sub-basin, Karnataka. In an effort to compare the accuracies of  $\lambda$ ET values obtained with the PM model approach proposed in the present study with other similar satellite-based approaches suggested by previous researchers, the following three methods were implemented with the same data set: 1) the Priestley-Taylor model with MODIS-derived LST-Fr trapezoidal scatter plots proposed by Laxmi and Nandagiri (2014) – hereinafter referred to as PT approach ( $\lambda$ ET<sub>PT</sub>) 2) the Cleugh et al. (2007) model in which G<sub>s</sub> is obtained using a simple relationship with LAI and used with the PM model – hereinafter referred to as PMC approach ( $\lambda$ ET<sub>PMC</sub>) and 3) the Leuning et al. (2008) model in which a biophysical approach is used to estimate G<sub>s</sub> for use with the PM model – hereinafter referred to as PML approach ( $\lambda$ ET<sub>PMC</sub>).

As regards modeling spatial AET patterns in the Hemavathi sub-basin, only the PM model approach proposed in the present study, a modified form of this method and the PT approach were implemented and validated using MOD16A2 ET product.

The primary structures of the methods adopted in this study are as follows.

1. This chapter provides a complete description of the methodology of the proposed algorithms which shows new simple, attractive features for estimating AET.

2.  $G_s$  parameter in PM model and  $\phi$  in the PT model are derived from trapezoidal scatter plots of LST versus  $F_r$ .
3. The developed PM and PT methods for AET estimation are validated using Asia flux towers data from sites located in different types of landscapes.
4. The validated PM and PT algorithms are then applied to map AET in a Sub-humid tropical Hemavathi sub-basin, Karnataka.

## 4.2 METHODOLOGY OF PENMAN-MONTEITH APPROACH

Standard procedures available in literature were used to convert remote sensing data and climate data into parameters/variables which appear in Eq. (4.1). Fig. (4.1) depicts the flow chart of steps involved in application of the PM model proposed in the present study to derive estimates of  $\lambda ET$  and AET using inputs from MODIS imagery and climate data. While the developed model provided output of  $\lambda ET$  for comparisons with flux tower measurements, AET values were estimated when the model was applied to the Hemavathi sub-basin. MATLAB<sup>®</sup> codes were developed for implementation. Step by step procedure is shown in a flowchart (Figure 4.1 and 4.2), followed by a description of the parameters and relevant equations involved in the estimation of AET by PM and PT approaches.

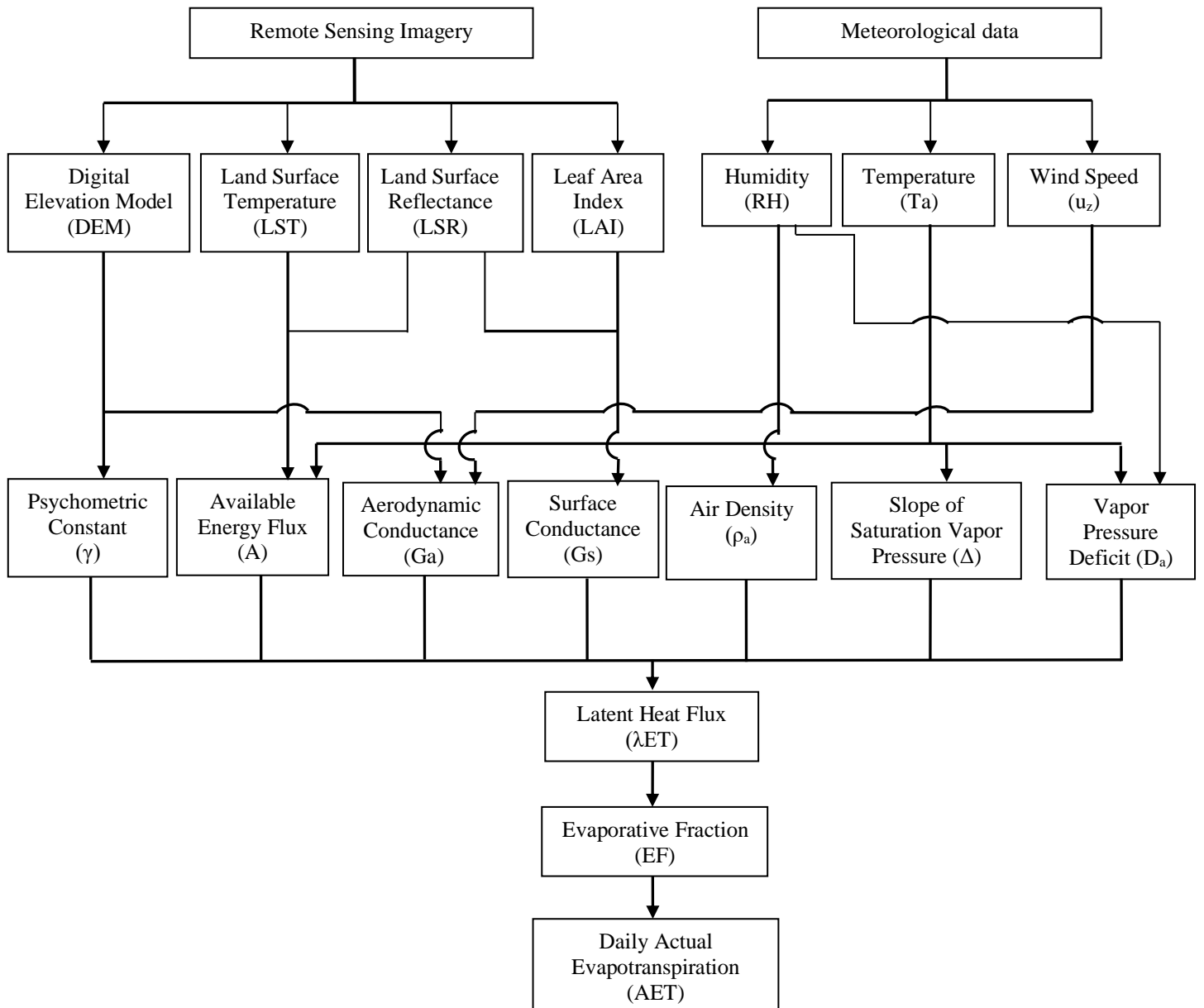


**Figure 4.1: Flowchart depicting the steps involved in the estimation of AET by the Penman-Monteith method**



### 4.3 METHODOLOGY OF PRIESTLEY-TAYLOR APPROACH

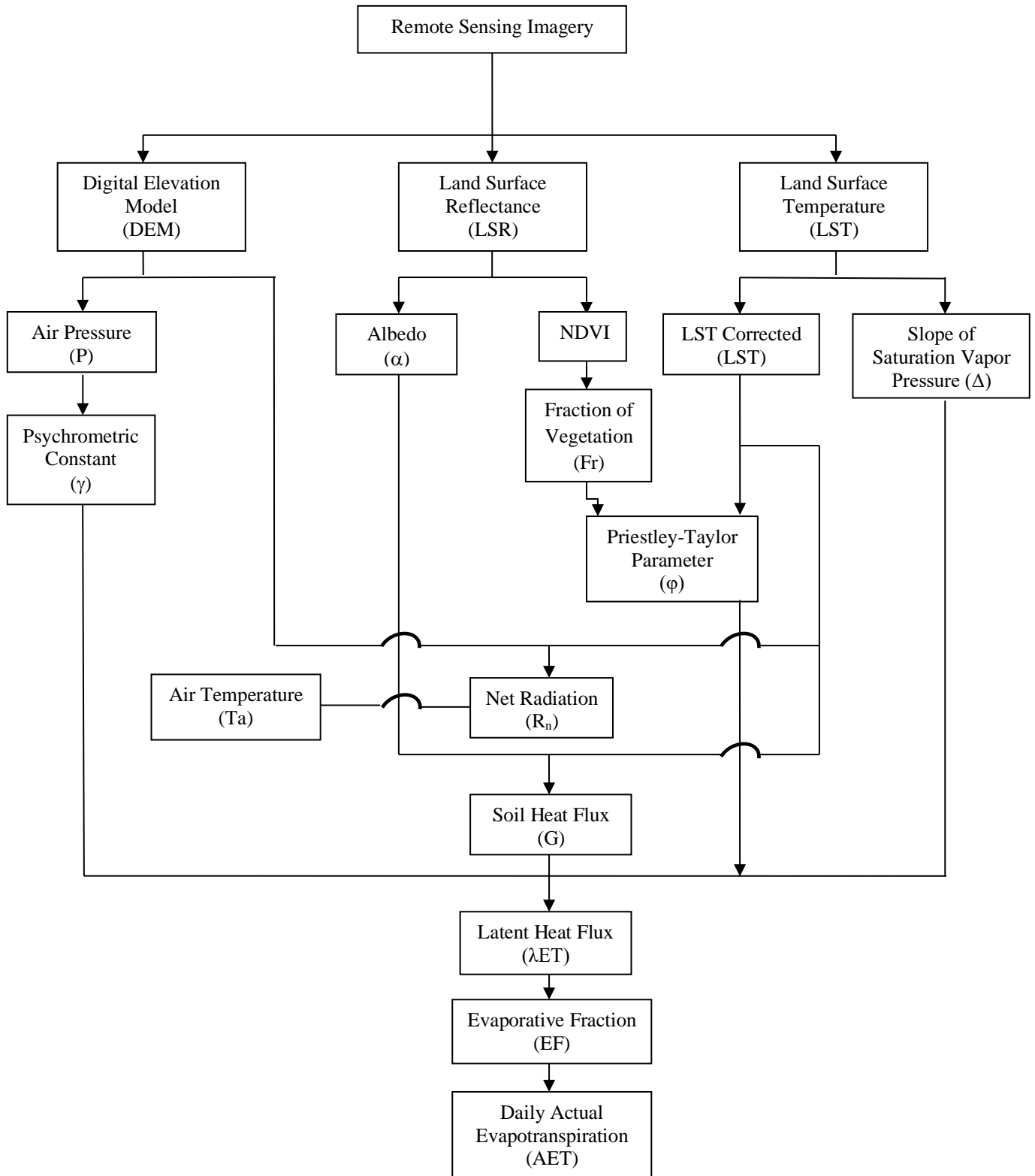


**Figure 4.2: Flowchart depicting the steps involved in the estimation of AET by Priestley-Taylor method**

#### 4.4 COMPUTATION OF VARIABLES IN PM AND PT EQUATIONS

The Penman-Monteith equation is briefly discussed with literature review in Article 2.2 (Chapter 2). The mathematical expression of latent heat flux ( $\lambda ET$ ) by the PM model is given by Equation (2.1) which can be rewritten as:

$$\lambda ET_{PM} = \frac{\frac{\Delta}{\gamma}(R_n - G) + \left(\frac{\rho_a c_p}{\gamma}\right) D_a Ga}{\frac{\Delta}{\gamma} + 1 + \frac{Ga}{Gs}} \quad (4.1)$$

Where,  $\lambda ET_{PM}$  = latent heat flux estimation by PM approach ( $W/m^2$ ),

$Ga$  = aerodynamic conductance ( $m/s$ ) =  $1/r_a$ ,

$Gs$  = bulk surface conductance ( $m/s$ ) =  $1/r_s$ ,

$R_n$  = net radiation of surface ( $W/m^2$ ),

$G$  = Soil heat flux ( $W/m^2$ ),

$\Delta$  = slope of saturated vapor pressure curve ( $kPa/^\circ C$ ),

$\gamma$  = psychrometric constant ( $kPa/^\circ C$ ),

$c_p$  = specific heat of moist air at constant pressure ( $MJ/kg/^\circ C$ ),

$\rho_a$  = mean density of air at constant pressure ( $kg/m^3$ ),

$D_a$  = vapor pressure deficit ( $e_s - e_a$ ) in which

$e_s$  = saturation vapor pressure ( $kPa$ ) at air temperature and

$e_a$  = actual vapor pressure ( $kPa$ ) at air temperature.

The Priestley-Taylor equation is briefly discussed with literature review in Article 2.3 (Chapter 2). The mathematical expression of latent heat flux ( $\lambda ET$ ) by the PT model is given by:

$$\lambda ET_{PT} = \phi \left[ (R_n - G) \frac{\Delta}{\Delta + \gamma} \right] \quad (4.2)$$

Where,  $\lambda ET_{PT}$  = Latent heat flux estimation by PT approach ( $W/m^2$ ),

$\phi$  = Priestley-Taylor parameter,

$R_n$  = net radiation of surface ( $W/m^2$ ),

$G$  = Soil heat flux ( $\text{W/m}^2$ ),

$\Delta$  = slope of saturated vapor pressure curve ( $\text{kPa}/^\circ\text{C}$ ),

$\gamma$  = psychrometric constant ( $\text{kPa}/^\circ\text{C}$ ).

All algorithms described in this chapter requires preliminary pre-processing of images which were performed using MODIS reprojection tool (MRT) and was converted to a standard format that can be read by MATLAB software. Geo-referencing, subsetting and pixel-wise analysis corresponding to the study area were performed using ArcGIS and ERDAS IMAGINE. The MODIS images were resampled to 1000 m resolution and ground elevations for each MODIS pixel were derived for the study area. Pixel-wise calculations using all the above necessary equations for each date of acquired MODIS images were carried out using MATLAB software. Specific few meteorological data were also used to calculate pixel-wise AET for the mentioned dates. Illustration of each parameter in PM and PT equations are given in the below sub-articles.

#### 4.4.1 Estimation of net radiation ( $R_n$ )

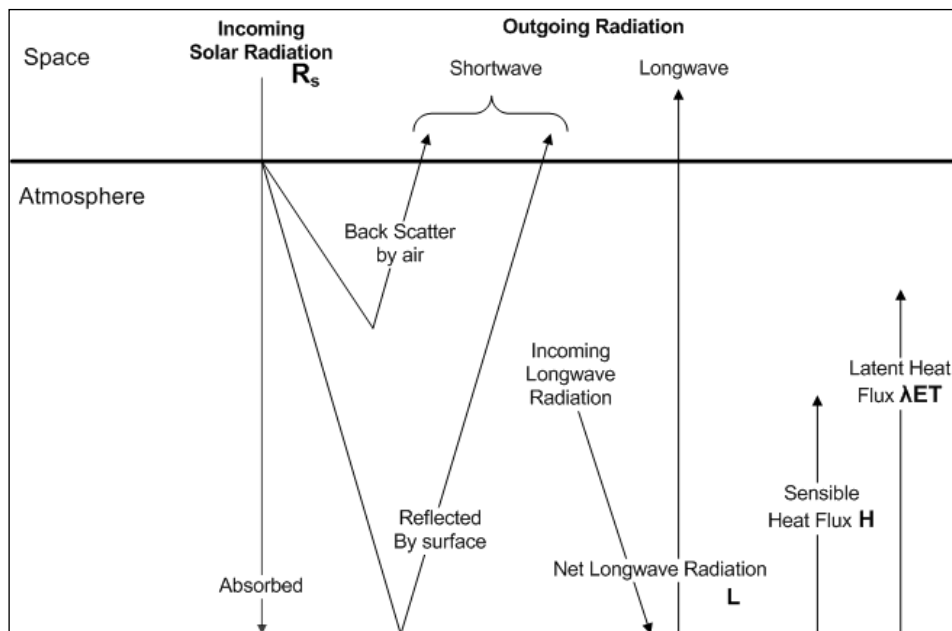


Figure 4.3: Surface Atmosphere Energy Exchange (Source: Gieske, 2005)

Figure 4.3 shows the simplified surface-atmosphere energy exchange, showing the main long and shortwave radiation components and latent heat flux, where incoming components are positive and outgoing components are negative. The total of the incoming and outgoing short and long wave components is the net radiation.

Net radiation is the dominant term in both PM and PT methods since it represents the source of energy that must be balanced by the thermodynamic equilibrium of the other terms. The net radiation can also be expressed as an electromagnetic balance of all incoming and outgoing fluxes reaching and leaving a flat horizontal and homogeneous surface. It may be computed as (Allen et al., 1998):

$$R_n = R_s(1 - \alpha) + R_i \downarrow - R_i \uparrow \quad (4.3)$$

Where  $\alpha$  = Surface albedo

$R_s$  = Incoming Solar radiation ( $W/m^2$ )

$R_i \downarrow$  = incoming longwave downward radiation ( $W/m^2$ )

$R_i \uparrow$  = outgoing longwave upward radiation ( $W/m^2$ )

#### 4.4.1.1 Incoming solar radiation ( $R_s$ )

Incoming of visible radiation and a limited portion of infrared energy (together sometimes called "shortwave radiation") from the Sun drive the Earth's climate system. Clouds, atmosphere reflect some of these incoming shortwave radiation. It is expressed as (Allen et al., 1998):

$$R_s = G_{sc} * d_r * \tau_{sw} * \cos\theta \quad (4.4)$$

Where,  $G_{sc}$  = Solar constant at the atmosphere top ( $1367 W/m^2$ )

$d_r$  = Inverse relative Earth-Sun distance

$\tau_{sw}$  = two way atmospheric transmissivity

$\theta$  = Solar zenith angle (radians)

##### 4.4.1.1.1 Inverse relative earth-sun distance ( $d_r$ )

The inverse relative distance earth-sun distance is given by (Allen et al., 1998):

$$d_r = 1 + 0.033 * \cos \left[ \frac{2\pi}{365} J \right] \quad (4.5)$$

Where,  $J$  = Sequential day of the year (Julian date) and the angle  $(J \times 2\pi/365)$  is in radians

#### 4.4.1.1.2 Two-way atmospheric transmissivity ( $\tau_{sw}$ )

$\tau_{sw}$  includes transmissivity of both diffuse (scattered) radiation and direct solar beam radiation to the surface. It is calculated assuming clear sky and relatively dry conditions using an elevation based relationship. It is expressed as (Allen et al., 1998):

$$\tau_{sw} = 0.75 + 2 \times 10^{-5} Z \quad (4.6)$$

Where,  $Z$  = Elevation (m)

#### 4.4.1.1.3 Solar zenith angle ( $\theta$ )

The angle between the sight from an observer on the earth to the sun and a vertical line extending upward from the observer is called the zenith angle ( $Z$ ). The amount of energy at the top of the atmosphere is a function of the solar zenith angle at certain latitude and time, and the distance between Sun and Earth. Solar zenith angle is obtained from LSR data (Allen et al., 1998).

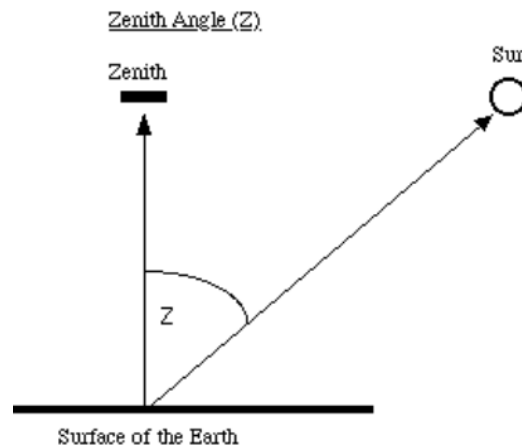


Figure 4.4: Solar zenith angle

#### 4.4.1.2 Long wave downward radiation ( $R_i\downarrow$ )

$R_i\downarrow$  ( $w/m^2$ ) radiation cannot be derived directly from remote sensors but can be determined from ground data or derived after atmospheric modeling. In this research work, ground-based temperature ( $T_a$ ) is replaced by satellite-based LST.  $R_i\downarrow$  varies with water vapor, air temperature, and atmospheric constituents. For the clear sky, the

concept of effective thermal infrared emissivity of the atmosphere ( $\epsilon_a$ ) introduces an overall emission value for all constituents. Long wave downward radiation is estimated using (Bastiaanssen, 1995):

$$R_i \downarrow = \epsilon_a \sigma \text{LST}^4 \quad (4.7)$$

Where,  $\sigma$  = Stefan-Boltzmann constant =  $5.67 \times 10^{-8}$  [W/m<sup>2</sup>/K<sup>4</sup>]

$\epsilon_a$  = Atmospheric emissivity

LST = Land surface temperature

#### 4.4.1.2.1 Atmospheric emissivity ( $\epsilon_a$ )

Emissivity is the ratio of the energy radiated by that object at a given temperature to the energy emitted by a blackbody of an object at the same temperature.  $\epsilon_a$  is calculated as (Bastiaanssen, 1995):

$$\epsilon_a = 0.85(-\ln \tau_{sw})^{0.09} \quad (4.8)$$

#### 4.4.1.3 Long wave upward radiation ( $R_i \uparrow$ )

$R_i \uparrow$ (w/m<sup>2</sup>) is the thermal radiation flux emitted from the earth's surface to the atmosphere. It is computed using the Stefan-Boltzmann equation (Bastiaanssen, 1995).

$$R_i \uparrow = \epsilon_s \sigma \text{LST}^4 \quad (4.9)$$

Where  $\epsilon_s$  = Surface emissivity calculated from NDVI

$\epsilon_s$  is computed as shown in the Eq. 4.9 (Van de Griend and Owe, 1993). The equation for estimating  $\epsilon_s$  from NDVI is valid only in the range  $0.16 \leq \text{NDVI} \leq 0.74$ . The method by Valor and Caselles (1996) could be used for a higher NDVI range.

$$\epsilon_s = 1.0094 + 0.047 * \ln (\text{NDVI}) \quad (4.10)$$

#### 4.4.2 Computation of albedo ( $\alpha$ )

Albedo ( $\alpha$ ) is the fraction of incident (shortwave) solar radiation reflected in all directions by the land surface. It is one of the critical parameters influencing the earth's climate (Pinty and Verstraete, 1992; Oleson et al., 2003; Gao et al., 2006; Cescatti et al., 2012). Surface albedo is important because it controls the amount of radiation

absorbed by the ground and determines the amount of energy available for heating the lower atmosphere, evaporating water, and driving the ecosystem processes that regulate greenhouse gas exchange (Rowe, 1991; Wang et al., 2002). It is calculated from linear combination bands following the Liang's model (Liang's 2001).

$$\alpha = 0.160R_1 + 0.291R_2 + 0.243R_3 + 0.116R_4 + 0.112R_5 + 0.081R_7 - 0.0015 \quad (4.11)$$

Where  $R_1$  to  $R_7$  = LSR of each band from MODIS data

#### 4.4.3 Estimation of soil heat flux (G)

Soil heat flux is the heat energy used to cool or warm the subsurface soil. It is theoretically proportional to the thermal conductivity and vertical temperature gradient in the subsurface soil. Soil heat flux is empirically estimated using a function by Bastiaanssen (2000) based on land surface temperature, albedo, and NDVI.

$$G = [LST - 273.15(0.0038 + 0.0074\alpha)(1 - 0.98NDVI^4)]R_n \quad (4.12)$$

#### 4.4.4 Slope of saturation vapor pressure curve ( $\Delta$ )

Slope of saturation vapor pressure curve (kpa/°C) is calculated as per Richards (1971).

$$\Delta = \frac{373.15e^*}{LST^2} (13.3185 - 3.952T_r - 1.9335T_r^2 - 0.5196T_r^3) \quad (4.13)$$

$$e^* = P \exp(13.3185T_r - 1.976T_r^2 - 0.6445T_r^3 - 0.1299T_r^4) \quad (4.14)$$

$$T_r = 1 - \frac{373.15}{LST} \quad (4.15)$$

Where  $T_r$  is radiometric temperature (K).

#### 4.4.5 Psychrometric constant ( $\gamma$ )

Psychrometric constant (kpa/°C) is calculated according to the research of FAO (Allen et al., 1998)

$$\gamma = 0.665 \times 10^{-3} P \quad (4.16)$$

$$P = 101.3 \left( \frac{293 - 0.0065 Z}{293} \right)^{5.26} \quad (4.17)$$

Where P is atmospheric pressure (kPa)

Z = Elevation (m)

#### 4.4.6 Estimation of Normalized Differential Vegetation Index (NDVI)

The Normalized Difference Vegetation Index (NDVI) is used to monitor changes in vegetation cover, productivity, phenology, as well as vegetation health status at both large spatial and long temporal scales (Celaya et al., 2010; Lunetta et al., 2006; Nemani et al., 2003; Pettorelli et al., 2005; Tucker et al., 2001). It is found that the upper asymptote of NDVI versus vegetation density usually occurs near 0.5-0.8 for dense vegetation and this upper limit depends on vegetation type, age and leaf water content (Paltridge and Platt, 1976). For bare soil NDVI tends to vary between -0.1 and 0.2 (Carlson and Ripley, 1997). It is expressed as:

$$NDVI = \frac{R_2 - R_1}{R_2 + R_1} \quad (4.18)$$

Where  $R_1$  and  $R_2$  = LSR values of the first and the second bands respectively of the MODIS images.

#### 4.4.7 Estimation of fraction of vegetation (Fr)

The fraction of vegetation (Fr) pertains to the part of a vegetation canopy having no patches of bare soil between plants, although small holes in the vegetation cover and sun flecks at the surface are permissible (Carlson et al., 1994; Carlson and Ripley, 1997). Fr is the primary index used for measuring the state and performance of the ecological environment. It has great significance for both ecology and society (Zhang et al., 2013), and Fr estimation of large areas has become a foundation for establishing global and regional climate and hydrological models. Pixel-wise Fr values are estimated from MODIS LSR product using the formula proposed by Carlson and Ripley (1997).

$$F_r = \left( \frac{NDVI - NDVI_{\min}}{NDVI_{\max} - NDVI_{\min}} \right)^2 \quad (4.19)$$



The minimum and maximum values of NDVI for each date are identified from computations made for all pixels using Eq. (4.17).

#### 4.4.8 Saturated vapor pressure ( $e_s$ ):

As saturation vapor pressure is related to air temperature, it can be calculated from the air temperature. The relationship is expressed as per Allen et al., (1998).

$$e_s = \frac{e^0(LST_{\max}) + e^0(LST_{\min})}{2} \quad (4.20)$$

$$e^0(LST) = 0.6108 \exp \left[ \frac{17.27 LST}{LST + 237.3} \right] \quad (4.21)$$

Where, LST = Land surface temperature (K)

$e^0(LST)$  = Saturation Vapor Pressure at air temperature (kPa)

#### 4.4.9 Actual vapor pressure ( $e_a$ ):

It is the amount of water vapor measurement in a volume of air and increases or decreases as the amount of water vapor varies. Air that attains its saturation vapor pressure has established an equilibrium with a flat surface of the water. The relationship is expressed as per Allen et al., (1998).

$$e_a = \frac{e^0(LST_{\min}) \frac{RH_{\max}}{100} + e^0(LST_{\max}) \frac{RH_{\min}}{100}}{2} \quad (4.22)$$

Where,  $e^0(LST_{\min})$  = Saturation Vapor Pressure at daily minimum temperature (kPa)

$e^0(LST_{\max})$  = Saturation Vapor Pressure at daily maximum temperature (kPa)

$RH_{\min}$  = minimum relative humidity (%)

$RH_{\max}$  = maximum relative humidity (%)

#### 4.4.10 Air density at constant pressure ( $\rho_a$ ):

The density of dry air can be calculated using the ideal gas law, expressed as a function of temperature and pressure as per Allen et al., (1998).

$$\rho_a = \frac{P}{T_v \cdot R} \quad (4.23)$$

$$T_V = \frac{LST}{1 - 0.378 \frac{e_a}{P}} \quad (4.24)$$

Where P = Atmospheric air pressure (kPa)

$T_V$  = Virtual temperature (K)

R = Specific gas constant (0.287 kJ/kg/K)

LST = Land surface temperature (K)

$e_a$  = Actual vapor pressure (kPa)

#### 4.4.11 Altitudinal correction of LST

LST is a good indicator of the energy balance at the Earth's surface and the greenhouse effect because it is one of the key parameters in the physics of land-surface processes on a regional as well as global scale. It is also required for a wide variety of climatic, hydrological, ecological and biogeochemical studies (Running, 1991; Zhang et al., 1995; Running et al., 1994; Nishida et al., 2003; Majumdar et al., 2012).

Hassan et al., (2007) suggested that  $LST_i$  should be corrected to a value representing the temperature at mean sea level by calculating the atmospheric pressure at each of the image pixels with respect to their elevations since  $LST_i$  is influenced by DEM. Eq. 4.17 is based on a simplified form of the ideal gas law for a neutrally-stratified atmosphere and a temperature of 293 K at a standard atmosphere (i.e., 101.3 kPa). Corrected land surface temperature (LST) is computed as per Hassan et al., (2007).

$$LST = LST_i \left[ \frac{p_0}{P} \right]^{-R/c_p} \quad (4.25)$$

Where  $LST_i$  = Image pixel temperature (K)

R = Gas constant (i.e.,  $0.287 \times 10^{-3}$  MJ/kg/K),

$c_p$  = Specific heat capacity of air ( $1.013 \times 10^{-3}$  MJ/kg/K)

$P_0$  = Standard air pressure (101.3 kPa)

#### 4.4.12 Computation of daily net radiation ( $R_{n \text{ daily}}$ )

$R_{n \text{ daily}}$  ( $\text{W/m}^2$ ) is expressed as (Almhab and Busu, 2007):

$$R_{n \text{ daily}} = R_{s \text{ daily}}(1 - \alpha) + R_i \downarrow - R_i \uparrow \quad (4.26)$$

Where  $R_{n \text{ daily}}$  = Daily average net radiation ( $\text{W/m}^2$ )

$R_{s \text{ daily}}$  = Daily average incoming shortwave radiation ( $\text{W/m}^2$ )

To convert  $\text{MJ/m}^2/\text{day}$  to  $\text{W/m}^2/\text{day}$ , there is a need to multiply  $R_{s \text{ daily}}$  by 11.5741

$$R_{s \text{ daily}} = 11.5741 \tau_{\text{sw}} R_a \quad (4.27)$$

Where,  $R_a$  = Extraterrestrial solar radiation ( $\text{MJ/m}^2/\text{day}$ )

##### 4.4.12.1 Extraterrestrial solar radiation ( $R_a$ )

The solar radiation received at the top of the earth's atmosphere on a horizontal surface is called the extraterrestrial solar radiation.  $R_a$ , for each day of the year and different latitudes, can be estimated from the solar constant, the solar declination and the time of the year. It is calculated by the procedure developed by Duffie and Beckman (2013).

$$R_a = \frac{24(60)}{\pi} K_0 dr [\omega_s \sin \psi \sin \delta + \cos \psi \cos \delta \sin \omega_s] \quad (4.28)$$

Where,  $K_0$  = Solar constant ( $0.0820 \text{ MJ/m}^2/\text{min}$ )

$dr$  = Inverse relative distance from Earth to Sun

$\omega_s$  = Sunset hour angle (radians)

$\psi$  = Latitude of each pixel (radians)

$\delta$  = Solar declination (radians)

Sunset hour angle is given by:

$$\omega_s = \arccos[-\tan \psi \tan \delta] \quad (4.29)$$

Solar declination is given by (Allen et al., 1998):

$$\delta = 0.409 \sin \left[ \frac{2\pi}{365} J - 1.39 \right] \quad (4.30)$$

#### 4.4.13 Estimation of aerodynamic conductance (Ga)

Aerodynamic conductance was estimated as per Leuning et al., (2008).

$$Ga = \frac{k^2 u_z}{\ln \left[ \frac{(z_m - d)}{z_{om}} \right] \ln \left[ \frac{(z_m - d)}{z_{ov}} \right]} \quad (4.31)$$

Where  $z_m$  = height of wind speed and humidity measurements (m),  $d$  = zero plane displacement height (m),  $z_{om}$  and  $z_{ov}$  = roughness lengths governing the transfer of momentum and water vapor (m),  $k$  = von Karman's constant (0.41),  $u_z$  = wind speed at height  $z_m$  (m/s). As suggested by Leuning et al., (2008), other variables were obtained as  $d = 2h/3$ ,  $z_{om} = 0.123h$  where  $h$  is canopy height and  $z_{ov} = 0.1z_{om}$ .

#### 4.4.14 Gs estimation from the trapezoidal scatter plot (LST versus Fr)

Considering total evapotranspiration flux ( $\lambda ET_{PM}$ ) to be the sum of transpiration flux from the canopy ( $\lambda E_c$ ) and evaporation flux from soil ( $\lambda E_s$ ), leads to (Leuning et al., 2008);

$$\lambda ET_{PM} = \frac{\frac{\Delta}{\gamma} (R_n - G)^c + \left( \frac{\rho_a c_p}{\gamma} \right) D_a Ga}{\frac{\Delta}{\gamma} + 1 + \frac{Ga}{Gc}} + \frac{f \frac{\Delta}{\gamma} (R_n - G)^s}{\frac{\Delta}{\gamma} + 1} \quad (4.32)$$

Where  $(R_n - G)^c$  and  $(R_n - G)^s$  represent available energy fractions absorbed by the canopy and soil surface respectively and  $Gc$  is bulk canopy conductance. An expression for  $G_s$  may be obtained by recasting Equation 2 as (Leuning et al., 2008);

$$G_s = Gc \left[ \frac{1 + \frac{\tau Ga}{\left( \frac{\Delta}{\gamma} + 1 \right) Gc} \left[ f - \frac{\left( \frac{\Delta}{\gamma} + 1 \right) (1-f) Gc}{Ga} \right] + \frac{Ga}{\frac{\Delta}{\gamma} Gi}}{1 - \tau \left[ f - \frac{\left( \frac{\Delta}{\gamma} + 1 \right) (1-f) Gc}{Ga} \right] + \frac{Ga}{\frac{\Delta}{\gamma} Gi}} \right] \quad (4.33)$$

Where  $\tau$  = fraction of total available energy absorbed by soil surface, i.e.,  $\tau = (R_n - G)^s / (R_n - G)$ ;  $\tau = \exp(-k_A LAI)$  where  $k_A$  is an extinction coefficient for available

energy,  $f$  = ratio of evaporation rate from soil ( $E_s$ ) to the equilibrium evaporation rate and  $G_i$  = climatological conductance, i.e.,  $G_i = \gamma (R_n - G) / (\rho_a c_p D_a)$ .

Figure (4.5) depicts a typical hypothetical triangular and trapezoidal scatter plot obtained by plotting pixel-wise values of LST versus  $Fr$  for a selected study area.

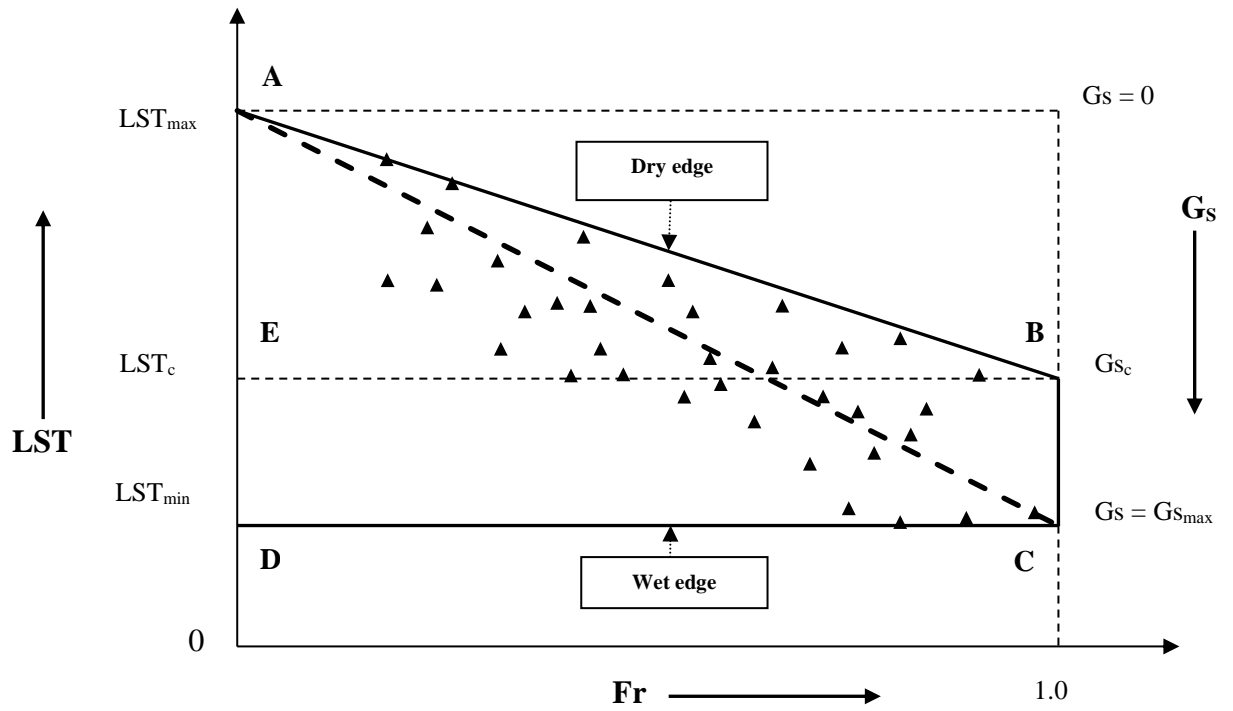


**Figure 4.5: Triangular and trapezoidal scatter plot of LST versus  $Fr$**

Although the interpretation of such a scatter plot is fairly well established (e.g. Laxmi and Nandagiri 2014), a brief description is given herein for the sake of completeness. Considering the trapezoid (labeled ABCD) in Figure 4.5, side DC is known as the ‘wet edge’ and the lowest values of LST occur along it. While point D represents wet bare soil, point C represents a fully vegetated wet surface and points in between possess varying proportions of bare soil and vegetation. Side AB is the ‘dry edge’ with LST values varying from the highest for dry bare soil (point A) to lower values for full vegetation (point B). Assuming that evaporative cooling is solely responsible for the reduction in LST, pixels with high LST values experience low evaporation/transpiration rates on account of soil moisture stress and vice versa. Therefore, it may be deduced that ET is zero for pixels located at point A and maximum for pixels located along the wet edge (DC). For other pixels located within the trapezoidal space, ET varies between these two extreme limits.

Accordingly, when implementing the PT method to estimate latent heat flux ( $\lambda ET_{PT}$ ), it is assumed that the parameter  $\phi$  assumes a value of 0 at point A ( $\phi_{min}$ ) and value of 1.26 ( $\phi_{max}$ ) along the wet edge. The value of  $\phi$  for any pixel lying within the trapezoidal space may then be obtained by applying a suitable interpolation algorithm (e.g. Tang et al., 2010; Laxmi and Nandagiri 2014) and ET may be estimated using the Priestley-Taylor equation.

In the present study, it is proposed that pixel-wise values of the bulk surface conductance parameter ( $G_s$ ) associated with the PM method may also be derived from the scatter plot of LST vs. Fr using a similar reasoning. As the first step in this direction, the limiting values of  $G_s$  have to be fixed at the vertices of the scatter plot. For simplicity, we initially consider the triangle ADC (Figure 4.5) and deduce the values of  $G_s$  at the vertices using the surface conductance model defined by Equation 4.33.

Considering point A first,  $Fr = 0$  and represents a completely bare soil. In the absence of a canopy, parameter  $\tau = 1.0$  and Equation 4.33 reduces to [Equation 10 of Leuning et al., (2008)],

$$G_s = \left[ \frac{\frac{\Delta}{\gamma} f G_a}{\left(\frac{\Delta}{\gamma} + 1\right) \left[\frac{\Delta}{\gamma} (1-f) + \frac{G_a}{G_i}\right]} \right] \quad (4.34)$$

But since at A,  $LST = LST_{max}$  soil evaporation flux is zero due to severe moisture stress and therefore  $f = 0$  is applicable, which upon substitution into Equation 4.34 yields  $G_s = 0$  resulting in  $\lambda ET = 0$  from Equation 4.1. Therefore, the minimum value of surface conductance ( $G_{smin}$ ) may be set to zero.

Considering point D, and recognizing that it again represents bare soil ( $Fr = 0$ ,  $\tau = 1.0$ ) but since  $LST = LST_{min}$  here, soil evaporation flux is at the maximum (equilibrium) rate due to high soil moisture levels and therefore  $f = 1.0$ .

Since,  $G_i = \gamma (R_n - G) / (\rho_a c_p D_a)$

$$G_{S_{\max}} = \left[ \frac{\Delta (R_n - G)}{\left(\frac{\Delta}{\gamma} + 1\right) \rho_a c_p D_a} \right] \quad (4.35)$$

It is interesting to note that according to Equation 4.35, for a bare soil surface with no moisture stress, the conductance appears to be a function of only existing climatic conditions. It has been shown out that evaporation from a bare soil takes place in three stages during which progressive drying of the soil profile occurs (e.g., Hillel, 1998; Qiu & Ben-Asher, 2010). The initial among these being the constant rate stage when the soil is wet and rate of moisture supply to the surface is equal to the evaporative demand. During this stage evaporation occurs at a constant rate and is controlled by external climatic conditions rather than by the properties of the soil profile (Hillel, 1998). Since Equation 4.35 is applicable to a constantly wet bare soil, evidently the initial constant rate stage is valid throughout, evaporation takes place at a constant rate determined by external climatic conditions only and the conductance depends only on ambient climatic conditions. A detailed discussion on the variation of  $G_s$  as defined by Equation 4.35 for a range of climatic conditions is presented in a subsequent section of this paper.

At point C (Fig. 1), since full canopy exists ( $Fr = 1.0$ ) parameter  $\tau = 0$  and Equation 4.33 reduces to [Equation 9 of Leuning et al., (2008)],

$$G_{S_{\max}} = G_c \left[ \frac{1 + \frac{G_a}{\frac{\Delta}{\gamma} G_i}}{1 + \frac{G_a}{\frac{\Delta}{\gamma} G_i}} \right] = G_c \quad (4.36)$$

Two important aspects with regard to Equation 4.35 and Equation 4.36 need to be highlighted. Firstly, since points D and C both lie on the same line, values of  $G_{S_{\max}}$  defined by Equation 4.35 and Equation 4.36 must be numerically equal to each other. This is on account of the fundamental assumption of the LST-Fr approach that since side DC (Figure 4.5) is the wet edge, evaporative flux is constant all along the edge and takes place at the potential rate controlled by prevailing climatic conditions. Although it has been noted that bulk surface conductance ( $G_s$ ) is in general influenced

by both climate and environmental variables (e.g, Alves and Pereira, 2000),  $G_{s_{max}}$  represents the upper limit of  $G_s$  for wet surfaces. Under wet conditions existing along side DC, evaporation from bare soil, evapotranspiration from soil and vegetation and transpiration from full vegetation will take place at the potential rate controlled by prevailing climatic conditions. Therefore, surface conductance assumes the maximum value ( $G_{s_{max}}$ ) under given conditions and may be computed explicitly from Equation 4.35 using climate data.

In summary, using the reasoning presented above, it may be deduced that the surface conductance for use with the PM model (Equation 4.1) may be set to a minimum value  $G_{s_{min}} = 0$  at point A in Figure 4.5 and to a maximum value  $G_{s_{max}}$  defined by Equation 4.35 along the wet edge DC. Accordingly, it is proposed that for any pixel (i) located within the triangular space ACD, a suitable value of surface conductance  $G_{s_i}$  may be assigned by interpolation between these two extreme values.

Considering the trapezoidal space ABCD (instead of triangle ACD), the only difference arises in assuming a reduction in  $G_s$  values for pixels located along the edge BC depending on the increase in LST, decrease in soil moisture and increase in the vapor pressure deficit ( $D_a$ ).

#### 4.4.15 Deriving pixel-wise $G_s$ and $\phi$ values from the LST-Fr scatter plot

Equations for assigning a value of surface conductance ( $G_s$ ) for each pixel in the LST-Fr trapezoidal space presented herein are adapted from equivalent equations given by Laxmi and Nandagiri (2014) for deriving pixel-wise values of the PT parameter ( $\phi$ ).

Considering the trapezoidal space defined by ABCD in Figure 4.5, the horizontal line BE is set off, thereby dividing the space into a triangular part ABE and a rectangular part EBCD. Representing constant LST along BE as  $LST_c$ , the corresponding value of  $G_{s_c}$  may be estimated using;

$$G_{s_c} = G_{s_{max}} \frac{(LST_{max} - LST_c)}{(LST_{max} - LST_{min})} \quad (4.37)$$



Next, the following three cases may arise depending on the position of a specific pixel ( $LST_i$ ,  $Fr_i$ ) in the trapezoidal space for which a surface conductance value ( $G_{s_i}$ ) needs to be assigned.

Case 1: When  $LST_i > LST_c$

$$G_{s_{min, i}} = G_{s_c} Fr_i \quad (4.38)$$

$$G_{s_{max, i}} = G_{s_{max}} \quad (4.39)$$

$$G_{s_i} = G_{s_{min, i}} + \frac{LST_{max} - LST_i}{LST_{max} - LST_c} (G_{s_c} - G_{s_{min, i}}) \quad (4.40)$$

Case 2: When  $LST_i = LST_c$

$$G_{s_i} = G_{s_c} = G_{s_{max}} \frac{(LST_{max} - LST_c)}{(LST_{max} - LST_{min})} \quad (4.41)$$

Case 3: When  $LST_i < LST_c$

$$G_{s_i} = G_{s_c} + G_{s_{max}} \frac{(LST_c - LST_i)}{(LST_{max} - LST_{min})} \quad (4.42)$$

Here  $G_{s_{max}}$  is defined by Equation 4.35. Implementation of Equations (4.37) to (4.42) requires input values of  $LST_{min}$ ,  $LST_{max}$ , and  $LST_c$  which can be obtained the trapezoidal plot of LST versus Fr.  $G_s$  values obtained in this manner may be used with Equation 4.1 with other relevant inputs to derive estimates of  $\lambda ET_{PM}$ .

Now, for any pixel (i) located within the trapezoidal space ABCD, a suitable value of surface conductance  $G_{s_i}$  may be assigned by interpolation between these two extreme values. Laxmi and Nandagiri (2014) presented equations for deriving values of the PT parameter ( $\phi$ ) for each pixel in the LST-Fr trapezoidal space. These equations were adapted in the present study to assign pixel-wise values of surface conductance ( $G_s$ ).  $G_s$  values obtained in this manner were used with Eq. (4.1) with other relevant inputs to derive estimates of  $\lambda ET_{PM}$  for each pixel.

Above same methodology and procedure is used to estimate  $\phi$  as per Laxmi and Nandagiri (2014) by taking  $\phi_{\max} = 1.26$  (AET=Maximum) along wet edge line due to Fr value 1 and  $LST_{\min}$  (high soil moisture condition) also it represents ‘equilibrium’ evaporation and transpiration rates. Conversely  $\phi_{\min} = 0$  (AET=0) along dry edge line due to Fr value 0 and  $LST_{\max}$  (low soil moisture condition).

Standard procedures available in literature were used to convert remote sensing data and climate data into parameters/variables which appear in Eq. (4.1). Fig. (4.2) depicts the flow chart of steps involved in application of the PM model proposed in the present study to derive estimates of  $\lambda ET$  and AET using inputs from MODIS imagery and climate data. While the developed model provided output of  $\lambda ET$  for comparisons with flux tower measurements, AET values were estimated when the model was applied to the Hemavathi sub-basin. MATLAB<sup>®</sup> codes were developed for implementation.

#### 4.4.16 Cleugh et al., (2007) bulk surface conductance model (PMC approach)

Cleugh et al., (2007) proposed a simple linear relationship between  $G_s$  and LAI of the form,

$$G_s = c_L LAI + g_{\min} \quad (4.43)$$

where  $c_L$  is mean surface conductance per unit leaf area index,  $g_{\min}$  is surface conductance controlling soil evaporation and LAI is leaf area index. Cleugh et al., (2007) recommend setting  $g_{\min} = 0$ .

Optimal values of  $c_L$  need to be obtained by minimizing the error between observed and estimated values of  $\lambda ET$ .

The Cleugh et al., (2007) approach (hereinafter referred to as PMC) involving application of Equations 15 and 1 to obtain estimates of latent heat flux ( $\lambda ET_{PMC}$ ) was implemented in the present study at each of the four flux tower sites MKL, PDF, IRI and SKR (Table 3.1) for the selected dates and times shown in Table 5.1. Considering a 5 km x 5 km area centred on each flux tower, MOD15A2 product was used to extract

pixel-wise values of LAI. Considering the range of  $c_L$  values: 0.0005 – 0.0037, obtained by Leuning et al., (2008) for 15 global flux sites, and a step of 0.0005, optimal values of  $c_L$  for each flux tower were obtained by trial such that the RMSE values between  $\lambda ET_{PMC}$  and  $\lambda ET_{Meas}$  were minimized for the selected times and dates.

#### 4.4.17 Leuning et al., (2008) bulk surface conductance model (PML approach)

Leuning et al., (2008) proposed the following equation to estimate the bulk stomatal conductance ( $G_c$ ) to enable computation of  $G_s$  using Equation 4.33 and subsequently,  $\lambda ET_{PM}$  using Equation 4.1.

$$G_c = \frac{g_{sx}}{k_Q} \ln \left[ \frac{Q_h + Q_{50}}{Q_h \exp(-k_Q LAI) + Q_{50}} \right] \left[ \frac{1}{1 + \frac{D_a}{D_{50}}} \right] \quad (4.44)$$

where  $g_{sx}$  is maximum stomatal conductance (m/s),  $k_Q$  is an extinction coefficient for shortwave radiation, LAI is Leaf Area Index,  $Q_h$  is the flux density of visible radiation at the top of canopy (MJ/m<sup>2</sup>/d),  $Q_{50}$  is visible radiation flux when stomatal conductance is half its maximum value (MJ/m<sup>2</sup>/d),  $D_a$  is vapor pressure deficit of air (kPa) and  $D_{50}$  is the vapor pressure deficit at which stomatal conductance is half its maximum value (kPa).

Accordingly, their model for  $G_s$  contains six unknown parameters:  $g_{sx}$ ,  $k_Q$ ,  $Q_{50}$ ,  $D_{50}$ ,  $k_A$  and  $f$  which need to be determined through calibration with measured  $\lambda ET$  values. Based on the results obtained from implementation at 15 flux tower sites they concluded that only two parameters  $g_{sx}$  and  $f$  need to be optimized while the others could be set to constant values without loss of much accuracy. As a further simplification, they proposed that  $g_{sx}$  values could also be fixed based on vegetation type as per the results documented in Kelliher et al., (1995) and only the soil evaporation parameter  $f$  needs to be optimized. Due to the limited nature of available measured flux data for calibration, this simpler methodology suggested by Leuning et al., (2008) was adopted.

Leuning et al., (2008) (herein after referred to as PML) approach were implemented separately at each of the four flux tower sites MKL, PDF, IRI and SKR (Table 3.1) for the selected dates and times shown in Table 5.1. As per their recommendation the following fixed values were assigned four parameters:  $k_A = k_Q = 0.6$ ,  $Q_{50} = 30 \text{ W/m}^2$  and  $D_{50} = 0.7 \text{ kPa}$  and  $Q_h = 0.45 R_s^*$  where  $R_s^*$  is incoming solar radiation, was used. Considering a 5 km x 5 km area centred on each flux tower, MODIS products, MOD09GA was used to compute  $R_s^*$  using LSR and MOD15A2 was used to extract LAI. Considering the vegetation type at each flux tower site (Table 3.1) values of  $g_{sx}$  were selected from Kelliher et al., (1995) and set to 0.0046, 0.0053, 0.0110 and 0.0053 m/s for the MKL, PDF, IRI and SKR sites respectively. A trial procedure in which  $f$  was varied over the limit 0 – 1.0 at steps of 0.1 was used to determine the optimal value of  $f$  for each flux tower which yielded minimum RMSE between flux values estimated by the PML approach ( $\lambda ET_{PML}$ ) and measured values ( $\lambda ET_{Meas}$ ) for the selected times and dates.

#### 4.4.18 Estimation of the evaporative fraction (EF)

The evaporative fraction is a ratio of latent heat flux to the available energy flux ( $R_n - G$ ) is estimated as per as per Tasumi et al., (2005). It has been used to characterize the energy partition over land surfaces and has the potential for inferring daily energy balance information based on midday remote sensing measurements.

$$EF = \frac{\lambda ET}{R_n - G} \quad (4.45)$$

#### 4.4.19 Calculation of daily AET

Since all parameters are estimated using instantaneous observation satellite sensors, 24 hours AET is estimated based on the assumption that EF remains constant through the latent heat of flux (Sugita and Brutsaert, 1991). The actual 24-hour AET can be estimated from the instantaneous evaporative fraction EF, and the daily averaged net

radiation  $R_{n \text{ daily}}$  (Morse et al., 2004). Assuming that the soil heat flux integrated over 24-hours ( $G_{\text{daily}}$ ) is negligible, AET rate over 24 hours can be calculated as:

$$AET_{\text{daily}} = \frac{8.64 \times 10^7 * EF(R_{n \text{ daily}} - G_{\text{daily}})}{\lambda \rho_w} \quad (4.46)$$

Where,  $\lambda$  = Latent heat of water ( $2.47 \times 10^6$  kJ/kg)

$\rho_w$  = Density of water ( $1000$  kg/m<sup>3</sup>)

## CHAPTER 5

### VALIDATION OF AET ALGORITHMS

---

#### 5.1 GENERAL

Results regarding the application of the developed PM algorithm in this research work was presented. Validation of PM algorithms with the help of flux towers data is shown in this chapter for different types of four landscapes. In an effort to compare the accuracies of  $\lambda ET$  values obtained with the PM model approach proposed in the present study with other similar satellite-based approaches suggested by previous researchers, the following three methods were implemented with the same data set: 1) the Priestley-Taylor model with MODIS-derived LST-Fr trapezoidal scatter plots proposed by Laxmi and Nandagiri (2014) – hereinafter referred to as PT approach ( $\lambda ET_{PT}$ ) 2) the Cleugh et al. (2007) model in which  $G_s$  is obtained using a simple relationship with LAI and used with the PM model – hereinafter referred to as PMC approach ( $\lambda ET_{PMC}$ ) and 3) the Leuning et al. (2008) model in which a biophysical approach is used to estimate  $G_s$  for use with the PM model – hereinafter referred to as PML approach ( $\lambda ET_{PML}$ ).

As regards modeling spatial AET patterns in the Hemavathi sub-basin, only the PM model approach proposed in the present study, a modified form of this method and the PT approach were implemented and validated using MOD16A2 ET product is presented in the next chapter.

#### 5.2 APPLICATION OF ALGORITHMS TO FLUX SITES

Latent heat flux values were estimated by using the Equations 4.1 to 4.44 and satellite imagery with flux tower data for each pixel in the different types of flux sites and the

selected six days. Detailed characteristics of the flux sites and the data used to code the algorithm in MATLAB, are given in Chapters 3 and 4.

### 5.3 RESULTS

#### 5.3.1 Variation of $G_{S_{max}}$ with climatic variables

Equation (4.35) indicates that the value of maximum surface conductance ( $G_{S_{max}}$ ) depends only on climatic variables. Variations in  $G_{S_{max}}$  values for a range of values of temperature ( $T$ ), available energy ( $R_n - G$ ) and vapor pressure deficit ( $D_a$ ) were examined. Figure 5.1 depicts variability in  $G_{S_{max}}$  values on account of increasing  $D_a$  for three conditions of available energy ( $R_n - G$ ). Air temperature ( $T$ ) was assumed to be 30 °C.

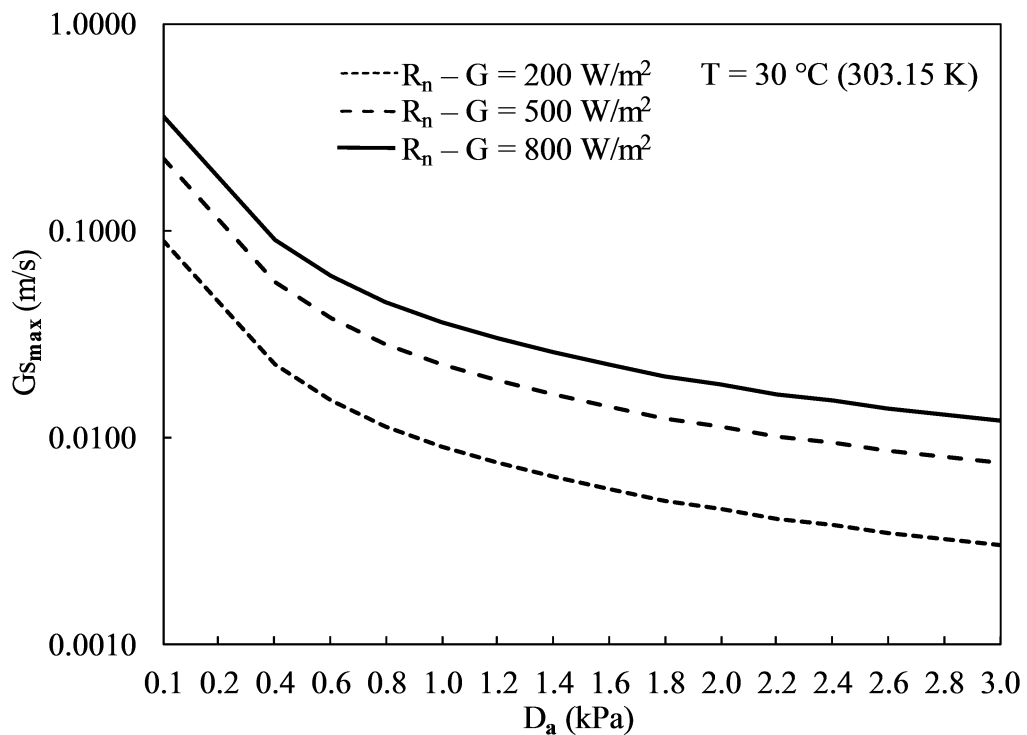


**Figure 5.1: Response of  $G_{S_{max}}$  (Equation 4.35) to  $D_a$  for different values of  $(R_n - G)$  at constant air temperature ( $T$ ) of 30 °C**

Although the nature of the overall response of  $G_{S_{max}}$  to changes in  $D_a$  and  $(R_n - G)$  depicted in Figure 5.1 is somewhat obvious to interpret from Equation (4.35), that is,  $G_s$  increases with available energy and decreases with increasing  $D_a$ , it still provides

useful information on the limits of  $G_{S_{\max}}$  values for different climatic conditions. Highest and lowest values of  $G_{S_{\max}}$  for  $D_a$  of 0.1 kPa and 3.0 kPa are: (0.0902, 0.003) for  $(R_n - G) = 200 \text{ W/m}^2$ , (0.2255, 0.0075) for  $(R_n - G) = 500 \text{ W/m}^2$  and (0.3608, 0.012) for  $(R_n - G) = 800 \text{ W/m}^2$  respectively. All three curves shown in Figure 5.1 could be described with a power equation of the form  $G_{S_{\max}} = a D_a^{-b}$  with a high value of the coefficient of determination ( $R^2$ ) of 0.9961. In all cases, the value of the exponent ( $b$ ) was equal to 1.251.

### 5.3.2 LST-Fr scatter plots

To demonstrate the applicability of the proposed methodology, six dates were selected for each flux tower site considering the following criteria: availability of relevant measurements at the tower, clear sky condition, availability of cloud-free MODIS satellite imagery and representation of summer, monsoon and winter seasons. However, due to non-availability of cloud-free MODIS imagery during the monsoon season, this criteria could not be met at a few sites. Table 5.1 lists the selected dates for each site. For each flux tower site, trapezoidal scatter plots of MODIS-derived LST values with altitudinal corrections versus Fr (Equation 4.19) were plotted for each selected date considering a  $5 \text{ km} \times 5 \text{ km}$  area centered on the tower. Out of the 24 (4 sites  $\times$  6 dates) scatter plots derived in this manner, for the sake of brevity, one sample plot for each site is shown in Figure 5.2. In each case, pixels in which the flux towers are located are depicted by the triangle symbol.

Values of  $LST_{\min}$ ,  $LST_{\max}$ , and  $LST_c$  which are required for estimation of pixel-wise values of  $G_s$  using Equations (4.38) to (4.42) have to be inferred from the trapezoidal plots of LST versus Fr. Tang et al., (2010) proposed an automated procedure for detection of the dry and wet edges in a triangular LST-Fr scatter plot which can be implemented to accurately infer  $LST_{\max}$  and  $LST_{\min}$ . However, Laxmi and Nandagiri (2014) used a visual approach to infer values of  $LST_{\min}$ ,  $LST_{\max}$ , and  $LST_c$  in a trapezoidal plot and showed that assumed errors of up to  $\pm 1 \text{ K}$  in LST values resulted in a maximum error of 4.57% in  $\lambda ET$  estimates by the PT method. Therefore, the simpler visual approach was adopted in the present study and accordingly, values of



$LST_{min}$ ,  $LST_{max}$ , and  $LST_c$  derived from the scatter plots are listed in Table 5.1 for each selected date at the four sites. Triangles ( $\blacktriangle$ ) in plots represent the pixel in which flux towers are located

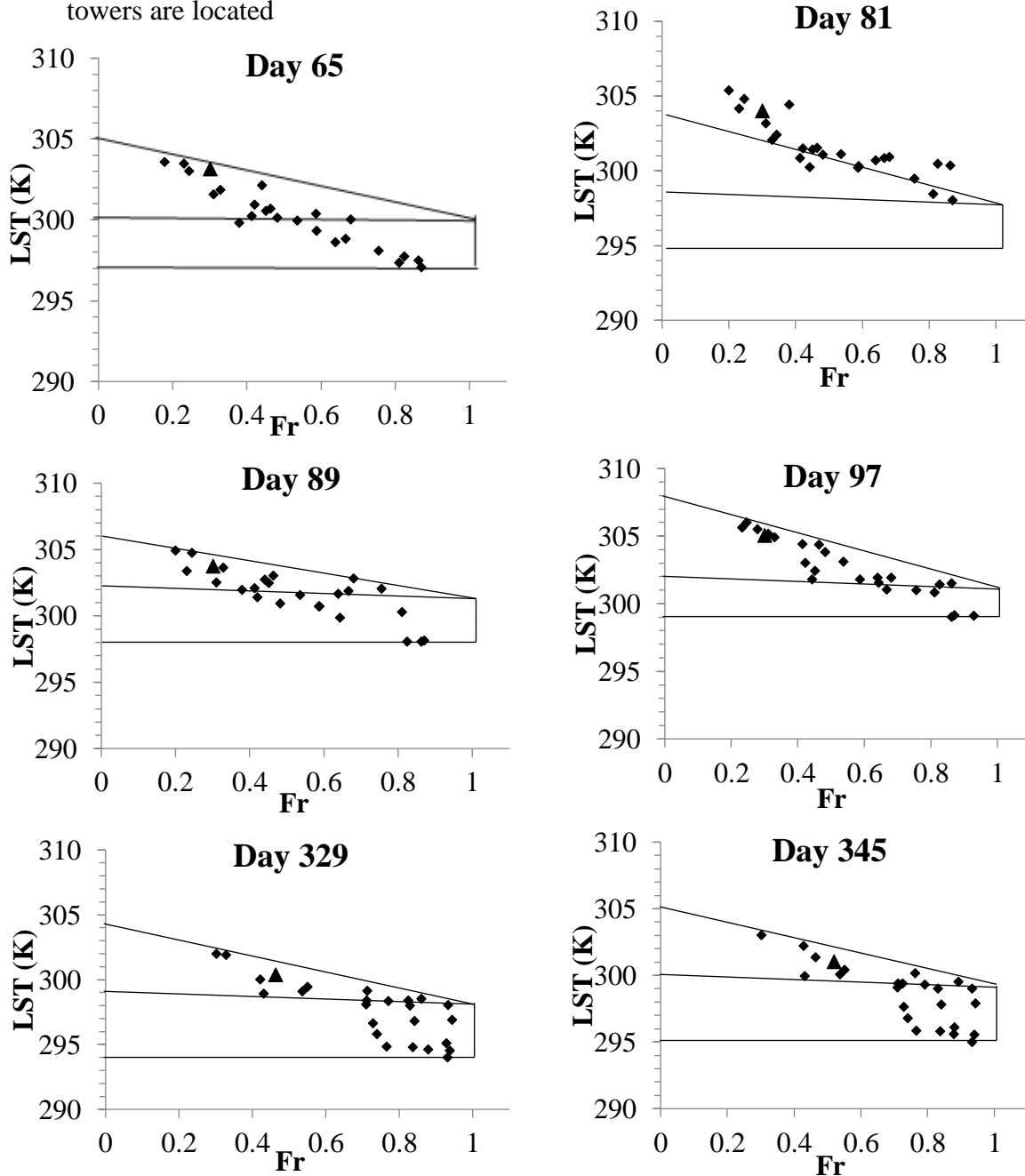


**Figure 5.2: Trapezoidal scatter plots of LST versus Fr for MKL flux tower**

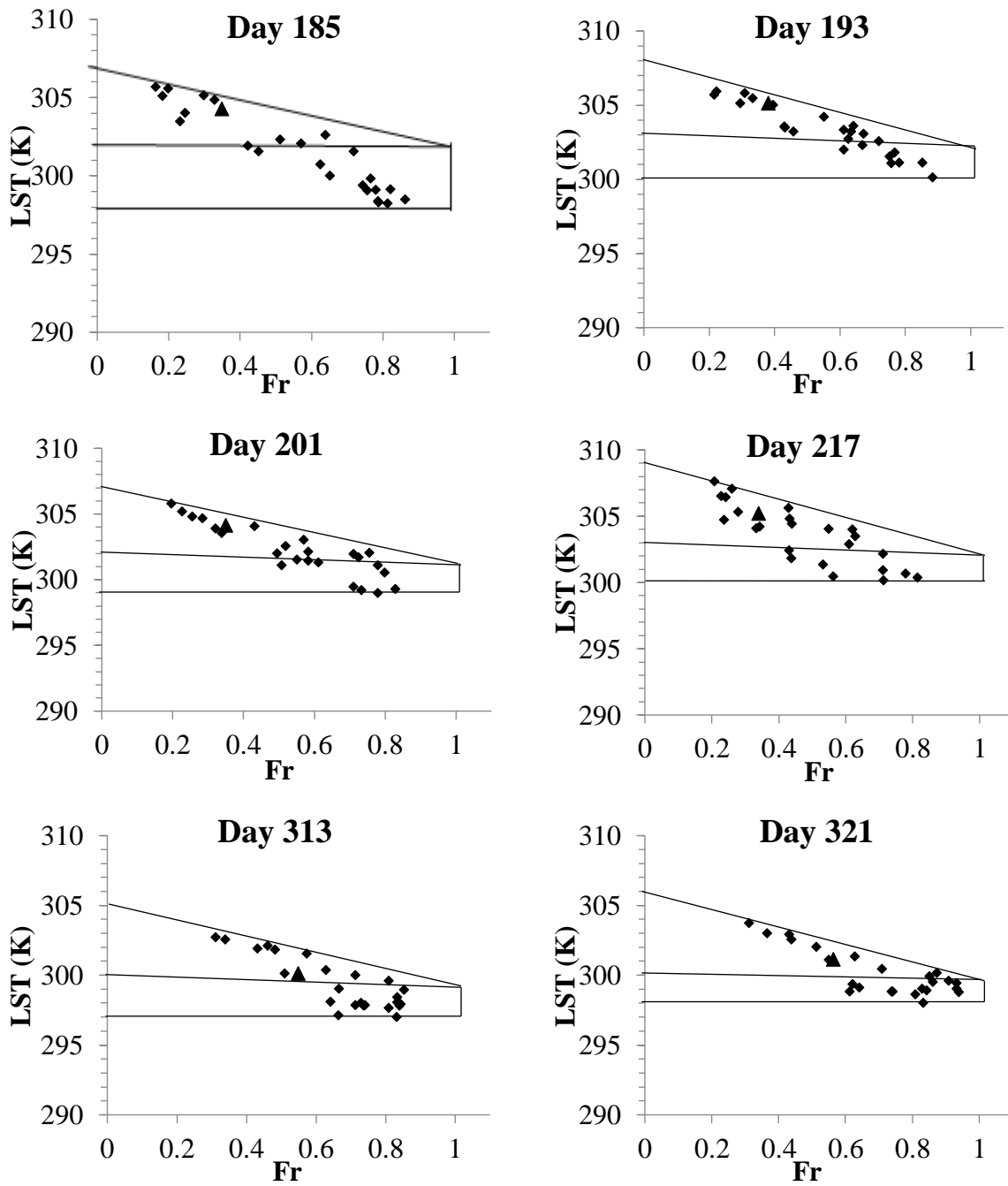


**Figure 5.3: Trapezoidal scatter plots of LST versus Fr for PDF flux tower**

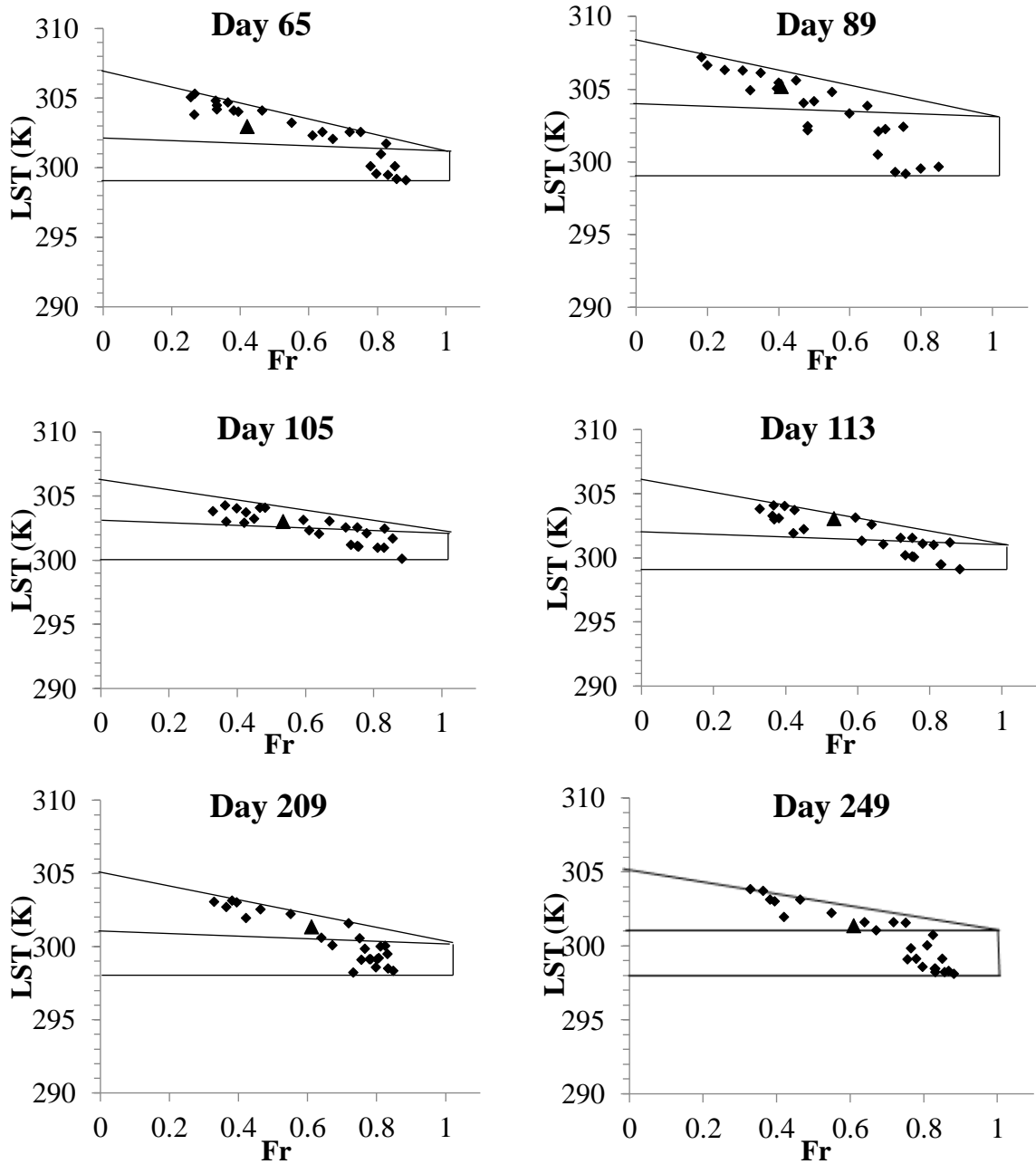


**Figure 5.4: Trapezoidal scatter plots of LST versus Fr for IRI flux tower**

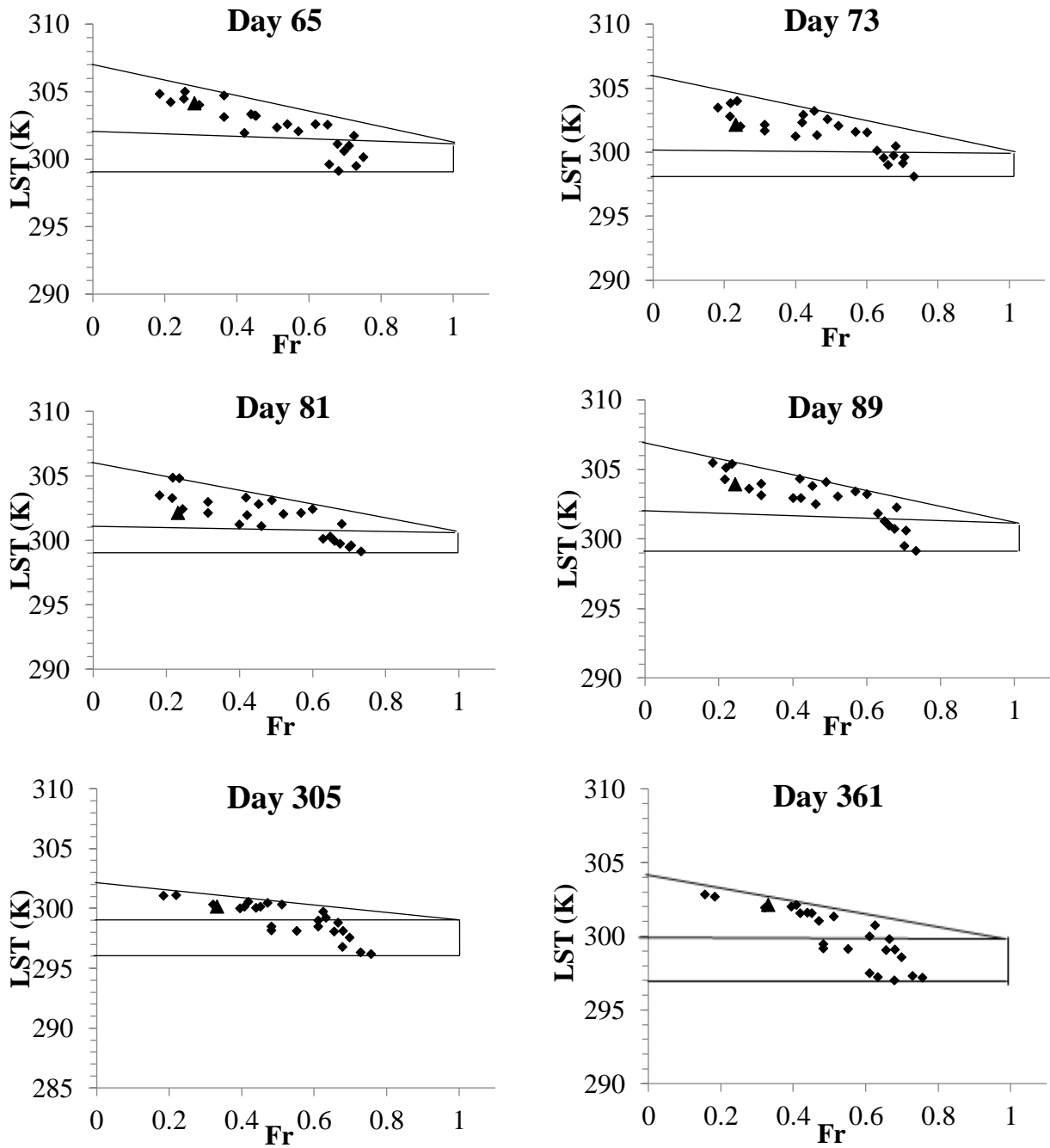


**Figure 5.5: Trapezoidal scatter plots of LST versus Fr for SKR flux tower**

**Table 5.1: LST values extracted from trapezoidal scatter plots on selected dates and times for each flux tower site**

Site	Date	Julian Day	Time (hrs)	LST <sub>min</sub> (K)	LST <sub>max</sub> (K)	LST <sub>c</sub> (K)
MKL	6 Mar 2004	65	11:15	297	305	300
	22 Mar 2004	81	11:15	298	307	302
	30 Mar 2004	89	11:15	298	306	302
	7 Apr 2004	97	11:15	299	308	302
	25 Nov 2004	329	11:15	294	304	299
	11 Dec 2004	345	11:15	295	305	300
PDF	4 Jul 2005	185	11:00	298	307	302
	12 Jul 2005	193	11:00	300	308	303
	20 Jul 2005	201	12:00	299	307	302
	5 Aug 2005	217	12:00	300	309	303
	9 Nov 2005	313	11:00	297	305	300
	17 Nov 2005	321	11:00	298	306	300
IRI	6 Mar 2010	65	11:30	299	307	302
	30 Mar 2010	89	11:30	299	308	304
	15 Apr 2010	105	11:30	300	306	303
	23 Apr 2010	113	12:00	299	306	302
	28 Jul 2010	209	11:00	298	305	301
	6 Sep 2010	249	11:30	298	305	301
SKR	6 Mar 2003	65	11:15	299	307	302
	14 Mar 2003	73	11:15	298	306	300
	22 Mar 2003	81	11:15	299	306	301
	30 Mar 2003	89	12:15	299	307	302
	1 Nov 2003	305	11:15	296	302	299
	27 Dec 2003	361	11:15	297	304	300

Also shown in Table 5.1 are the times at which flux computations were made by the proposed methodology for each date at each site. On comparing these times with the

satellite overpass times for each site shown in Table 3.1, it can be seen that at the MKL site flux computations correspond exactly with the satellite overpass time for all dates. For the other sites, however, on a few dates computations had to be made considering averaging periods which deviated from the satellite overpass times by 30 mins to 60 mins due to non-availability of measured data of  $\lambda ET$  or other climate variables.

### 5.3.3 Computed $G_{s_{max}}$ values

Values of  $G_{s_{max}}$  computed with Equation 4.35 using climatic data measured at each flux tower on the selected dates and times are listed in Table 5.2. The highest value of  $G_{s_{max}}$  across the sites was 0.0132 m/s ( $R_s = 75.76$  s/m) and the lowest was 0.0108 m/s ( $R_s = 92.59$  s/m). High values of  $G_{s_{max}}$  were obtained at the PDF site especially during the monsoon season (Julian Days 193, 201 and 217). This may be due to the fact that this site is located in a tropical evergreen forest with an average annual rainfall of 2231 mm (Table 3.1) and therefore vapor deficit ( $D_a$ ) values are likely to be lower on account of higher moisture availability. On the other hand, at the SKR site which is located in tropical desert climate with annual rainfall of only 1300 mm, the computed values of  $G_{s_{max}}$  were consistently lower due to higher values of  $(R_n - G)$ . At the IRI site, high values of  $G_{s_{max}}$  were obtained even during the summer days, probably on account of irrigation being provided to the paddy crop (Table 3.1). Overall, the range of  $G_{s_{max}}$  values obtained at these tropical sites appear consistent with a value of 0.013 m/s for tropical rainforest reported by Kelliher et al., (1995). However, it is to be noted that since  $G_{s_{max}}$  values have been calculated using only climatic variables (Equation 4.35), the effect of measurement errors cannot be ruled out.

### 5.3.4 Pixel-wise variability of computed $G_s$ and $\lambda ET_{PM}$ values

By setting the minimum value of  $G_{s_{min}} = 0$  and using values of  $G_{s_{max}}$  derived using Equation 4.35 (Table 5.2),  $G_s$  values for each pixel ( $G_{s_i}$ ) in the 5 km  $\times$  5 km area surrounding the flux tower sites were computed using Equations 4.38-4.42. LST constants obtained from the scatter-plots of LST-Fr (Table 5.1) were used in implementing these equations. Minimum, maximum and mean values of  $G_s$  obtained for the 25 pixels around the flux tower for each site and day/time are listed in Table

5.2. For the pixels with high LST, the minimum  $G_s$  values ranged between 0.003 m/s ( $R_s = 333.33$  s/m) and 0.004 m/s ( $R_s = 250$  s/m). For pixels located on the wet edge with minimum values of LST (Fig. 4.5), maximum values of  $G_s$  were equal to the corresponding values of  $G_{s_{max}}$  (Table 5.2). Mean  $G_s$  values varied over the range 0.006 m/s ( $R_s = 166.67$  s/m) and 0.0087 m/s ( $R_s = 114.94$  s/m) across the sites.

Minimum, maximum and mean values of  $\lambda ET_{PM}$  computed using Equation 4.1 for the pixels surrounding the flux tower sites are shown in Figures 5.2 – 5.5 for locations. While the value of  $G_s$  for each pixel was obtained using Equations 4.38 -4.42, climatic variables measured at the flux tower were used as input to Equation 4.1 since the spatial extent of the study area was only 25 km<sup>2</sup>. Therefore, the variation in  $\lambda ET_{PM}$  values across the pixels was solely on account of variations in  $G_s$  values caused by variations in LST and  $G_{s_{max}}$  and not due to variations in climate variables. Despite this, significant spatial variations in  $\lambda ET_{PM}$  values can be seen for all the sites/dates. Across all the pixels and dates, minimum values of  $\lambda ET_{PM}$  ranged between 162.47 W/m<sup>2</sup> and 254.58 W/m<sup>2</sup>, whereas the maximum values varied between 202.68 W/m<sup>2</sup> and 299.79 W/m<sup>2</sup> (Figure 5.6). The minimum mean value of  $\lambda ET_{PM}$  was 165.18 W/m<sup>2</sup> and 282.64 W/m<sup>2</sup>. The highest values of  $\lambda ET_{PM}$  were obtained at the wet PDF site on Julian Day 217 which corresponds to the monsoon season (Figure 5.6). It can be seen from Figure 5.6 that the lowest values of  $\lambda ET_{PM}$  were obtained at the relatively drier MKL site during the summer season. Moderate to low values of  $\lambda ET_{PM}$  were obtained for the other two sites.

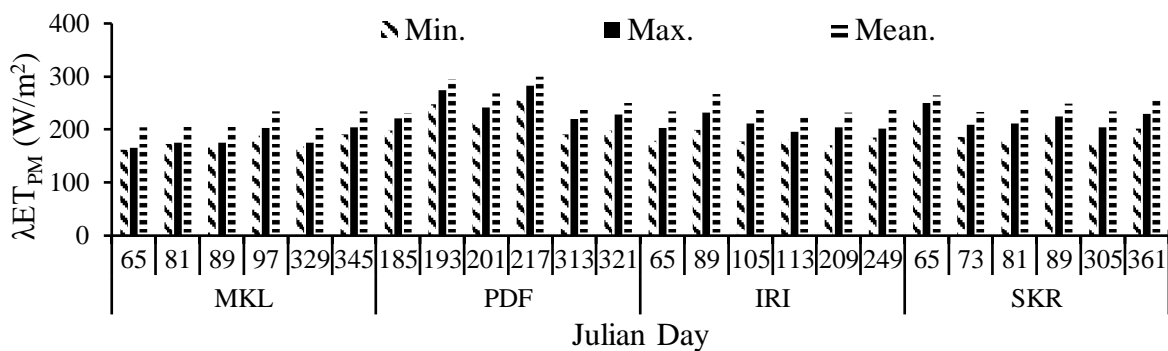


**Figure 5.6: Variability of computed pixel-wise  $\lambda ET_{PM}$  values for selected dates in each flux site area**

**5.3.5 Comparison of computed and measured values of latent heat flux by PM approach**

The accuracy of the instantaneous  $\lambda ET_{PM}$  values estimated by the methodology adopted in this study were assessed through comparison with values of latent heat flux measured at the flux towers ( $\lambda ET_{Meas}$ ). For this purpose,  $\lambda ET_{PM}$  values estimated for the pixels in which the flux towers were located (Fig. 5.2) were extracted and compared with measured instantaneous  $\lambda ET_{Meas}$  values for the averaging period corresponding to or closest to the satellite overpass time for the location of the flux tower (see Article 4.2). Fig. 5.7 depicts these comparisons for the six selected dates separately for the four flux towers.

**Table 5.2: Variability of computed pixel-wise  $G_s$  values for selected dates in each flux site area and values of  $G_{smax}$  computed using Equation 4.35**

Flux Tower	Julian Day	Gs (m/s)		
		Min.	Max.	Mean
MKL	65	0.0034	0.0113	0.0069
	81	0.0032	0.0112	0.0061
	89	0.0032	0.0127	0.0060
	97	0.0038	0.0124	0.0080
	329	0.0038	0.0128	0.0062
	345	0.0035	0.0108	0.0061
PDF	185	0.0032	0.0114	0.0061
	193	0.0037	0.0132	0.0081
	201	0.0035	0.0125	0.0075
	217	0.0038	0.0132	0.0087
	313	0.0039	0.0118	0.0069
	321	0.0040	0.0116	0.0083
IRI	65	0.0038	0.0117	0.0069
	89	0.0033	0.0132	0.0060



	105	0.0040	0.0131	0.0065
	113	0.0040	0.0123	0.0069
	209	0.0039	0.0114	0.0063
	249	0.0039	0.0118	0.0063
SKR	65	0.0033	0.0118	0.0069
	73	0.0035	0.0114	0.0083
	81	0.0034	0.0116	0.0079
	89	0.0034	0.0123	0.0075
	305	0.0030	0.0114	0.0062
	361	0.0030	0.0109	0.0061

Fig. (5.7 a) shows that the PM method consistently overestimates flux values at the MKL site. On the other hand there is consistent underestimation at the PDF site (Fig. 5.7 b) with the deviations being more pronounced for higher values of flux. Lower values of flux are overestimated and higher values are underestimated at the IRI site (Fig. 5.7 c). Fig. (5.7 d) indicates that at the SKR site, estimated values  $\lambda ET_{PM}$  compare favourably with  $\lambda ET_{Meas}$  on all dates except one (Julian day 305) when a large overestimate is obtained. Upon examination, it was found that on this date at the SKR site an extraordinarily large value of  $R_n = 683.59 \text{ W/m}^2$  was recorded at the flux tower which resulted in a high value of  $\lambda ET_{PM}$ .

Since the comparisons depicted in Fig. (5.7) provide only a qualitative assessment of the accuracy of  $\lambda ET_{PM}$  values, a quantitative error assessment was carried out by computing various model performance measures. Considering  $\lambda ET_{PM}$  and  $\lambda ET_{Meas}$  values for six dates at each site, the following performance measures were calculated – coefficient of determination ( $R^2$ ), root mean squared error (RMSE), percent bias (PBIAS) and the intercept (a) and slope (b) terms of a linear regression fit ( $y = a + bx$ ). Results are shown in Table 5.2.

From the results depicted in Fig. 5.7 and Table 5.2 it may be concluded that the PM model (Equation 4.1) implemented with  $G_s$  values derived from the scatter-plot of MODIS LST vs.  $F_r$  yielded instantaneous  $\lambda ET$  values which compared quite favourably with those measured at four flux towers. Model performance measures obtained in this study (Table 5.2) are comparable and in some cases better than those obtained by previous studies involving satellite-based implementations of the PM model. This is notwithstanding the fact that none of the previous studies have focused on tropical regions of south-east Asia. It can be seen from Table 5.3 that the range of  $R^2$  values obtained in the present study (0.85 – 0.96) are higher than those reported in literature and the range of RMSE values obtained (18.27 – 33.79  $W/m^2$ ) are better than the lowest/highest values reported earlier (e.g., Cleugh et al., 2007; Mu et al., 2007; Yebra et al., 2013). The only exception is the recent study by Amazirh et al., (2017) in which RMSE values between 12 – 13  $W/m^2$  were obtained for irrigated wheat crops in Morocco.

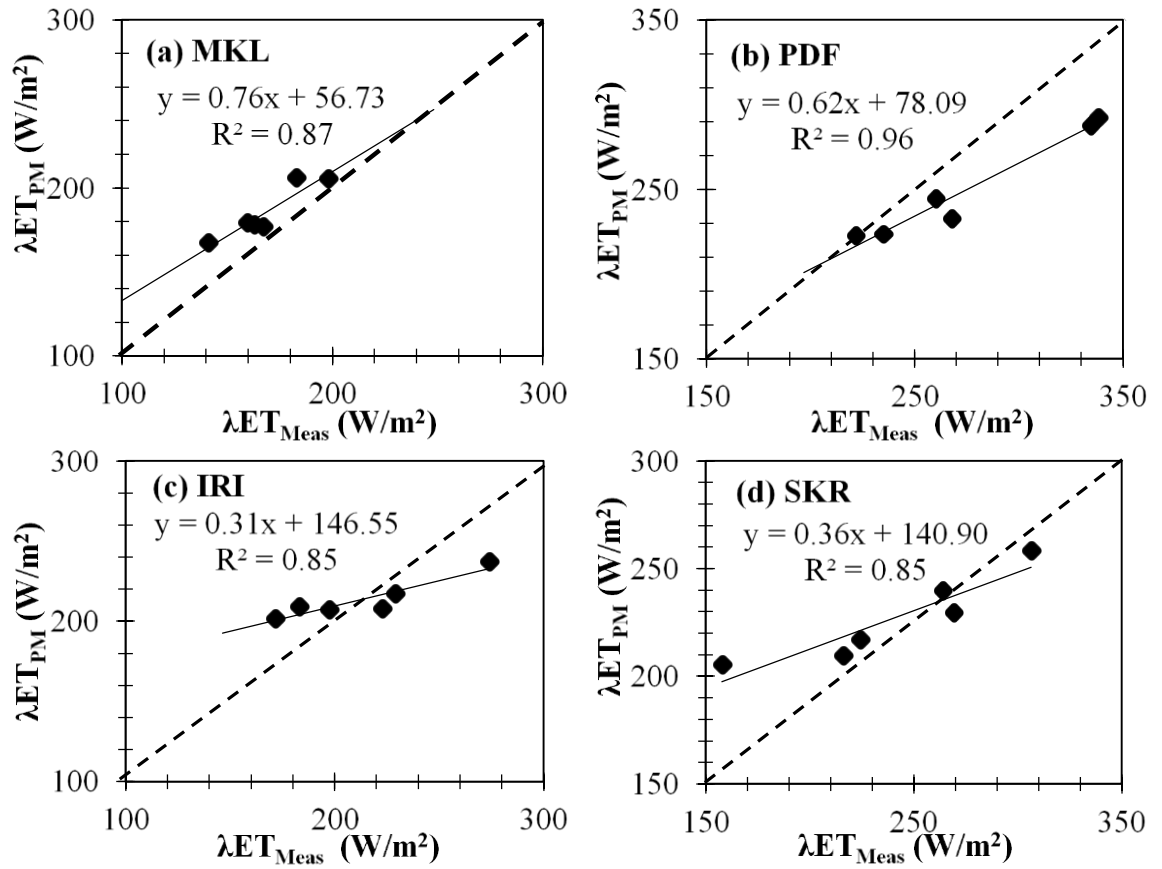


**Figure 5.7: Comparison of instantaneous latent heat flux values computed by the Penman-Monteith method proposed in the present study ( $\lambda ET_{PM}$ ) with those measured ( $\lambda ET_{Meas}$ ) on selected dates/times at the flux towers located at MKL (b) PDF (c) IRI and (d) SKR**

**Table 5.3: Performance measures computed using latent heat flux values measured on six dates at each of the four flux towers ( $\lambda ET_{Meas}$ ) and flux values obtained by the approach proposed in the present study ( $\lambda ET_{PM}$ )**

Flux Tower	R <sup>2</sup>	RMSE (W/m <sup>2</sup> )	PBIAS (%)	a	b
MKL	0.87	18.27	10.05	56.73	0.76
PDF	0.96	31.42	-9.31	78.09	0.62
IRI	0.85	23.74	0.26	146.55	0.31
SKR	0.85	33.79	-5.44	140.90	0.36

**Table 5.4: Performance measures computed using latent heat flux values measured on six dates at each of the four flux towers ( $\lambda ET_{Meas}$ ) and flux values obtained by the PT ( $\lambda ET_{PT}$ ), PMC ( $\lambda ET_{PMC}$ ) and PML ( $\lambda ET_{PML}$ ) approaches**

Flux Tower	PT approach					PMC approach					PML approach				
	$R^2$	RMSE (W/m <sup>2</sup> )	PBIAS (%)	a	b	$R^2$	RMSE (W/m <sup>2</sup> )	PBIAS (%)	a	b	$R^2$	RMSE (W/m <sup>2</sup> )	PBIAS (%)	a	b
MKL	0.94	18.34	10.46	48.98	0.81	0.88	22.71	12.91	57.68	0.79	0.86	21.50	12.07	59.10	0.77
PDF	0.87	27.12	-6.30	91.43	0.61	0.96	36.22	-11.21	78.54	0.60	0.95	36.11	-11.27	73.74	0.62
IRI	0.77	23.59	2.16	144.06	0.35	0.76	25.38	-1.86	149.63	0.28	0.82	25.34	-2.23	148.77	0.27
SKR	0.72	32.70	-3.60	141.24	0.37	0.86	36.19	-7.37	138.87	0.35	0.86	36.43	-7.70	137.08	0.35

### 5.3.6 Comparison with Laxmi and Nandagiri (2014)

From results shown in Table 5.4, it can be seen that the PT approach yielded more accurate estimates of  $\lambda ET_{PT}$  in comparison to the PMC and PML approaches. Although  $R^2$  values were higher for both the PMC and PML methods, RMSE and PBIAS values were lower for the PT approach. Also, a and b values were slightly superior for the PT method.

Comparison of results for the PT approach (Table 5.4) with those for the PM model of the present study (Table 5.3) it can be seen that in terms of  $R^2$  the PM model was better at all flux tower sites except MKL. However, in most cases the PT approach yielded lower values of RMSE indicating slightly higher accuracy. For the present approach PBIAS values were lower for the MKL and IRI sites but higher for the other two sites. Values of a and b were very similar for both approaches. Overall, it can be said that for the dataset used in this study, both the PM model of the present study and the PT model of Laxmi and Nandagiri (2014) performed on par.

### 5.3.7 Comparison with Cleugh et al., (2007)

Application of the PMC method (Equations 4.43 and 4.1), yielded optimal values of  $c_L = 0.0020, 0.0015, 0.0025$  and  $0.0015$  for the MKL, PDF, IRI and SKR sites respectively. Performance of the model was evaluated by computing  $R^2$ , RMSE, PBIAS, a and b statistics using  $\lambda ET_{PMC}$  and  $\lambda ET_{Meas}$  values at each flux tower for the selected times and dates. Results of the performance evaluation of the PMC approach are shown in Table 5.4 and may be compared with the methodology of the present study. In terms of  $R^2$ , the PMC method yields higher values at the MKL and SKR sites in comparison the method proposed in the present study. At the IRI site, the value of  $R^2$  is lower for the PMC method and the same value of  $R^2$  is yielded by both methods at the PDF site. On the other hand, the PMC method yields higher values of both RMSE and PBIAS at all four sites in comparison to the present method indicating the slight superiority of the latter approach. Small differences exist in statistics a and b between the two approaches. Overall, it can

be seen that the PMC method performs reasonably well in reproducing the magnitudes of  $\lambda ET$  at all the flux tower sites.

### 5.3.8 Comparison with Leuning et al., (2008)

However, methodology is been described in Chapter 4, despite being biophysically-based, use of the Leuning et al., (2008) bulk conductance model with the PM equation requires optimization of model parameters using observed ET values. Furthermore, since their approach is data intensive and involves use of six unknown parameters, accuracy of estimated ET values may be constrained by associated uncertainties.

In implementing the PML approach, optimal values of  $f = 0.60, 0.80, 0.80$  and  $0.70$  were obtained for the MKL, PDF, IRI and SKR sites respectively. Performance statistics of the PML model computed using  $\lambda ET_{PML}$  and  $\lambda ET_{Meas}$  values at each flux tower for the selected times and dates are listed in Table 5.4.

From the results shown in Tables 5.3 and 5.4, it can be seen that values of  $R^2$  obtained in the present study are higher at all sites except the SKR site where the PML approach yields a marginally higher value. On the other hand, RMSE values obtained by the present approach are significantly lower, so also values of PBIAS. In terms of performance statistics a and b, marginal differences exist between the two approaches. Overall, it is evident that the performance of the approach proposed in the present study is comparable and somewhat better than the PML approach for the data used in this study.

From Tables 5.3 and 5.4 it can be seen that although the magnitudes of PBIAS values differ between the four approaches tested, the sign remains the same for all sites except one indicating that nature of bias (under-estimation or over-estimation) is the same. A discussion on the possible reasons for bias is presented in the subsequent section of this chapter.

### 5.3.9 Discussion

From the results shown in Tables 5.3 and 5.4 it is clear that the performances of all four approaches tested (present study, PT, PMC and PML) are more or less the same with the performance of the proposed LST-Fr approach being slightly superior for the dataset used in this study. However, two aspects need to be highlighted in evaluating relative model performances: 1) both the PMC and PML approaches use empirical relationships of varying complexity to estimate  $G_s$  from LAI data which require on-site calibration with measured flux data. Also, it is interesting to note from Table 5.4 that the single parameter  $G_s$ -LAI relationship of Cleugh et al., (2007) (PMC approach) performs on par with the more complex relationship proposed by Leuning et al., (2008) (PML approach). Given the fact that LAI values which are used as input in the PMC approach vary over a limited range especially for forests, it appears that a constant value of  $G_s$  determined via calibration is able to estimate the magnitudes of  $\lambda ET$  at a given location with reasonable accuracy. While calibration ensures satisfactory performance, it limits the general applicability of both methods notwithstanding some efforts by Leuning et al., (2008) to assign parameter values based on general vegetation classes. On the other hand, the performance of the methodology proposed in this study must be viewed in the context that it is calibration-free and yet provides accurate estimates of  $\lambda ET$  at all four flux tower sites 2) it is well known that moisture levels exert significant influence on  $G_s$  and accounting for this in the  $\lambda ET$  estimation procedure will provide a more physically-based approach. In this regard, among the four approaches considered, only the methodology proposed in the present study considers the effect of moisture variability on  $G_s$  since implicit in the LST-Fr plot (Figure 4.5) is an inverse relationship between LST and moisture. This may be the reason for the slightly superior performance of the present method (Table 5.3).

Also, it is likely that  $G_a$  computed using Equation 4.31 may have been the cause for the consistent bias. For example, Leuning et al., (2008) note that atmospheric stability can modify  $G_a$  values by up to  $\pm 25\%$ . Schellekens et al., (2000) found that the PM model yielded significantly low wet canopy  $\lambda ET$  in a tropical rain forest in Puerto Rico most likely on account of advection, low  $G_a$  and rainfall. Furthermore, errors in PM model

estimates at low to intermediate values of  $Da$  have been reported by Whitley et al., (2009) and Cleverly et al., (2013) in Australia. Pending further investigations on the accuracy of  $G_a$  values computed using Equation 4.31 in wet tropical regions, results of the present study can only confirm that the source of bias in  $\lambda ET$  estimates cannot be attributed to the  $G_s$  parameter. The role of instrumental, measurement and computational errors, both systematic and random, in Eddy Covariance flux tower measurements of climate variables and  $\lambda ET_{Meas}$  cannot be ruled out.

It may be concluded that from the Table 5.4 results that the PT model (Eq. 4.2) implemented with  $\phi$  values derived from the scatter-plot of MODIS LST versus  $Fr$  yielded favorably good  $\lambda ET$  results when at four flux towers. Model performance by PT approach for tropical regions of south-east Asia obtained in this study (Table 5.4) is showing favorably good results than those obtained by previous studies. For example, Nishida et al., (2003) applied the PT model for estimating EF and reported after validation of the algorithm by using AmeriFlux stations data as standard error = 0.17 and  $R^2 = 0.71$ . Wang et al., (2007) enhanced the applicability of the Priestley-Taylor method of Jiang and Islam (2001) and results show that ET can be reasonably predicted with a correlation coefficient that varies from 0.84 to 0.95 and a bias that ranges from 3  $W/m^2$  to 15  $W/m^2$  and RMSE varying from 30  $W/m^2$  to 40  $W/m^2$ . Tang et al., (2010) applied the parameterization of Jiang and Islam (1999) in which results indicated that their approach was accurate enough at least in most cases for the estimation of regional AET by showing RMSE of this comparison as 25.07  $W/m^2$ . Yao et al., (2011) developed a triangular VI method to estimate the PT parameter for AET estimation in arid and semi-arid regions and the bias of estimated daily ET deviating from the corresponding ground-measured ET is -8.66  $W/m^2$  and the RMSE is 21.55  $W/m^2$ . Laxmi and Nandagiri (2014) estimated actual evapotranspiration (AET) by an approach based on the PT method and comparison of estimated and measured fluxes in 2003 yielded root mean square error (RMSE) of 64.73  $W/m^2$  which reduced to 18.65  $W/m^2$  when one day was treated as an outlier because of instrument error. From Table 5.4, It can be seen that the range of  $R^2$  values obtained for PT approach from Table 5.4 (0.72 – 0.94) are well than those reported in the literature and the range of RMSE values obtained (18.34 – 32.70  $W/m^2$ ) are good than the values reported earlier.



Despite providing accurate estimates of instantaneous latent heat flux at all four tower sites (Figure 5.7, Tables 5.3 and 5.4) the methodology proposed in this study appears to exhibit a weakness in terms of a consistent bias in flux estimates at all four sites. However, as pointed out earlier, the PT, PMC and PML methodologies also exhibited the same pattern of bias which implies that the source of bias is apparently not the  $G_s$  estimation methodology but possible discrepancies in the implementation of Equation 4.1 and/or errors in measured flux values.

## CHAPTER 6

## APPLICATION TO THE HEMAVATHI SUB-BASIN

**6.1 GENERAL**

Satellite remote sensing technology is recognized to map AET regional to large scale patterns in an economically feasible manner. The present study was taken up to estimate actual evapotranspiration (AET) by Penman-Monteith (PM) model and Priestley-Taylor (PT) models using Moderate Resolution Imaging Spectroradiometer (MODIS) satellite data and to compare performances with MOD16 Global Terrestrial Evapotranspiration Data Set (MOD16A2). The PM method proposed in the present study, the PT method (Laxmi and Nandagiri, 2014) and the PMCH method (Choudhary et al., 1986) were implemented in the Hemavathi sub-basin to map spatial patterns of daily AET. Relevant MODIS products were downloaded and sub-setted to the basin area and climate records for the Belur station were used for the purpose. The analysis was carried out for two dates in summer and two dates in winter separately for the years 2007 and 2012. These years were selected since the year 2007 experienced relatively high rainfall during summer and winter than the year 2012. The dates selected were Julian days 57, 65, 345 and 353 separately for the years 2007 and 2012 (total of 8 days). For each date, trapezoidal scatter plots of MODIS-derived LST values versus Fr were plotted by considering 1 km<sup>2</sup> pixels in the study area of 304 km<sup>2</sup>. Values of LST<sub>min</sub>, LST<sub>max</sub>, and LST<sub>c</sub> which are required for the pixel-wise estimation of G<sub>s</sub> and  $\phi$  values were extracted from the trapezoidal plots.

**6.2 APPLICATION OF THE VALIDATED PM AND PT ALGORITHMS**

Implementation of Equations 4.1 to 4.46 using MODIS data along with climate data yielded AET values for each pixel in the Hemavathi sub-basin for the selected dates. Detailed characteristics of the study area and data used to code the algorithm in MATLAB are given in Chapters 3 and 4. The final objective is to apply the validated PM and PT (Laxmi and Nandagiri, 2014) models to estimate AET in a Sub-humid

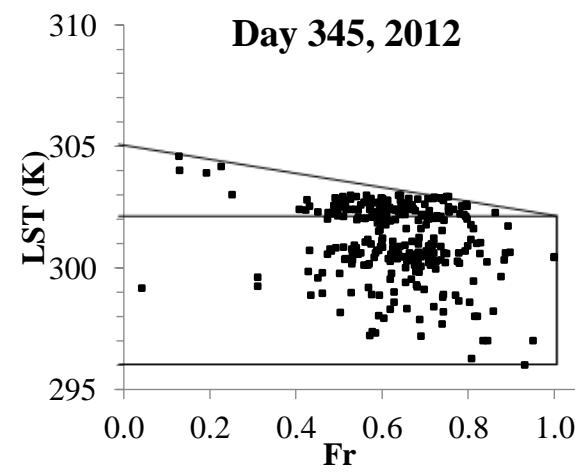
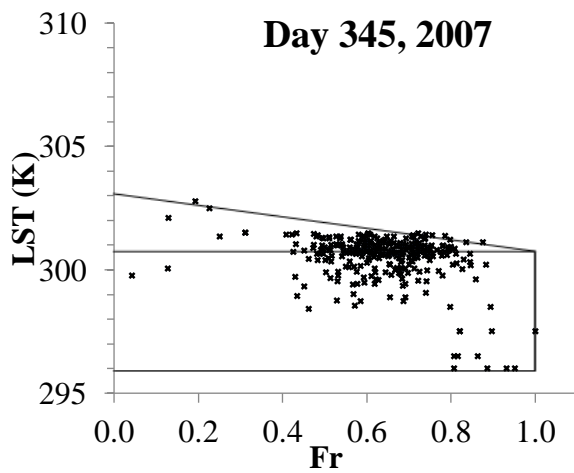
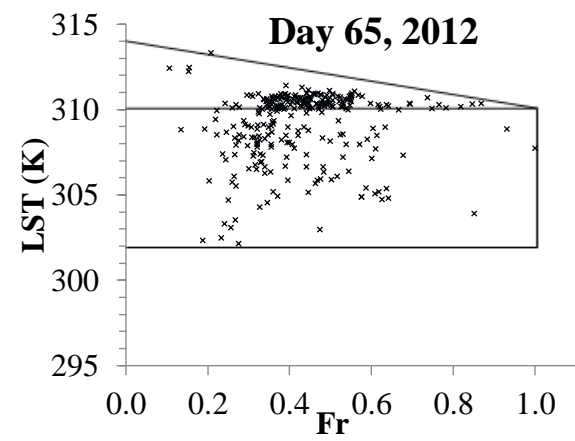
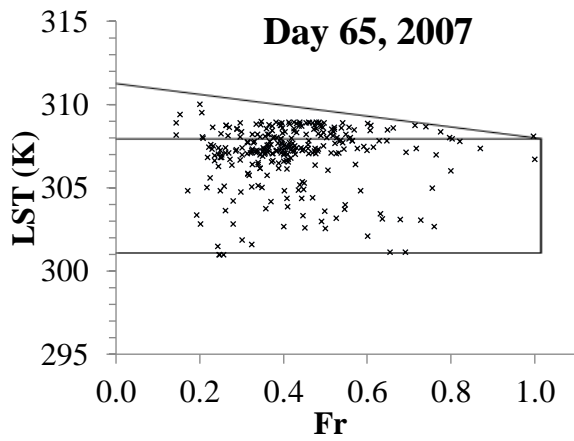
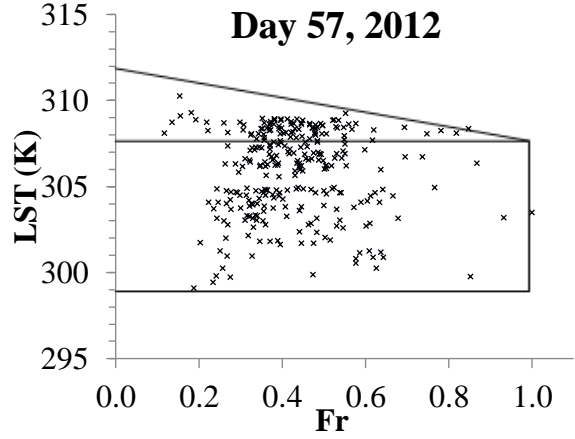
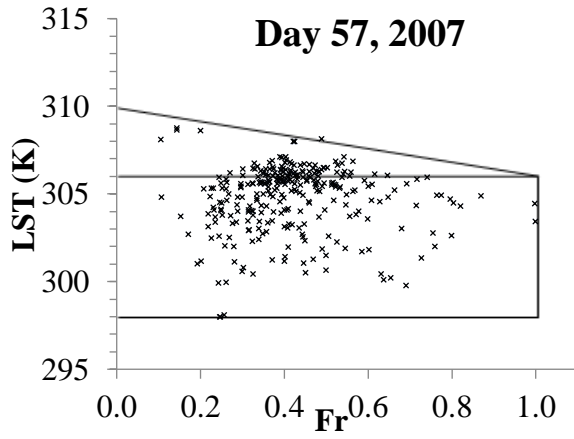
tropical Hemavathi sub-basin and to compare the results with MOD16A2 data are discussed.

For each day, estimated AET values by the PT approach ( $AET_{PT}$ ), PM model of the present study with  $G_a$  computed using Leuning et al. (2008) equation ( $AET_{PM}$ ) and with  $G_a$  computed using Choudhary et al. (1986) equation ( $AET_{PMCH}$ ) for each of the 304 pixels were extracted and compared with the corresponding pixel-wise MOD16A2 ET estimates. Accuracies of estimated AET values obtained by the relative to MOD16 estimates were assessed by computing performance statistics of  $R^2$ , RMSE, PBIAS and a and b values.

## 6.3 RESULTS AND DISCUSSION

### 6.3.1 LST-Fr scatter plots

To validate the applicability of the proposed trapezoidal approach methodology to estimate  $G_s$  and  $\phi$ , two days in each of summer and winter season of 2007 and 2012 were selected. Table 6.1 lists the LST values for the selected dates. For each date, trapezoidal scatter plots of MODIS-derived LST values with altitudinal corrections versus Fr were plotted for each selected date considering study area of 304 km<sup>2</sup>. Out of the eight dates scatter plots derived in this manner, for the sake of brevity, one sample plot for summer and winter of 2007 and 2012 is shown in Fig. (6.1). As per the methodology, trapezoidal scatter plots of LST versus Fr values were plotted. Values of  $LST_{min}$ ,  $LST_{max}$ , and  $LST_c$  which are required for the estimation of pixel-wise values of  $G_s$  and  $\phi$  using Eqs. (4.38) To (4.42) have to be inferred from the trapezoidal plots of LST versus Fr. However, Fr values exhibited significant seasonal changes due to wetness and temperature conditions. LST values of  $LST_{min}$ ,  $LST_{max}$ , and  $LST_c$  were derived from the trapezoidal scatter plots in Figure (6.1). It was observed from Figure 6.1 that trapezoidal scatter plots exhibited Fr and LST pixelwise variations with respect to the different seasons due to wetness and temperature conditions.



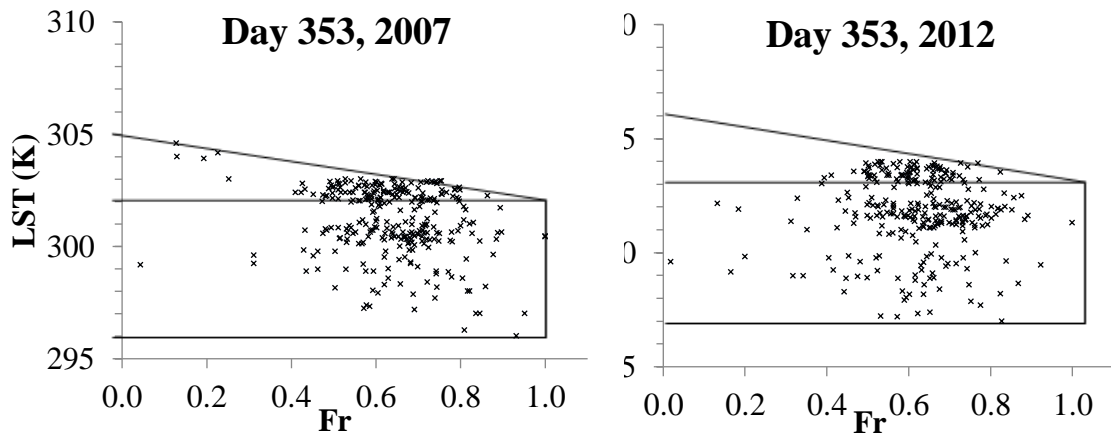


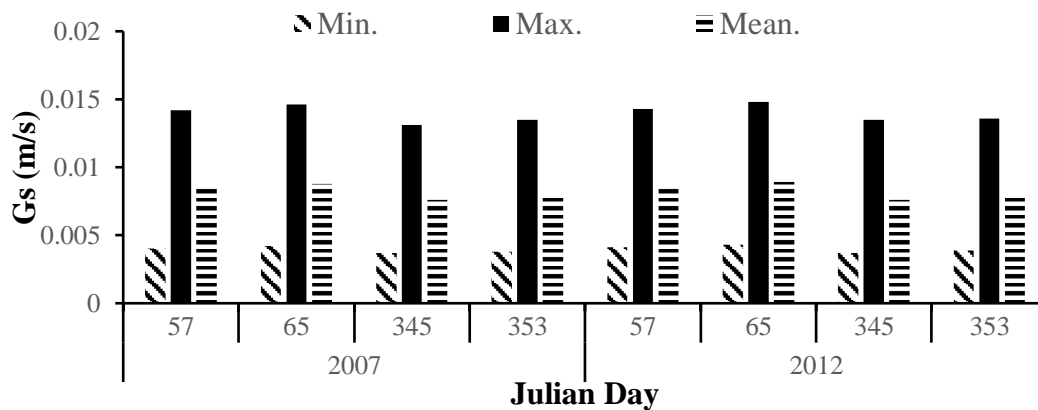
Figure 6.1: Trapezoidal scatter plots of LST versus Fr

Table 6.1: LST values extracted from trapezoidal scatter plots on selected dates

Year	Date	Julian day	LST <sub>min</sub> (K)	LST <sub>max</sub> (K)	LST <sub>c</sub> (K)
2007	26-Feb	57	298	310	306
	6-Mar	65	301	311	308
	11-Dec	345	296	303	301
	19-Dec	353	296	305	302
2012	26-Feb	57	299	312	308
	5-Mar	65	302	314	310
	10-Dec	345	296	305	302
	18-Dec	353	297	306	303

### 6.3.2 Pixel-wise variability of computed $G_s$ and $\phi$ with AET values

LST values obtained from the scatter-plots of LST-Fr (Table 6.1) were used in deriving minimum, maximum and mean values of  $G_s$  with AET values obtained. Minimum  $G_s$  values from Figure 6.2 ranged between 0.0037 and 0.0043 were observed for the pixels with high LST and low moisture content. Maximum  $G_s$  values ranged between 0.0131 and 0.0148 were observed for the pixels with minimum LST on the wet edge (Fig. 4.5). Mean  $G_s$  values varied over the range 0.0076 and 0.0089 across the sites depending on the wetness and temperature conditions.



**Figure 6.2: Variability of computed pixel-wise min, max and mean  $G_s$  values and values of  $G_{smax}$  computed using Eq. 4.35**

Estimated AET minimum, maximum and mean values for the pixels in the study are shown in Figure 6.3. Across all the pixels and dates for PMCH approach, minimum values of AET ranged between 1.85 mm and 2.14 mm, whereas the maximum values varied between 4.11 mm and 5.32 mm (Figure 6.3). The mean values of AET ranged between 2.45 mm and 3.11 mm. The highest values of AET is obtained for the high LST, which corresponds to the summer season of Julian day 65, 2012. It can be seen that the lowest values of AET were obtained in the winter season due to low LST and less moisture.

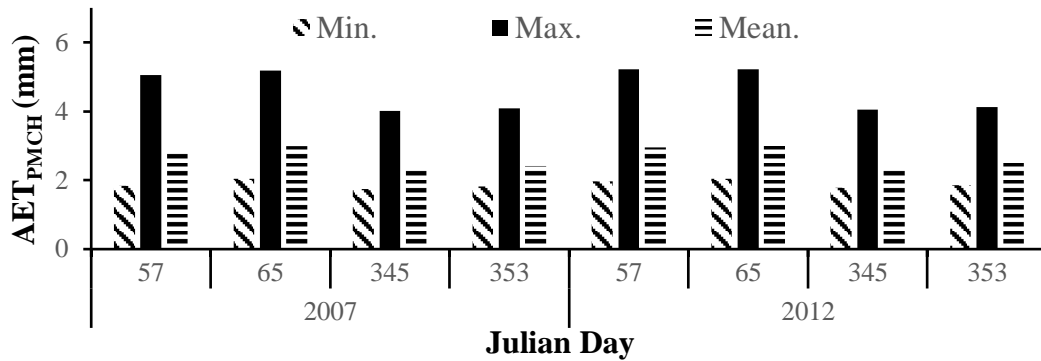


**Figure 6.3: Variability of computed pixel-wise min, max and mean  $AET_{PMCH}$  values**

Similarly, LST values obtained from the scatter-plots of LST-Fr (Table 6.1) were used in deriving minimum, maximum and mean values of  $\phi$  with AET values were obtained. Minimum  $\phi$  values from Figure 6.4 ranged between 0.25 and 0.38 were observed for the pixels with high LST and low moisture content. Maximum  $\phi$  values are 1.26 observed for the pixels with minimum LST on the wet edge (Figure 4.5). Mean  $\phi$  values ranged between 0.71 and 0.89 across the sites depending on the wetness and temperature conditions.

Estimated AET minimum, maximum and mean values for the pixels in the study area are shown in Figure 6.5. Across all the pixels and dates for PT approach, minimum values of AET ranged between 1.98 mm and 2.27 mm, whereas the maximum values varied between 4.21 mm and 5.47 mm (Figure 6.5). The mean values of AET ranged between 2.58 mm and 3.06 mm. The highest values of AET is obtained for the high LST, which corresponds to the summer season of Julian day 65, 2012. It can be observed that the lowest values of AET were obtained in the winter season due to low LST and less moisture.

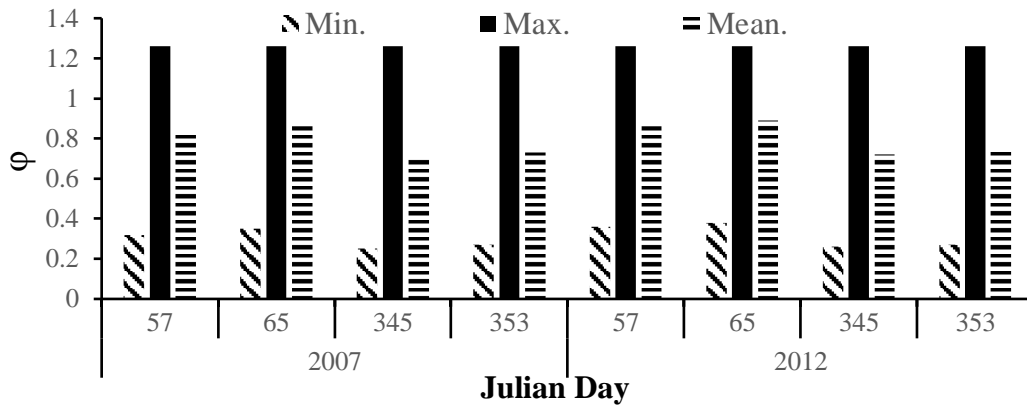


Figure 6.4: Variability of computed pixel-wise min, max and mean  $\phi$  values

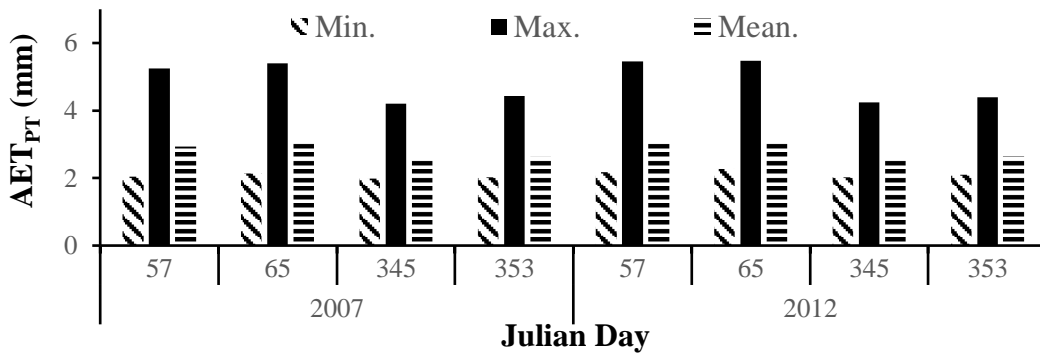
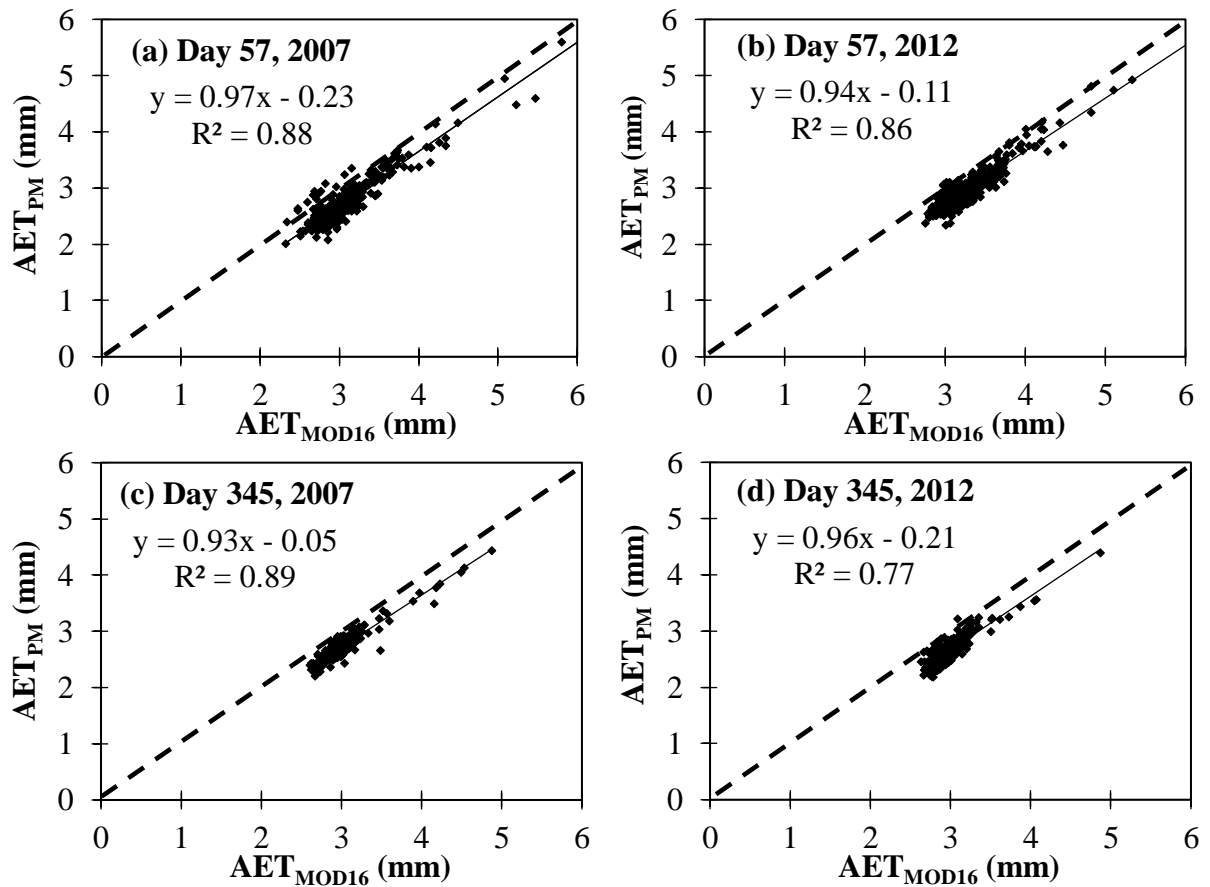


Figure 6.5: Variability of computed pixel-wise min, max and mean  $AET_{PT}$  values

### 6.3.3 Pixelwise comparison of estimated AET by PM and PT and approaches with MOD16A2

Estimated AET values by PM and PT models for the 304 pixels were extracted and compared with MOD16A2 pixelwise for the study area. AET estimated by PM, PT and PMCH models is compared with MOD16A2 shown in Figures 6.6, 6.7 and 6.8, the following performance measures results were calculated and tabulated in Table 6.2 – coefficient of determination ( $R^2$ ), root mean squared error (RMSE), percent bias (PBIAS) and the intercept (a) and slope (b) terms of a linear regression fit ( $y = a + bx$ ).





**Figure 6.6: Comparison of average AET estimated by PM and MOD16A2 for sample days (a) Day 57, 2007 (b) Day 57, 2012 (c) Day 345, 2007 (d) Day 345, 2012**

Fig. (6.6) AET estimated by MOD16 Global Terrestrial Evapotranspiration Data Set is found to be higher than PM approach for all the days and LU/LC classes by yielding good correlation coefficient ( $R$ ) of 0.77 to 0.90, RMSE of 0.28 to 0.38 mm and PBIAS of -7.04 % to -12.41 %. Results of the performance evaluation of the  $AET_{PM}$  approach are shown in Table 6.2 and is being compared with the PMCH approach. PM method yields slightly higher values of both RMSE and PBIAS when compared with PMCH approach due to the overestimation of  $G_a$ .

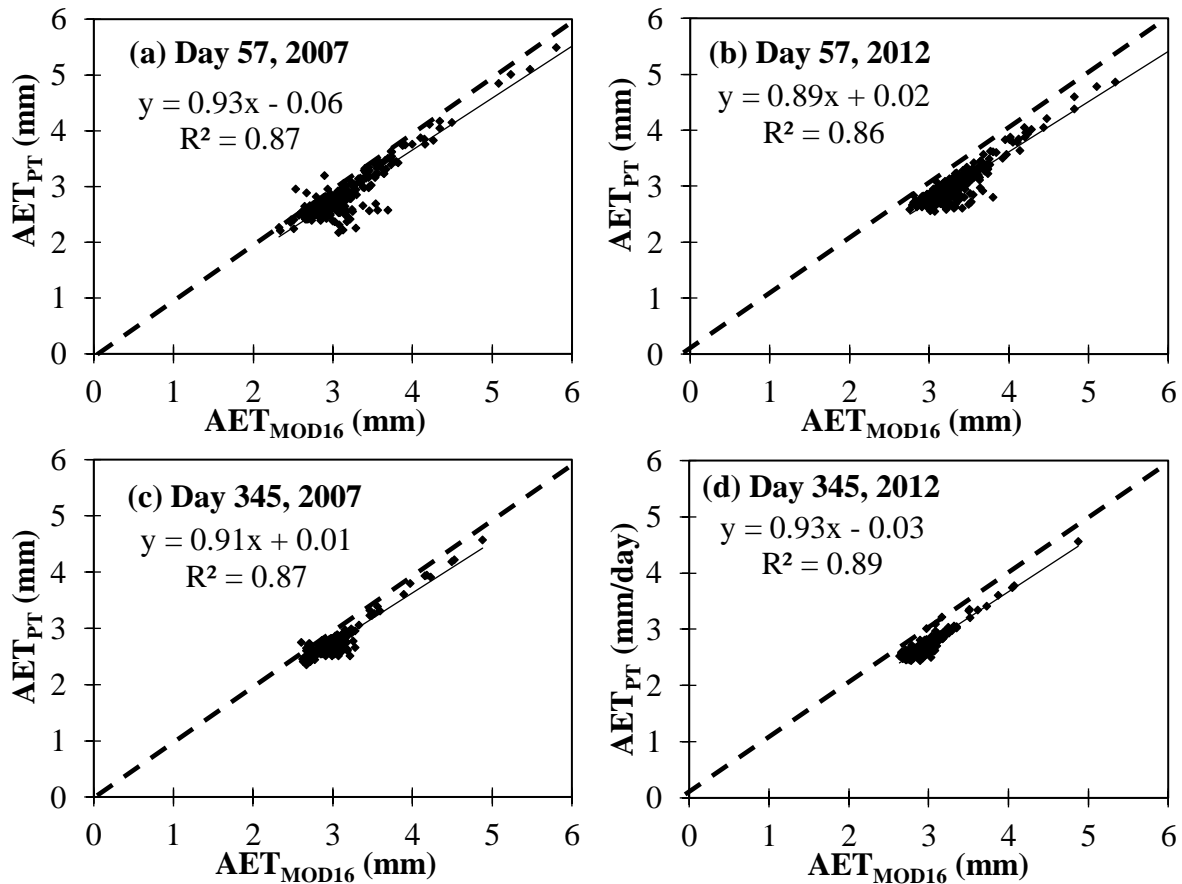


**Figure 6.7: Comparison of average AET estimated by PT and MOD16A2 for sample days (a) Day 57, 2007 (b) Day 57, 2012 (c) Day 345, 2007 (d) Day 345, 2012**

Fig. (6.7) AET estimated by MOD16 Global Terrestrial Evapotranspiration Data Set is found to be higher than Priestley-Taylor approach for all the days and LU/LC classes by yielding good correlation coefficient (R) of 0.84 to 0.89, RMSE of 0.27 to 0.35 mm and PBIAS of -8.27 % to -10.06 %. Results of the performance evaluation of the  $AET_{PT}$  approach are shown in Table 6.2. PT method yields reasonably lower values of both RMSE and PBIAS for all the selected days of summer and winter seasons when compared with PM approach.

### 6.3.4 Aerodynamic conductance estimation by Choudhary et al., (1986)

Performance evaluation of AET estimation methods relative to MOD16A2 estimates shows that the PM model proposed in the present study with  $G_a$  computed using the Leuning et al. (2008) equation ( $AET_{PM}$ ) performed reasonably well but yielded slightly high values of PBIAS. A similar finding was noted with regard to the PM, PMC and PML models when tested with flux tower data (Chapter 5). As pointed out in Article 5.3.9, it was felt that the aerodynamic conductance ( $G_a$ ) could be a possible reason for this bias. Therefore, alternative equations for computing  $G_a$  were identified from a review of literature (Thom, 1975; Verma et al., 1976; Hatfield et al., 1983; Mahrt and Ek, 1984; Choudhary et al., 1986; Xie, 1988; Viney, 1991; Yang et al., 2001). Liu et al., (2007) evaluated the relative performances of various  $G_a$  equations and found that the equation proposed by Choudhary et al., (1986) yielded reasonably accurate estimates with low RMSE, which was simple and requires fewer data inputs compared to other methods. Therefore, the Choudhary et al., (1986) equation for  $G_a$  was selected as an alternative to the Leuning et al. (2008) equation for  $G_a$ .

Accordingly, the Choudhary et al., (1986) approach involving the application of Equations 6.1, 4.46 and 4.1 to obtain estimates of AET was implemented in the present study area (hereinafter referred to as PMCH).

Aerodynamic conductance was estimated as per Choudhary et al., (1986).

$$G_a = \frac{k^2 u_z}{\ln \left[ \frac{(z_m - d)}{z_{om}} \right] \ln \left[ \frac{(z_m - d)}{z_{ov}} \right]} (1 - \beta Ri_B)^{-3/4} \quad (6.1)$$

$$Ri_B = \frac{g}{Ta} \frac{(Ta - Ts) (z_m - d)}{u_z^2} \quad (6.2)$$

Where  $z_m$  = height of wind speed and humidity measurements (m),  $d$  = zero plane displacement height (m),  $z_{om}$  and  $z_{ov}$  = roughness lengths governing the transfer of momentum and water vapor (m),  $k$  = von Karman's constant (0.41),  $u_z$  = wind speed at height  $z_m$  (m/s). As suggested by Leuning et al., (2008), other variables were obtained as  $d = 2h/3$ ,  $z_{om} = 0.123h$  where  $h$  is canopy height,  $z_{ov} = 0.1z_{om}$ ,  $Ri_B$  = Richardson

number,  $T_a$  = air temperature ( $^{\circ}\text{C}$ ),  $T_s$  = surface temperature ( $^{\circ}\text{C}$ ),  $g$  = gravitational acceleration ( $\text{m/s}^2$ ) and  $\beta$  = thermal expansion coefficient taken as 5.

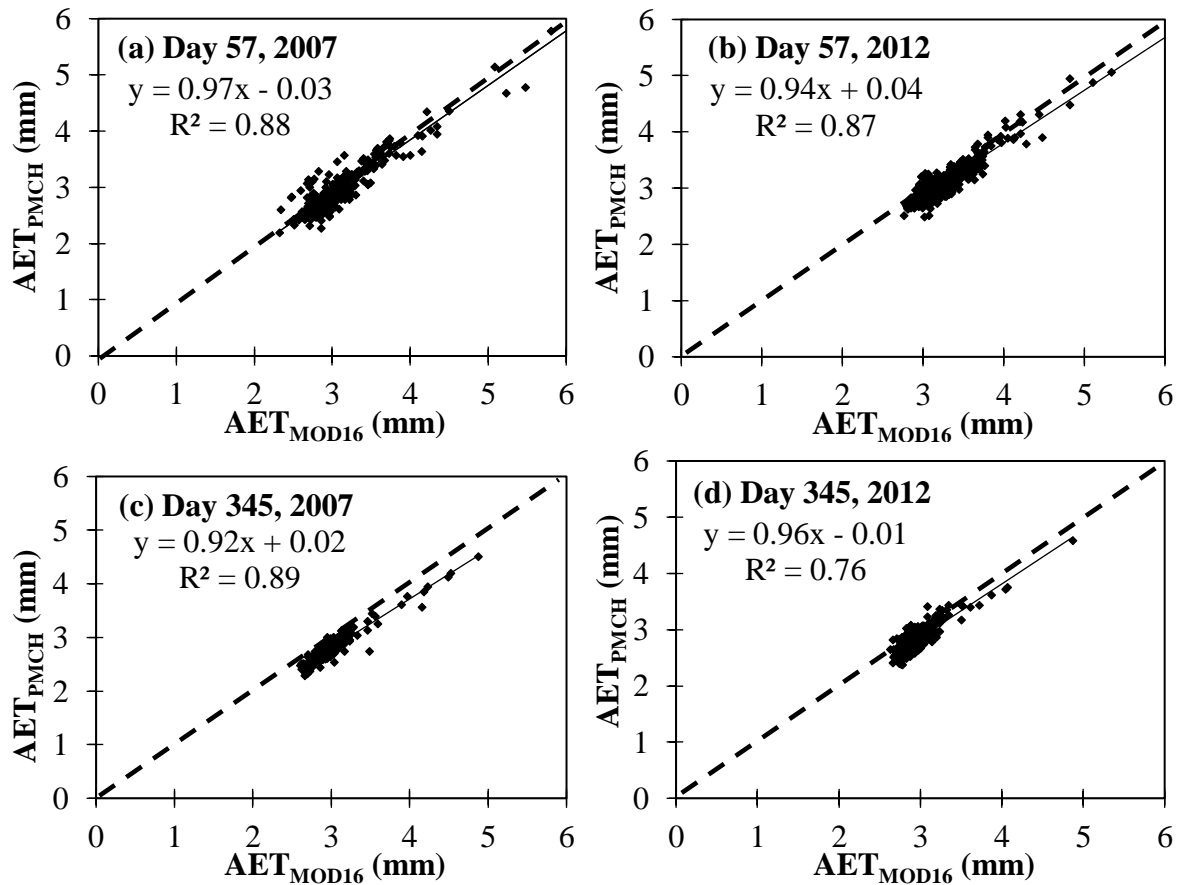


**Figure 6.8: Comparison of average AET estimated by PMCH and MOD16A2 for sample days (a) Day 57, 2007 (b) Day 57, 2012 (c) Day 345, 2007 (d) Day 345, 2012**

Fig. (6.8) AET estimated by MOD16 Global Terrestrial Evapotranspiration Data Set is found to be higher than PMCH approach for all the days and LU/LC classes by yielding good correlation coefficient ( $R$ ) of 0.76 to 0.90, RMSE of 0.19 to 0.25 mm and PBIAS of -2.64 % to -7.74 %. Results of the performance evaluation of the AET<sub>PMCH</sub> approach are shown in Table 6.2 is being compared with the PM approach of the present study. PMCH method yields lower values of both RMSE and PBIAS for all the dates in comparison to the present PM method indicating reasonably accurate results. The PM model proposed in the present study with  $G_a$  computed using the Choudhary et al. (1986) equation turned out to be the best model as indicated by the lowest values of RMSE, although  $R^2$  were similar. Also, use of the Choudhary et al. (1986) equation

reduced PBIAS values significantly for all days considered (Table 6.2). Small differences exist in statistics a and b between the two approaches. Overall, it can be seen that the PMCH method performs reasonably well in reproducing the magnitudes of AET for all the selected days of summer and winter seasons.

Results of the performance evaluation of AET estimation methods relative to MOD16A2 estimates are shown in Table 6.2. It can be seen that the PM model proposed in the present study with  $G_a$  computed using the Leuning et al. (2008) equation ( $AET_{PM}$ ) performed reasonably well for both the wet and dry years. High values of  $R^2$  and reasonably low values of RMSE were obtained but the PBIAS values were somewhat high. Also, it can be seen from Table 6.2 that the PM model yielded relatively poorer estimates for the winter days of the drier year 2012. The performance of the PT model was quite similar to the PM model with similar performance statistics being recorded. However, slightly lower RMSE values were obtained for this model on some days. The PM model proposed in the present study with  $G_a$  computed using the Choudhary et al. (1986) equation turned out to be the best model as indicated by the lowest values of RMSE, although  $R^2$  were similar. Also, use of the Choudhary et al. (1986) equation reduced PBIAS values significantly for all days considered (Table 6.2).

**Table 6.2: Performance measures computed comparing pixel-wise MOD16A2 values in the Hemavathi sub-basin on eight dates with AET estimates obtained by the PM ( $AET_{PM}$ ), PT ( $AET_{PT}$ ) and PMCH ( $AET_{PMCH}$ ) approaches**

Year	Julian Day	PM					PT					PMCH				
		R <sup>2</sup>	RMSE (mm)	PBIAS (%)	a	b	R <sup>2</sup>	RMSE (mm)	PBIAS (%)	a	b	R <sup>2</sup>	RMSE (mm)	PBIAS (%)	a	b
2007	57	0.88	0.38	-10.31	-0.23	0.97	0.87	0.34	-9.03	-0.06	0.93	0.88	0.23	-4.08	-0.03	0.97
	65	0.90	0.36	-8.73	-0.13	0.95	0.88	0.35	-8.27	-0.05	0.93	0.90	0.20	-3.38	0.06	0.95
	345	0.89	0.30	-9.35	-0.05	0.93	0.87	0.29	-9.14	0.01	0.91	0.89	0.23	-6.83	0.02	0.92
	353	0.86	0.31	-10.06	-0.21	0.97	0.86	0.27	-8.80	0.01	0.91	0.86	0.25	-7.74	-0.14	0.97
2012	57	0.87	0.34	-9.06	-0.11	0.94	0.86	0.35	-9.51	0.02	0.89	0.87	0.22	-4.74	0.04	0.94
	65	0.81	0.28	-7.04	-0.15	0.98	0.84	0.33	-10.06	0.11	0.86	0.80	0.20	-2.64	-0.03	0.98
	345	0.77	0.36	-11.34	-0.21	0.96	0.89	0.27	-8.65	-0.03	0.93	0.76	0.19	-4.76	-0.01	0.96
	353	0.78	0.38	-12.41	-0.24	0.96	0.88	0.30	-9.72	-0.09	0.93	0.77	0.21	-5.74	-0.04	0.96

Literature review relating to spatial pixel-wise AET estimates comparison with MOD16A2 (Autovino et al., 2016; Cherif et al., 2015; Ruhoff et al., 2013; Ke et al., 2017) are presented and results interpreted that MOD16A2 overestimated AET in all the studies given below. AET estimated by MOD16A2 is found to be slightly higher than Penman-Monteith and Priestley-Taylor approaches for all the days. Autovino et al., (2016) estimated AET by PM model and later compared with measured AET fluxes showed mean RMSE of 0.52 mm/day. Also, the comparison between MOD16A2 and the proposed approach showed that MOD16A2 overestimated AET by reporting mean RMSE of 0.83 mm/day. Cherif et al., (2015) improved the accuracy of estimating AET by remotely sensed energy balance model and results were compared with MOD16A2, attaining  $R^2$  of 0.61 and an RMSE of 0.92 mm/day. Ruhoff et al., (2013) examined the accuracy of the MOD16A2 algorithm at sugar-cane plantation (USE) and natural savannah vegetation (PDG). Comparison between 8-day average MOD16A2 estimates and flux tower measurements yielded  $R^2$  of 0.78 to 0.81, mean RMSE of 0.78 and 0.46 mm/day, at PDG and USE, respectively. Ke et al., (2017) results showed that fusion of Landsat VIs produced the best accuracy of predicted AET ( $R^2 = 0.52-0.97$ , RMSE = 0.47–3.0 mm/8 days when compared with MOD16A2. The downscaled 30 m AET had good agreement with MOD16A2 (RMSE = 0.42–3.4 mm/8 days). From Table 6.2, It can be seen that the range of  $R^2$  and RMSE performance measures to estimate AET using PT, PM and PMCH models when compared with the MOD16A2 data yielded favourably good results.

## 6.3.5 Spatial AET estimated by PM, PT and PMCH approaches

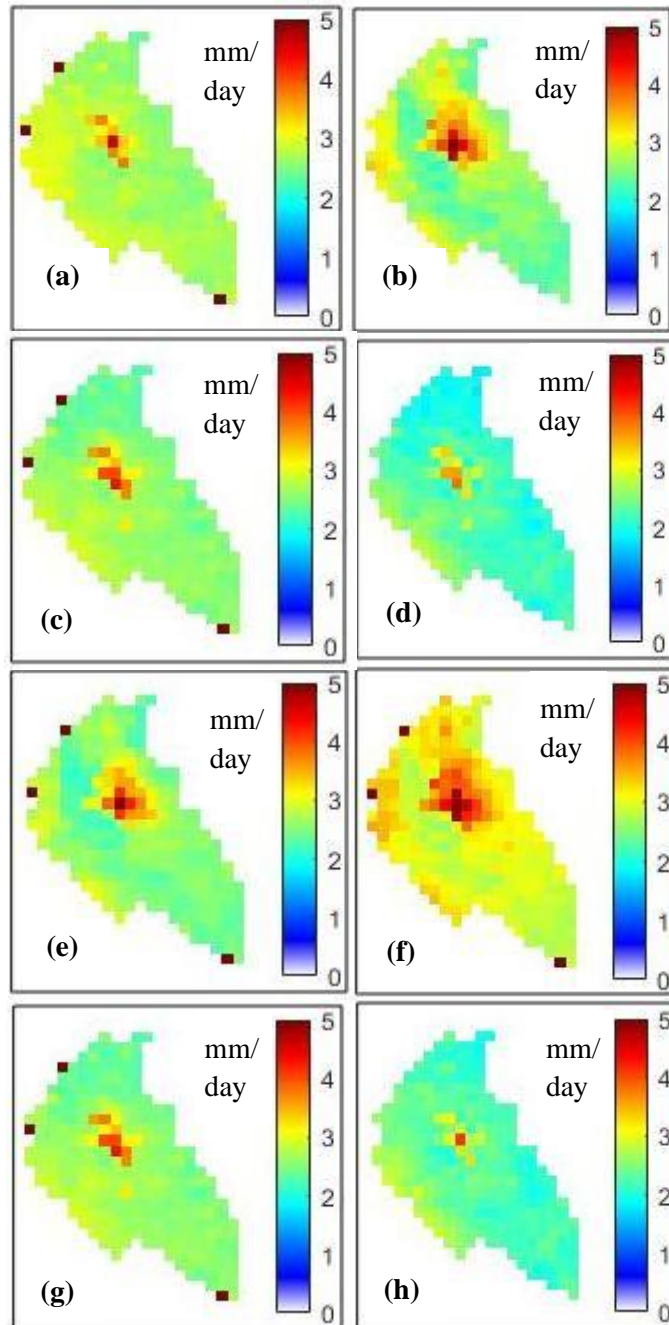


**Figure 6.9: Spatial variation of AET by PM approach in Hemavathi sub-basin for a) Day 57, 2007 (b) Day 65, 2007 (c) Day 345, 2007 (d) Day 353, 2007 (e) Day 57, 2012 (f) Day 65, 2012 (g) Day 345, 2012 (h) Day 353, 2012**



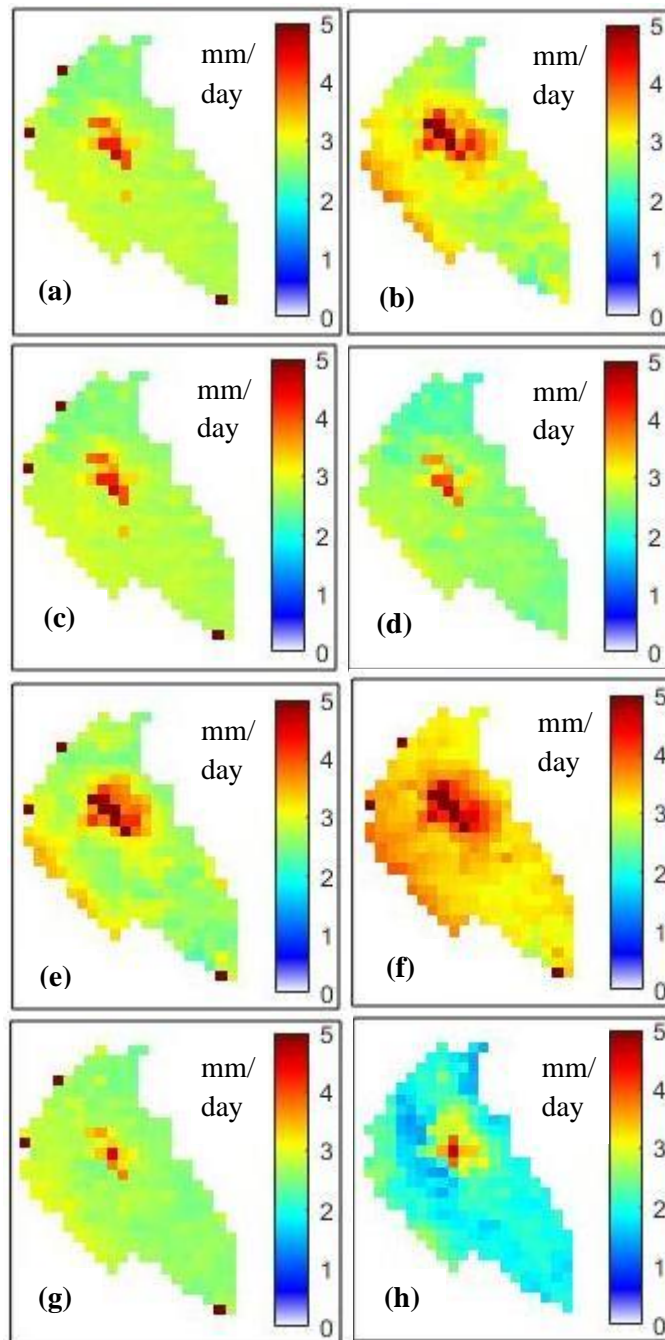


**Figure 6.10: Spatial variation of AET by PT approach in Hemavathi sub-basin for a) Day 57, 2007 (b) Day 65, 2007 (c) Day 345, 2007 (d) Day 353, 2007 (e) Day 57, 2012 (f) Day 65, 2012 (g) Day 345, 2012 (h) Day 353, 2012**

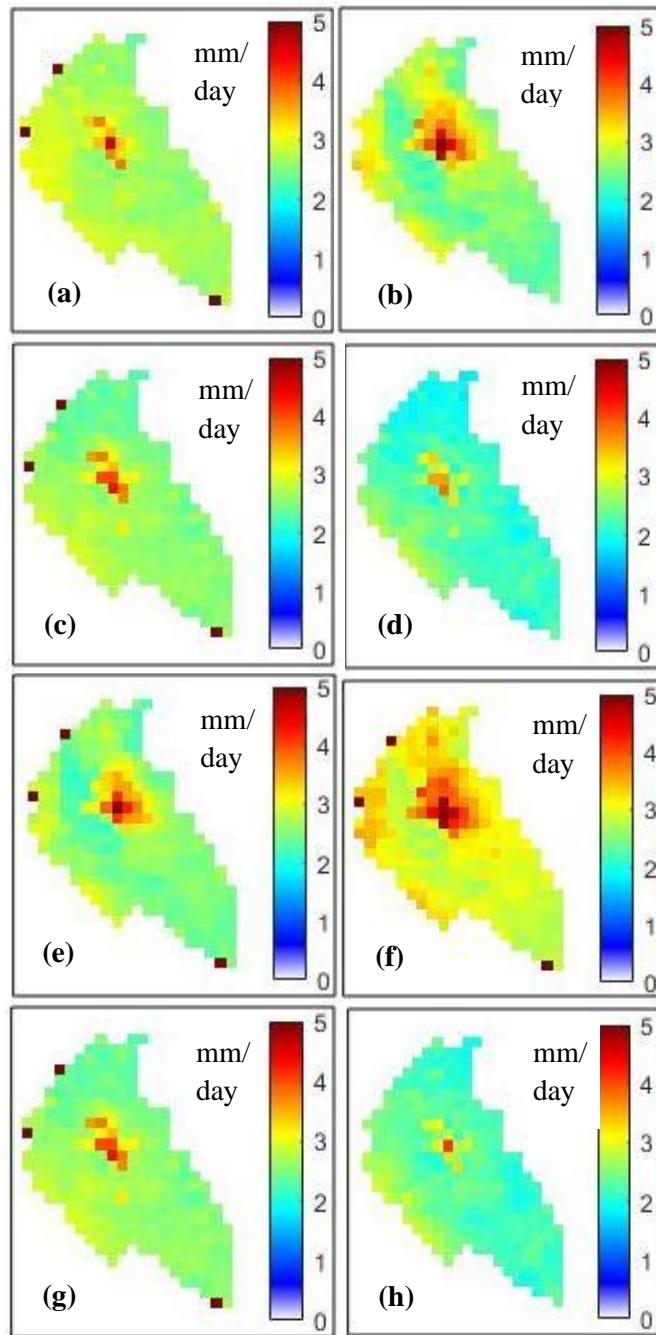


**Figure 6.11: Spatial variation of AET by PMCH approach in Hemavathi sub-basin for a) Day 57, 2007 (b) Day 65, 2007 (c) Day 345, 2007 (d) Day 353, 2007 (e) Day 57, 2012 (f) Day 65, 2012 (g) Day 345, 2012 (h) Day 353, 2012**

Daily evapotranspiration mapping was estimated from the equations given in Chapter 4. Below Figures (6.9, 6.10 and 6.11) shows AET estimated by PM, PT and PMCH approaches. Using the pixel-wise values of AET, maps showing the spatial variability were prepared. As an example, the maps obtained using  $AET_{PMCH}$  values are shown in Figure 6.2 for all the dates considered in 2007 and 2012. The variations of AET over the basin appear to be influenced by topography, type of LU/LC, LST and moisture availability conditions. AET in higher elevations of the basin is observed to be consistently higher than the lower elevations during both summer and winter seasons of 2007 and 2012. Expectedly, average AET values are higher in the summer season than in winter for both 2007 and 2012 years due to high LST. AET during the winter of 2012 was slightly lower than the winter of 2007 for most of the classes on account of very less moisture in 2012 due to less rainfall in monsoon season. The spatial distribution of the estimated AET is higher in Waterbodies, followed by Plantation/Orchard and Crop/Mixed farming LU/LC classes. It is found to be low in the built-up and Barren/Wasteland LU/LC classes.

## CHAPTER 7

## SUMMARY AND CONCLUSIONS

**7.1 GENERAL**

The main objective of this research work was to develop a novel approach involving MODIS-retrieved Land Surface Temperature (LST) – Fraction of Vegetation (Fr) trapezoidal scatter plot to model bulk surface conductance ( $G_s$ ) for use with the PM model for estimating latent heat flux ( $\lambda ET$ ) or Actual Evapotranspiration (AET) and validating PM algorithm for computation of daily AET. Validation of PM and PT models were done by using flux towers data. The validated PM and PT (Laxmi and Nandagiri, 2014) models were later applied to map spatial variability of daily AET in a tropical catchment and to evaluate model accuracies by comparing performances with MOD16A2 data in the Hemavathi river sub-basin (304 km<sup>2</sup>) which is located in Karnataka State. The study addresses a typical condition where developing country like India faces scarcity of ground based data like flux towers for validation of AET on the one side, whereas, on the other side, good quality global satellite data at acceptable spatial resolutions, advanced GIS tools are readily available for modeling. Hence, the development of PM and PT approaches to estimate AET is implemented by using satellite imagery and ground based measurements with the help of GIS interface and MATLAB.

In this chapter, a summary of the work carried out is presented by listing conclusions from the obtained results and discussions. Also, limitations of the study and scope for future research are presented.

**7.2 CONCLUSIONS**

- i. In this research work a novel approach involving MODIS-retrieved Land Surface Temperature (LST) – Fraction of Vegetation (Fr) trapezoidal scatter plot is used to model bulk surface conductance ( $G_s$ ) for use with the PM model for latent heat flux ( $\lambda ET$ ).  $G_{s_{max}}$  equation has been derived as a function of only climate variables ( $\Delta$ ,  $R_n$ ,  $G$ ,  $\gamma$  and  $D_a$ ) which can be calculated using recorded data. This equation can provide an upper bound to ongoing and future efforts

aimed at developing models for  $G_s$  using environmental and biophysical variables.

- ii. Estimated values of  $\lambda ET_{PM}$  obtained using the proposed approach were validated with instantaneous flux values measured on six selected dates at four flux towers located in tropical south-east Asia. Excellent comparisons were obtained between tower measured  $\lambda ET$  and those estimated by the proposed approach for all four flux tower locations ( $R^2 = 0.85 - 0.96$ ;  $RMSE = 18.27 - 33.79 \text{ W/m}^2$ ). Results obtained from the proposed methodology were also compared with alternative methods proposed by previous researchers, the simple Cleugh et al. (2007) approach (PMC) and the somewhat more complex Leuning et al. (2008) approach (PML). Results by all methods were comparable.
- iii. The novel LST-Fr contextual scatter-plot approach developed in the present study proved to be a simple and accurate method. Most importantly, unlike the other methods tested, the present method is calibration-free and does not require measured flux data for optimizing model parameters.
- iv. A methodology for implementation of the PM and PT (Laxmi and Nandagiri, 2014) models to estimate spatial AET in the Hemavathi river sub-basin ( $304 \text{ km}^2$ ) was developed using MODIS products and ground-based climate records. Since comparisons with flux tower data revealed a small but consistent bias, an alternative equation for computing the aerodynamic conductance ( $G_a$ ) proposed by Choudhary et al. (1986) was used to see if the bias could be eliminated.
- v. Accuracies of AET estimates for eight selected dates in 2007 and 2012 were evaluated through comparison with the MOD16A2 ET product. Excellent comparisons were obtained with the average RMSE being  $0.30 \text{ mm/day}$ . The PM model approach proposed in this study with the Choudhary et al. (1986) equation for  $G_a$  yielded the best estimates of AET in the Hemavathi sub-basin.

- vi. The framework for implementing the spatial contextual information approach to derive operational estimates of daily AET over large spatial domains has been developed and validated in this study.
- vii. Spatial maps for Hemavathi sub-basin indicated that AET during the winter of 2012 was slightly lower than the winter of 2007 for most of the classes on account of lower moisture in 2012 due to less rainfall in monsoon season. The estimated AET was higher in Waterbodies, followed by Plantation/Orchard and Crop/Mixed farming LU/LC classes. It was found to be low in the built-up and Barren/Wasteland LU/LC classes.
- viii. The methodology developed in this study has the potential to provide reasonably accurate regional/catchment scale land surface evapotranspiration estimates using satellite imagery in a convenient manner with minimal data inputs.

### **7.3 LIMITATIONS OF THE STUDY**

- i. Due to the non-availability of flux towers data in India during the work, PM and PT algorithms were applied in Southeast Asian regions.
- ii. Algorithms need to be evaluated further using Indian flux towers data.
- iii. The study was conducted confined to days on which cloud-free MODIS images were available.
- iv. In the application of algorithms to Hemavathi sub-basin, ground-based climate data were available for only one station, hence spatial variability in climate was not taken into account.

#### 7.4 SCOPE FOR FUTURE STUDIES

- i. Diverse satellite imagery like AVHRR and Landsat with finer spatial resolution may be used to compare the performances with MODIS imagery.
- ii. The developed algorithms may be implemented at the catchment scale using interpolated climate data obtained from climate stations or from gridded data.
- iii. Automated procedures for extracting  $LST_{\min}$ ,  $LST_{\max}$ , and  $LST_c$  from trapezoidal scatter plots may be developed.
- iv. Efforts need to be made to use the methodologies proposed in this study to obtain continuous time series of AET. This will be useful in water balance studies and calibration of hydrological models.
- v. The proposed approach may be extended to develop AET maps for larger spatial scales such as State, Country or Global.

## REFERENCES

---

Allen, R. G., Pereira, L. S., Raes, D., & Smith, M. (1998). "Crop evapotranspiration-Guidelines for computing crop water requirements-FAO Irrigation and drainage paper 56". *Fao, Rome*, 300(9), D05109.

Alves, I., & Pereira, L. S. (2000). "Modelling surface resistance from climatic variables?". *Agricultural Water Management*, 42(3), 371-385.

Ayenew, T. (2003). "Evapotranspiration estimation using thematic mapper spectral satellite data in the Ethiopian rift and adjacent highlands." *J. Hydrol.*, 279(1–4), 83–93.

Allen, R. G., Tasumi, M., Morse, A., Trezza, R., Wright, J. L., Bastiaanssen, W., Kramber, W., Lorite, I., and Robison, C. W. (2007). "Satellite-Based Energy Balance for Mapping Evapotranspiration with Internalized Calibration (METRIC)-Applications". *J. Irrig. Drain. Eng.*, 133(4), 395–406.

Ambast, Sunil K., Ashok K. Keshari, and Ashvani K. Gosain. "Estimating regional evapotranspiration using remote sensing: Application to some low level canal system, India." *Journal of Irrigation and Drainage Engineering* 134, no. 1 (2008): 13-25.

Anderson, M. C., Norman, J. M., Kustas, W. P., Houborg, R., Starks, P. J., and Agam, N. (2008). "A thermal-based remote sensing technique for routine mapping of land-surface carbon, water and energy fluxes from field to regional scales." *Remote Sens. Environ.*, 112(12), 4227–4241.

Autovino, D., Minacapilli, M., and Provenzano, G. (2016). "Modelling bulk surface resistance by MODIS data and assessment of MOD16A2 evapotranspiration product in an irrigation district of Southern Italy." *Agric. Water Manag.*, 167, 86–94.

Amazirh, A., Er-Raki, S., Chehbouni, A., Rivalland, V., Diarra, A., Khabba, S., ... & Merlin, O. (2017). "Modified Penman–Monteith equation for monitoring evapotranspiration of wheat crop: Relationship between the surface resistance and remotely sensed stress index. *Biosystems engineering*, 164, 68-84.



- Beven, K. (1979). "A sensitivity analysis of the Penman-Monteith actual evapotranspiration estimates". *Journal of Hydrology.*, 44, 169–190.
- Brutsaert W. and Stricker H. (1979). "An advection aridity approach to estimate actual regional Evapotranspiration." *Water Resources Research*, 15 (2), 443-450.
- Bastiaanssen, W. G. M. (1995). *Regionalization of surface flux densities and moisture indicators in composite terrain: a remote sensing approach under clear skies in Mediterranean climates*. Dr. Thesis, Wageningen Agric. Univ. Wageningen Netherlands.
- Bastiaanssen, W. G. M. (2000). "SEBAL-based sensible and latent heat fluxes in the irrigated Gediz Basin, Turkey." *J. Hydrol.*, 229(1–2), 87–100.
- Batra, N., Islam, S., Venturini, V., Bisht, G., and Jiang, L. (2006). "Estimation and comparison of evapotranspiration from MODIS and AVHRR sensors for clear sky days over the Southern Great Plains." *Remote Sens. Environ.*, 103(1), 1–15.
- Carlson, T. N., Gillies, R. R., & Perry, E. M. (1994). "A method to make use of thermal infrared temperature and NDVI measurements to infer surface soil water content and fractional vegetation cover". *Remote sensing reviews*, 9(1-2), 161-173.
- Carlson, T. N., and Ripley, D. A. (1997). "On the relation between NDVI, fractional vegetation cover, and leaf area index." *Remote Sens. Environ.*, 62(3), 241–252.
- Choudhury, B. J., Reginato, R. J., & Idso, S. B. (1986). "An analysis of infrared temperature observations over wheat and calculation of latent heat flux." *Agricultural and Forest Meteorology*, 37(1), 75-88.
- Cleugh, H. A., Leuning, R., Mu, Q., and Running, S. W. (2007). "Regional evaporation estimates from flux tower and MODIS satellite data." *Remote Sens. Environ.*, 106(3), 285–304.
- Cescatti, A., Marcolla, B., Vannan, S. K. S., Pan, J. Y., Román, M. O., Yang, X., ... & Migliavacca, M. (2012). "Intercomparison of MODIS albedo retrievals and in situ measurements across the global FLUXNET network". *Remote sensing of*

*environment*, 121, 323-334.

Cleverly, J., Chen, C., Boulain, N., Villalobos-Vega, R., Faux, R., Grant, N., ... & Eamus, D. (2013). "Aerodynamic resistance and Penman–Monteith evapotranspiration over a seasonally two-layered canopy in semiarid central Australia." *Journal of Hydrometeorology*, 14(5), 1562-1570.

Cherif, I., Alexandridis, T. K., Jauch, E., Chambel-Leitao, P., & Almeida, C. (2015). "Improving remotely sensed actual evapotranspiration estimation with raster meteorological data". *International Journal of Remote Sensing*, 36(18), 4606-4620.

Doorenbos, J., and Pruitt, W. O. (1977). "Crop water requirements". FAO irrigation and drainage. *Land and Water Development Division, FAO, Rome*, 144.

Doorenbos, J. and Kassam, A.H. (1979). "Yield response to water". FAO irrigation and drainage, Food and Agriculture Organization, Rome, 193.

De Bruin, H. A. R. (1983). "A model for the Priestley-Taylor parameter  $\alpha$ ". *Journal of Climate and Applied Meteorology*, 22(4), 572-578.

Duffie, J. A., & Beckman, W. A. (1991). "Solar engineering of thermal processes". New York: John Wiley Publications.

Er-Raki, S., Amazirh, A., Ayyoub, A., Khabba, S., Merlin, O., Ezzahar, J., & Chehbouni, A. (2016, October). "Integrating thermal surface temperature into Penman-Monteith model for estimating evapotranspiration and crop water stress of orange orchard in semi-arid region." In *International Symposium on Sensing Plant Water Status-Methods and Applications in Horticultural Science 1197* (pp. 89-96).

Fisher, J. B., Tu, K. P., and Baldocchi, D. D. (2008). "Global estimates of the land-atmosphere water flux based on monthly AVHRR and ISLSCP-II data, validated at 16 FLUXNET sites." *Remote Sens. Environ.*, 112(3), 901–919.

Goward, S. N., Cruickshanks, G. D., & Hope, A. S. (1985). "Observed relation between thermal emission and reflected spectral radiance of a complex vegetated landscape". *Remote Sensing of Environment*, 18(2), 137-146.

- Goward, S. N., and Hope, A. S. (1989). "Evapotranspiration from combined reflected solar and emitted terrestrial radiation: Preliminary FIFE results from AVHRR data." *Adv. Sp. Res.*, 9(7), 239–249.
- Gieske, A., & Meijninger, W. (2005). "High density NOAA time series of ET in the Gediz Basin, Turkey". *Irrigation and drainage systems*, 19(3-4), 285-299.
- Gao, W., Lu, Q., Gao, Z., Wu, W., Du, B., & Slusser, J. (2006). "Analysis of temporal variations of surface albedo from MODIS". In *Remote Sensing and Modeling of Ecosystems for Sustainability III* (Vol. 6298, p. 62981G).
- Glenn, E. P., Huete, A. R., Nagler, P. L., Hirschboeck, K. K., & Brown, P. (2007). "Integrating remote sensing and ground methods to estimate evapotranspiration". *Critical Reviews in Plant Sciences*, 26(3), 139-168.
- Gamage, N., Smakhtin, V., & Perera, B. J. C. (2011, December). "Estimation of actual evapotranspiration using remote Sensing data. In *19th International congress on modelling and simulation*", Perth, Australia (pp. 12-16).
- García, M., Sandholt, I., Ceccato, P., Ridler, M., Mougín, E., Kergoat, L., Morillas, L., Timouk, F., Fensholt, R., and Domingo, F. (2013). "Actual evapotranspiration in drylands derived from in-situ and satellite data: Assessing biophysical constraints." *Remote Sens. Environ.*, 131, 103–118.
- Hatfield, J. L., Perrier, A., & Jackson, R. D. (1983). "Estimation of evapotranspiration at one time-of-day using remotely sensed surface temperatures". In *Developments in Agricultural and Managed Forest Ecology* (Vol. 12, pp. 341-350).
- Hillel, D. 1998. "Environmental soil physics." Academic Press Ltd, 771p.
- Huntingford, C., and Monteith, J. L. (1998). "The behaviour of a mixed-layer model of the convective boundary layer coupled to a big leaf model of surface energy partitioning." *Boundary-Layer Meteorol.*, 88(1), 87–101.

Hassan, Q. K., Bourque, C. P. A., Meng, F. R., and Cox, R. M. (2007). "A wetness index using terrain-corrected surface temperature and normalized difference vegetation index derived from standard MODIS products: An evaluation of its use in a humid forest-dominated region of Eastern Canada." *Sensors*, 7(10), 2028–2048.

Jiang, L., and Islam, S. (1999). "A methodology for estimation of surface evapotranspiration over large areas using remote sensing observations." *Geophys. Res. Lett.*, 26(17), 2773–2776.

Jiang, L., & Islam, S. (2001). "Estimation of surface evaporation map over southern Great Plains using remote sensing data". *Water resources research*, 37(2), 329-340.

Kelliher, F. M., Leuning, R., Raupach, M. R., & Schulze, E. D. (1995). "Maximum conductances for evaporation from global vegetation types". *Agricultural and Forest Meteorology*, 73(1-2), 1-16.

Kustas, W. P., & Norman, J. M. (1996). "Use of remote sensing for evapotranspiration monitoring over land surfaces". *Hydrological Sciences Journal*, 41(4), 495-516.

Ke, Y., Im, J., Park, S., & Gong, H. (2017). "Spatiotemporal downscaling approaches for monitoring 8-day 30 m actual evapotranspiration". *ISPRS Journal of Photogrammetry and Remote Sensing*, 126, 79-93.

Liang, S. (2001). "Narrowband to broadband conversions of land surface albedo I: Algorithms". *Remote sensing of environment*, 76(2), 213-238.

Loukas, A., Vasiliades, L., Domenikiotis, C., and Dalezios, N. R. (2005). "Basin-wide actual evapotranspiration estimation using NOAA/AVHRR satellite data." *Phys. Chem. Earth*, 30(1-3 SPEC. ISS.), 69–79.

Lunetta, R. S., Knight, J. F., Ediriwickrema, J., Lyon, J. G., & Worthy, L. D. (2006). "Land-cover change detection using multi-temporal MODIS NDVI data". *Remote sensing of environment*, 105(2), 142-154.

- Liu, S., Lu, L., Mao, D., & Jia, L. (2007). "Evaluating parameterizations of aerodynamic resistance to heat transfer using field measurements". *Hydrology and Earth System Sciences Discussions*, 11(2), 769-783.
- Leuning, R., Zhang, Y. Q., Rajaud, A., Cleugh, H., and Tu, K. (2008). "A simple surface conductance model to estimate regional evaporation using MODIS leaf area index and the Penman-Monteith equation." *Water Resour. Res.*, 44(10).
- Lizarraga-Celaya, C., Watts, C. J., Rodríguez, J. C., Garatuza-Payan, J., Scott, R. L., & Saiz-Hernandez, J. (2010). "Spatio-temporal variations in surface characteristics over the North American Monsoon region". *Journal of arid environments*, 74(5), 540-548.
- Li, X., Liang, S., Yuan, W., Yu, G., Cheng, X., Chen, Y., ... & Liu, S. (2014). "Estimation of evapotranspiration over the terrestrial ecosystems in China". *Ecohydrology*, 7(1), 139-149.
- Laxmi, K., and Nandagiri, L. (2014). "Latent heat flux estimation using trapezoidal relationship between MODIS land surface temperature and fraction of vegetation-application and validation in a humid tropical region." *Remote Sens. Lett.*, 5(11), 981–990.
- Monteith, J.L. (1965). "Evaporation and environment". In: *The State and Movement of Water in Living Organisms*, Volume 19, pp. 205–234.
- Mukammal, E. I., & Neumann, H. H. (1977). "Application of the Priestley-Taylor evaporation model to assess the influence of soil moisture on the evaporation from a large weighing lysimeter and class A pan". *Boundary-Layer Meteorology*, 12(2), 243-256
- Morton F.I. (1983). "Operational estimates of Areal Evapotranspiration and their significance to the science and practice of hydrology." *Journal of Hydrology*, 66, 1-76.
- McNaughton, K. G., & Jarvis, P. G. (1983). "Predicting effects of vegetation changes on transpiration and evaporation". *Water deficits and plant growth*, 7, 1-47.

- Mahrt, L. and Ek, M. (1984). "The influence of atmospheric stability on potential evaporation." *J. Clim. Appl. Meteorol.*, 23, 222–234.
- McNaughton, K. G., & Spriggs, T. W. (1989). "An evaluation of the Priestley and Taylor equation and the complementary relationship using results from a mixed-layer model of the convective boundary layer". *Estimation of areal evapotranspiration*, 177, 89-104.
- Morse, A., Kramber, W. J., Wilkins, M., Allen, R. G., & Tasumi, M. (2003, July). "Preliminary computation of evapotranspiration by land cover type using Landsat TM data and SEBAL". In *IGARSS 2003. 2003 IEEE International Geoscience and Remote Sensing Symposium. Proceedings (IEEE Cat. No. 03CH37477)* (Vol. 4, pp. 2956-2958).
- Mu, Q., Heinsch, F. A., Zhao, M., and Running, S. W. (2007). "Development of a global evapotranspiration algorithm based on MODIS and global meteorology data." *Remote Sens. Environ.*, 111(4), 519–536.
- Mu, Q., Zhao, M., and Running, S. W. (2011). "Improvements to a MODIS global terrestrial evapotranspiration algorithm." *Remote Sens. Environ.*, 115(8), 1781–1800.
- Majumdar, T. J., Pal, S. K., & Bhattacharya, A. K. (2012). "Generation of emissivity and land surface temperature maps using MODIS TIR data for lithological mapping over the Singhbhum-Orissa Craton". *Journal of the Geological Society of India*, 80(5), 685-699.
- Nemani, R. R., & Running, S. W. (1989). "Estimation of regional surface resistance to evapotranspiration from NDVI and thermal-IR AVHRR data". *Journal of Applied meteorology*, 28(4), 276-284.
- Nishida, K., Nemani, R. R., Running, S. W., & Glassy, J. M. (2003). "An operational remote sensing algorithm of land surface evaporation". *Journal of Geophysical Research: Atmospheres*, 108(D9).

- Nemani, R. R., Keeling, C. D., Hashimoto, H., Jolly, W. M., Piper, S. C., Tucker, C. J., ... & Running, S. W. (2003). "Climate-driven increases in global terrestrial net primary production from 1982 to 1999". *science*, 300(5625), 1560-1563.
- Oleson, K. W., Bonan, G. B., Schaaf, C., Gao, F., Jin, Y., & Strahler, A. (2003). "Assessment of global climate model land surface albedo using MODIS data". *Geophysical Research Letters*, 30(8).
- Penman, H. L. (1948). "Natural Evaporation from Open Water, Bare Soil and Grass." *Proc. R. Soc. A Math. Phys. Eng. Sci.*, 193(1032), 120–145.
- Priestley, C. H. B., and Taylor, R. J. (1972). "On the Assessment of Surface Heat Flux and Evaporation Using Large-Scale Parameters." *Mon. Weather Rev.*, 100(2), 81–92.
- Paltridge, G. W., & Proctor, D. (1976). "Monthly mean solar radiation statistics for Australia. *Solar Energy*", 18(3), 235-243.
- Pinty, B., & Verstraete, M. M. (1992). "On the design and validation of surface bidirectional reflectance and albedo models". *Remote Sensing of Environment*, 41(2-3), 155-167.
- Pereira, A. R. (2004). "The Priestley-Taylor parameter and the decoupling factor for estimating reference evapotranspiration." *Agric. For. Meteorol.*, 125(3–4), 305–313.
- Pettorelli, N., Vik, J. O., Mysterud, A., Gaillard, J. M., Tucker, C. J., & Stenseth, N. C. (2005). "Using the satellite-derived NDVI to assess ecological responses to environmental change. *Trends in ecology & evolution*", 20(9), 503-510.
- Patel, N. R., Rakhesh, D., & Mohammed, A. J. (2006). "Mapping of regional evapotranspiration in wheat using Terra/MODIS satellite data". *Hydrological sciences journal*, 51(2), 325-335.
- Qiu, G. Y., & Ben-Asher, J. (2010). "Experimental determination of soil evaporation stages with soil surface temperature". *Soil Science Society of America Journal*, 74(1), 13-22.

Richards, J. M. (1971). "A simple expression for the saturation vapour pressure of water in the range -50 to 140°C." *J. Phys. D. Appl. Phys.*, 4(4), L15.

Rowe, C. M. (1991). "Modeling land-surface albedos from vegetation canopy architecture". *Physical Geography*, 12(2), 93-114.

Running, S. W. (1991). "Computer simulation of regional evapotranspiration by integrating landscape biophysical attributes with satellite data". In *Land Surface Evaporation* (pp. 359-369).

Ruhoff, A. L., Paz, A. R., Aragao, L. E. O. C., Mu, Q., Malhi, Y., Collischonn, W., ... & Running, S. W. (2013). "Assessment of the MODIS global evapotranspiration algorithm using eddy covariance measurements and hydrological modelling in the Rio Grande basin". *Hydrological Sciences Journal*, 58(8), 1658-1676.

Sugita, M., & Brutsaert, W. (1991). "Daily evaporation over a region from lower boundary layer profiles measured with radiosondes". *Water Resources Research*, 27(5), 747-752.

Schellekens, J., Bruijnzeel, L. A., Scatena, F. N., Bink, N. J., & Holwerda, F. (2000). "Evaporation from a tropical rain forest, Luquillo Experimental Forest, eastern Puerto Rico". *Water Resources Research*, 36(8), 2183-2196.

Sumner, D. M., and Jacobs, J. M. (2005). "Utility of Penman-Monteith, Priestley-Taylor, reference evapotranspiration, and pan evaporation methods to estimate pasture evapotranspiration." *J. Hydrol.*, 308(1-4), 81-104.

Senay, G. B., Budde, M., Verdin, J. P., and Melesse, A. M. (2007). "A coupled remote sensing and simplified surface energy balance approach to estimate actual evapotranspiration from irrigated fields." *Sensors*, 7(6), 979-1000.

Scanlon, B. R., Zhang, Z., Reedy, R. C., Pool, D. R., Save, H., Long, D., Chen, J., Wolock, D. M., Conway, B. D., and Winester, D. (2015). "Hydrologic implications of GRACE satellite data in the Colorado River Basin." *Water Resour. Res.*, 51(12), 9891-9903.



- Sun, H. (2016). "Two-stage trapezoid: A new interpretation of the land surface temperature and fractional vegetation coverage space". *IEEE Journal of Selected Topics in Applied Earth Observations and Remote Sensing*, 9(1), 336-346.
- Thom, A. S. (1975). "Momentum, mass and heat exchange of plant communities." *Vegetation and the Atmosphere, Academic Press, London*, 57–109.
- Tucker, C. J., Slayback, D. A., Pinzon, J. E., Los, S. O., Myneni, R. B., & Taylor, M. G. (2001). "Higher northern latitude normalized difference vegetation index and growing season trends from 1982 to 1999". *International journal of biometeorology*, 45(4), 184-190.
- Tasumi, M., Trezza, R., Allen, R. G., and Wright, J. L. (2005). "U.S. Validation Tests on the SEBAL Model for Evapotranspiration via Satellite." *Irrig. Drain. Syst.*, 19(3–4), 223–249.
- Tang, R., Li, Z. L., and Tang, B. (2010). "An application of the Ts-VI triangle method with enhanced edges determination for evapotranspiration estimation from MODIS data in arid and semi-arid regions: Implementation and validation." *Remote Sens. Environ.*, 114(3), 540–551.
- Tang, R., Li, Z. L., Jia, Y., Li, C., Sun, X., Kustas, W. P., and Anderson, M. C. (2011). "An intercomparison of three remote sensing-based energy balance models using Large Aperture Scintillometer measurements over a wheat-corn production region." *Remote Sens. Environ.*, 115(12), 3187–3202.
- Utset, A., Farré, I., Martínez-Cob, A., and Caverro, J. (2004). "Comparing Penman-Monteith and Priestley-Taylor approaches as reference-evapotranspiration inputs for modeling maize water-use under Mediterranean conditions." *Agric. Water Manag.*, 66(3), 205–219.
- Verma, S. B., Rosenberg, N. J., Blad, B. L., and Baradas, M. W. (1976). "Resistance-energy balance method for predicting evapotranspiration: Determination of boundary layer resistance and evaluation of error effects", *Agronomy J.*, 68, 776–782.

Van de Griend, A. A., & OWE, M. (1993). "On the relationship between thermal emissivity and the normalized difference vegetation index for natural surfaces". *International Journal of remote sensing*, 14(6), 1119-1131.

Viney, N. R. (1991). "An empirical expression for aerodynamic resistance in the unstable boundary layer". *Boundary-Layer Meteorology*, 56(4), 381-393.

Valor, E., & Caselles, V. (1996). "Mapping land surface emissivity from NDVI: Application to European, African, and South American areas". *Remote sensing of Environment*, 57(3), 167-184.

Wang, S., Chen, W., and Cihlar, J. (2002). "New calculation methods of diurnal distribution of solar radiation and its interception by canopy over complex terrain." *Ecol. Modell.*, 155(2–3), 191–204.

Wang, K., Wang, P., Li, Z., Cribb, M., & Sparrow, M. (2007). "A simple method to estimate actual evapotranspiration from a combination of net radiation, vegetation index, and temperature". *Journal of Geophysical Research: Atmospheres*, 112(D15).

Whitley, R., Medlyn, B., Zeppel, M., Macinnis-Ng, C., & Eamus, D. (2009). "Comparing the Penman–Monteith equation and a modified Jarvis–Stewart model with an artificial neural network to estimate stand-scale transpiration and canopy conductance". *Journal of Hydrology*, 373(1-2), 256-266.

Wang, X., Wang, W., & Jiang, Y. (2015). "Combining the trapezoidal relationship between land surface temperature and vegetation index with the Priestley-Taylor equation to estimate evapotranspiration". *Proceedings of the International Association of Hydrological Sciences*, 368, 379-384.

Xie, X. (1988). An improved energy balance-aerodynamic resistance model used estimation of evapotranspiration on the wheat field [J]. *Acta Meteorologica Sinica*, 1.

Yang, K., Tamai, N., and Koike, T. (2001). "Analytical solution of surface layer similarity equations.", *J. Appl. Meteorol.*, 40, 1647–1653.

- Yuan, W., Liu, S., Yu, G., Bonnefond, J. M., Chen, J., Davis, K., Desai, A. R., Goldstein, A. H., Gianelle, D., Rossi, F., Suyker, A. E., and Verma, S. B. (2010). "Global estimates of evapotranspiration and gross primary production based on MODIS and global meteorology data." *Remote Sens. Environ.*, 114(7), 1416–1431.
- Yao, Y. (2011). "Simple method to determine the Priestley–Taylor parameter for evapotranspiration estimation using Albedo-VI triangular space from MODIS data." *J. Appl. Remote Sens.*, 5(1), 053505.
- Yao, Y., Liang, S., Cheng, J., Liu, S., Fisher, J. B., Zhang, X., Jia, K., Zhao, X., Qin, Q., Zhao, B., Han, S., Zhou, G., Zhou, G., Li, Y., and Zhao, S. (2013). "MODIS-driven estimation of terrestrial latent heat flux in China based on a modified Priestley-Taylor algorithm." *Agric. For. Meteorol.*, 171–172, 187–202.
- Yebra, M., Van Dijk, A., Leuning, R., Huete, A., & Guerschman, J. P. (2013). "Evaluation of optical remote sensing to estimate actual evapotranspiration and canopy conductance". *Remote Sensing of Environment*, 129, 250-261.
- Yang, Y., Anderson, M. C., Gao, F., Hain, C. R., Semmens, K. A., Kustas, W. P., Noormets, A., Wynne, R. H., Thomas, V. A., and Sun, G. (2017). "Daily Landsat-scale evapotranspiration estimation over a forested landscape in North Carolina, USA, using multi-satellite data fusion." *Hydrol. Earth Syst. Sci.*, 21(2), 1017–1037.
- Zhang, L., Lemeur, R., & Goutorbe, J. P. (1995). "A one-layer resistance model for estimating regional evapotranspiration using remote sensing data". *Agricultural and Forest Meteorology*, 77(3-4), 241-261.
- Zhang, K., Kimball, J. S., Mu, Q., Jones, L. A., Goetz, S. J., and Running, S. W. (2009). "Satellite based analysis of northern ET trends and associated changes in the regional water balance from 1983 to 2005." *J. Hydrol.*, 379(1–2), 92–110.
- Zhang, K., Kimball, J. S., Nemani, R. R., & Running, S. W. (2010). "A continuous satellite-derived global record of land surface evapotranspiration from 1983 to 2006". *Water Resources Research*, 46(9).

Zhang, F., Tiyip, T., Ding, J., Sawut, M., Johnson, V. C., Tashpolat, N., & Gui, D. (2013). "Vegetation fractional coverage change in a typical oasis region in Tarim River Watershed based on remote sensing". *Journal of Arid Land*, 5(1), 89-101.

Zhang, K., Kimball, J. S., and Running, S. W. (2016). "A review of remote sensing based actual evapotranspiration estimation." *Wiley Interdiscip. Rev. Water*, 3(6), 834–853.

## PAPERS PUBLISHED FROM THIS RESEARCH

---

---

**Sanjay Shekar N. C.** and Lakshman Nandagiri (2016). “Actual Evapotranspiration Estimation using a Penman-Monteith Model.” *International Journal of Advances in Agricultural and Environmental Engineering (IJAAEE)*, ISSN 2349-1523, 3 (1), 161-164.

**Sanjay Shekar N. C.** and Lakshman Nandagiri (2016). “Latent Heat Flux Estimation in a Sub-Humid Tropical Region using a Satellite-Based Penman-Monteith Model.” *International Conference on Civil, Environment and Waste Mgmt (CEWM)*, ISBN: 978-93-84422-61-5, 84-87.

**Sanjay Shekar N. C.** and Lakshman Nandagiri (2019). “Penman-Monteith Evapotranspiration Model with Bulk Surface Conductance Derived from Remotely Sensed Spatial Contextual Information.” *International Journal of Remote Sensing (IJRS)*, ISSN: 1366-5901, 41 (4), 1486-1511.

**Sanjay Shekar N. C.** and Lakshman Nandagiri (2019). “Evaluation of Evapotranspiration Estimates by Penman-Monteith and Priestley-Taylor models with MOD16A2.” *Journal of Indian Society for Remote Sensing (JIRS)*, ISSN: 0255-660X (Under Preparation).

## RESUME

---

Name: Mr. Sanjay Shekar N C

Register number: AM13P02

Date of Birth: 29<sup>th</sup> March, 1988

Father's Name: Mr. Chandrashekar N M

Permanent address: #1060, Sri Jenukallu,  
Dr. Shivakumar Swamiji Arch, 7<sup>th</sup> main,  
10<sup>th</sup> Cross, Jnanabharathi 2<sup>nd</sup> Stage,  
Bangalore -560056

E-mail: sanjayshekarnc@gmail.com

Phone: +91 9535274064

